DUAL ENERGY ELECTRON STORAGE RING COOLER DESIGN FOR RELATIVISTIC ION BEAMS

by

Bhawin Dhital
M.S. January 2013, Tribhuvan University, Nepal
M.S. May 2018, Old Dominion University

A Dissertation Submitted to the Faculty of
Old Dominion University in Partial Fulfillment of the
Requirements for the Degree of

DOCTOR OF PHILOSOPHY

PHYSICS

OLD DOMINION UNIVERSITY
December 2022

Approved by:

Geoffrey A. Krafft (Director)

Fanglei Lin (Member)

Jean R Delayen (Member)

Desmond Cook (Member)

Hani Elsayed-Ali (Member)

ABSTRACT

DUAL ENERGY ELECTRON STORAGE RING COOLER DESIGN FOR RELATIVISTIC ION BEAMS

Bhawin Dhital
Old Dominion University, 2022
Director: Dr. Geoffrey A. Krafft

Collider experiments demand small beam emittances in order to achieve high luminosity. For light particles such as electrons, there exists a natural synchrotron radiation damping resulting in low emittance beams at equilibrium. In the case of heavy particle beams such as proton or ion beams, there is no significant synchrotron radiation damping effect and some cooling mechanism is needed to get to low emittance beams. A dual energy storage ring cooler is a novel concept proposed to cool hadron beams at higher energies. The design consists of two rings: a low energy ring and a high energy ring connected by the energy recovering linac (ERL) that provides the necessary energy difference. The low energy ring has an electron cooler where the cooling interaction takes place between the electron and hadron beams whereas electron beam going through the high energy ring undergoes synchrotron radiation damping. In this document, we present a possible design of a dual energy storage ring-based electron cooler for high energy proton beam cooling suitable for the Electron Ion Collider (EIC) to be built at Brookhaven National laboratory (BNL). A special feature of a dual energy storage ring cooler design is that the electron beam energy in the low energy section must be tuned to match the hadron beam velocity in the cooling section, and the electron beam energy in the high energy section is chosen to provide an adequate synchrotron radiation damping. In addition, the ring optics design is carried out considering chromaticity correction, dynamic aperture, momentum aperture, beam lifetime, radiation damping and the intrabeam scattering effect. Finally, the cooling performance is simulated for 275 GeV proton beams at the top energy of the EIC. In such a collider it is desirable to cool the hadron beams to balance the emittance growth rates due to intra-beam scattering (IBS) to maintain a high luminosity during the collision runs. In such a situation, a dual energy storage ring based cooler could be a practical approach to be used for hadron beam cooling.

ACKNOWLEDGMENTS

I want to thank all people who have helped me and supported me during my PhD. First of all, I would like to thank my research supervisor Dr. Geoffrey A. Krafft, for providing me this great opportunity to work on this novel cooler design concept and having faith in me to work on this project. Dr. Krafft is a great professor and a great physicist having enthusiasm both in teaching and physics research. We had a lot of discussions in his office at CEBAF regarding the problems in a dual energy storage ring cooler. I feel proud of him and myself being his PhD student. I am very grateful to have Dr. Fanglei Lin as my thesis supervisor, who has provided me with direction, insight, motivation and support to obtain my Ph.D. at Jefferson Lab. Dr. Lin has taught me and trained me with different skills being very patient during my research. Her hard work and leadership played the vital role for the completion of my dissertation.

I am thankful to Dr. Jean Delayen who suggested me to work on this cooler project. Besides serving on my thesis committee, he has provided me with a lot of suggestions during my research. I would also like to thank Dr. Desmond Cook and Dr. Hani Elsayed-Ali for serving on my thesis committee and providing valuable suggestions and feedback during annual reviews and thesis evaluation meetings.

A special thanks goes to Dr. Vasiliy Morozov for his great ideas and support in this project. He provided with physics ideas and various simulation and numerical codes to carry out this research work. I would also like to thank all people at CASA at Jefferson Lab where I have spent almost four years working in this project. My sincere thanks goes to Dr. Todd Satogata, CASA director for his great support and guidance during my time at CASA. Dr. Satogata helped me with editing my thesis and provided a lot of suggestions. In addition, I would like to thank Dr. Slava Derbenev, Dr. Andrew Hutton, Dr. Yuhong Zhang, Dr. Steve Benson and Dr. He Zhang for all the discussions, suggestions and insights into various problems in storage ring based cooler design. I also would like to thank Dr. Alex Bogacz and Dr. Rui Li for the fruitful discussion in accelerator physics. I would like to thank all people and friends at CASA and in Jefferson Lab.

My sincere thanks goes to the Physics Department at Old Dominion university for providing me support for my graduate studies. I am very thankful to people at Physics Department, especially Ms. Lisa Okun and Ms. Annette Guzman-Smith for their continuous support academically and in person.

I want to remember all my friends and classmate at ODU. Their friendship will be deep

in my heart forever.

Finally, I want to express my most gratitude to my parents and my wife Gita for letting me pursue my dreams. They are my rock-firm supporters and they always do their best to support me. Thank you.

TABLE OF CONTENTS

Page

Page

LIST OF TABLES

LIST OF FIGURES

CHAPTER 1

INTRODUCTION

One goal of modern high-energy particle accelerators and colliders is to achieve a higher luminosity. Such a higher luminosity demands smaller beam emittances. For light particles such as electrons and positrons, there exists a natural synchrotron radiation damping leading to low emittance beams in equilibrium. However, this damping effect is negligible in the case of heavy particle beams consisting of protons or ions. In this case, we need to apply an external mechanism to cool the heavy particle beam in order to achieved smaller beam sizes and ultimately higher luminosity.

An Electron-Ion Collider (EIC) is to be built at Brookhaven National Laboratory (BNL) [1]. In such a collider to maintain a luminosity of $L = 10^{34}\,\mathrm{cm}^{-2}\,\mathrm{s}^{-1}$ during long collision runs, it is desirable to cool the hadron beams to balance the emittance growth rates due to intrabeam scattering (IBS). To date, the proposed highest proton beam energy is 275 GeV and preserving the emittance long-term requires some cooling mechanism with cooling rates that exceed the IBS growth rates.

Electron storage rings have been considered as a coolers since the late 1970s. However, no such ring has been built for this purpose at present and thus it remains uncertain whether strong hadron cooling is possible by this means. The concept of electron cooling of hadron beams with strongly enhanced synchrotron radiation damping by using wigglers in a single energy storage ring has been thoroughly studied [2, 3]. In this thesis we propose a novel concept that greatly expands the range of applicability of storage-ring electron coolers by significantly boosting the electron beam energy in the damping section using superconducting radio frequency (SRF) cavities.

Any damping wigglers in the damping section enhance the synchrotron radiation emitted eventually leading to decreased damping times. Later, our calculations will note that the cost of using long wiggler sections is more expensive than using SRF cavities to boost the energy in the high energy section to provide sufficient synchrotron radiation damping. This conclusion allows us to give up the idea of the use of damping wigglers in the high energy ring.

To cool the hadron beam in the energy range of 41-275 GeV, the required cooling electron beam energy is in the range of 22-150 MeV. In such a low electron beam energy, the intrabeam

scattering (IBS) effect is very strong giving very short IBS times of the order of tens of milliseconds. Furthermore, the synchrotron radiation damping effect is very weak giving long damping times of the order of second up to a minute. To get the balance between IBS and radiation damping, we propose a dual energy storage ring with a high energy section to enhance the synchrotron radiation and a low energy section for cooling.

1.1 RESEARCH GOALS AND OBJECTIVES

The main goal of this research work was to explore the possibilities inherent in a new type of accelerator arrangement called an energy recovered loop accelerator. The idea is to create an ion beam cooler based on a high current electron storage ring. The goal of the dual energy storage ring project is to design an electron storage ring that provides the best possible solution to the emittance degradation due to all heating effects in ion storage rings and colliders. If we succeed, such a cooler will significantly improve the emittance and lifetimes of ion beams and therefore, improve the collider performance. The proposed dual energy storage ring cooler consists of two rings: the low energy cooler ring and the high energy damping ring operate at markedly different energies. These two rings are connected by an energy recovering superconducting RF structure. Initially, we proposed to make the use of wigglers in the high energy section to enhance the synchrotron damping effect. Later our calculations showed that for damping ring designs above around 350 MeV, it is less costly to omit wigglers and increase the energy of the high energy ring to achieve a required radiation damping rate. Now, instead of wigglers, our design uses SRF cavities to increase the energy of the high energy ring to 500 MeV which provides enough damping to the electron beam to reach the required equilibrium.

In this thesis, the following aspects of dual-energy storage ring design will be discussed:

- Design and improvement of prototype linear optics of a storage-ring electron cooler, including beam transverse stability.
- Optimization of cooler parameters.
- Analytic estimation of intra-and-inter beam scattering and space charge effects.
- Estimation of equilibrium emittances.
- Single-particle tracking, including non-linearities, of the dual-energy ring design.

Work on HOM impedance measurements for the SRF accelerating structure and coherent synchrotron radiation and beam break up should be carried out in future work. We have

completed all other remaining milestones. We have derived new formulas to calculate the equilibrium electron beam parameters in a dual energy storage ring. Now we have understood a lot of parameters in a dual energy storage ring design including the design and stability. A journal paper on dual-energy ring coolers summarizing our findings has been completed.

1.2 ORGANIZATION OF THE DISSERTATION

This dissertation is organized in the following way: Chapter 1 provides a brief introduction to the importance of hadron beam cooling and luminosity requirements in a collider. Chapter 2 discusses the beam dynamics in a storage ring, starting with the basic concepts of co-ordinate systems and phase-space coordinates. Chapter 2 also reviews the general theory of transverse and longitudinal beam dynamics that are used in a dual energy storage ring to study the stability criteria. Further, the basic concept on synchrotron radiation including equilibrium energy spread and emittance in a single energy storage ring is explained in detail. Chapter 3 is followed by a more detailed explanation of the electron cooling mechanism along with a model for cooling rate. At the end of this chapter, a brief introduction of a dual energy storage ring cooler design is presented. Chapter 4 introduces a specific dual energy storage ring design with a detailed explanation of longitudinal and transverse stability. We derived the equilibrium electron beam parameters in a dual energy storage ring and calculate the damping times and IBS times in all three dimensions. Intensive numerical calculation is carried out to study the dynamic aperture and momentum aperture in a dual energy storage ring. Based on the momentum aperture, Touschek lifetime calculations are carried out both in simulation and theory. Chapter 5 provides cooling forces formulas and the methods and results of simulating electron cooling of the EIC proton beam using the JSPEC simulation package [4]. Finally, in Chapter 6, we summarize the findings of our research and provide a guideline for future works with some possible applications of a dual energy storage ring beyond beam cooling.

CHAPTER 2

THEORY OF ELECTRON STORAGE RINGS

Many facilities based on electron storage rings are used to conduct research in a wide variety of fields. As many electron storage rings have been built, their design and performance may be computed in great detail. Another widely known application of storage rings is to particle colliders, where two beams moving in opposite directions collide. The design of a dedicated electron storage ring requires significant study beyond the simple layout and linear optics design, but we need to begin here, and then extend the usual design procedures for storage rings to the two-energy ring case. The guiding and focusing of a charged particle beam in a circular accelerator rely on a series of magnetic elements, separated by field-free drift spaces, that form the accelerator lattice. Relativistic electrons in storage rings usually radiate synchrotron radiation when the electrons go through the bending magnets (dipoles) in the arcs.

2.1 BEAM DYNAMICS

A beam is composed of charged particles. The dynamics of a beam moving along a particle accelerator depend on the interaction of charged particles with electromagnetic fields. The Lorentz force acting on the particles in an electromagnetic field is given by

$$\mathbf{F} = q[\mathbf{E} + \mathbf{v} \times \mathbf{B}], \tag{1}$$

where q is the electric charge of the particle, $\mathbf{E}$ is the electric field, $\mathbf{v}$ is the particle velocity, and $\mathbf{B}$ is the magnetic field. The study of evolution of particle trajectories under the influence of Lorentz forces is called beam dynamics. A fundamental approximation of beam dynamics relies only on linear fields and is called linear optics.

In modern accelerators, particles gain energy from time-varying electric fields, while static magnetic fields bend and confine the beam of particles transversely. Magnets such as dipoles and quadrupoles bend and focus or defocus the beam during beam transport and form the basis for the linear approximation. Beyond the linear approximation, sextupole and octupole magnets are used to correct non-linear optical aberration. Synchrotron rings are often constructed with basic "cells" such as FODO cells, which are arrangements of focusing

and defocusing quadrupoles that provide a net focusing to the beam. The strong focusing concept [5] changed the way focusing arrangements are constructed for modern large particle accelerators.

The first task for a new accelerator design is to define a reference trajectory or closed orbit. A charged particle with ideal position, momentum, and timing follows that reference trajectory. When the accelerator is linearly stable, all other particles in a beam will follow trajectories close to that reference trajectory. In a circular accelerator where a particle of electric charge q is circulating in a reference trajectory of radius ρ, a Cartesian coordinate system (x, y, z) is defined with respect to the location of the reference particle of momentum p_0 as shown in Fig. 1.

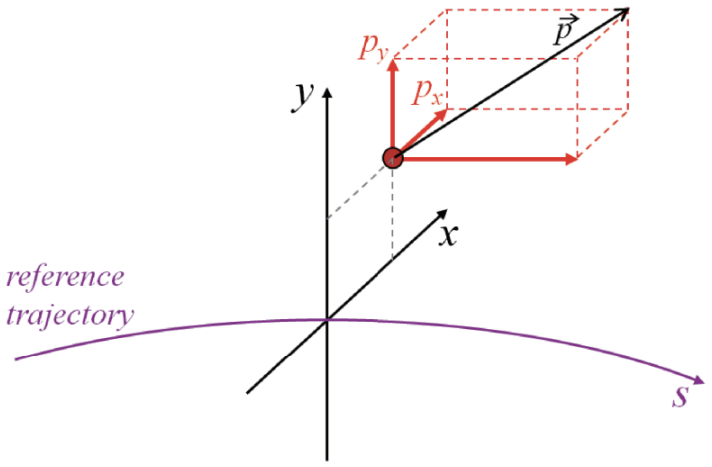

FIG. 1: Reference Trajectory and Coordinate System.

In Fig. 1 the curved path is the reference trajectory. Nearly all particles have differences in position, momentum, and/or time from the reference trajectory; these particles move along paths slightly different from the reference trajectory. To describe the perturbative motion of these particles around the reference trajectory, we define particle coordinates

$(x(s), y(s), z(s))$, with respect to the ideal particle. In this frame, particle coordinates are $(x(s), p_x(s), y(s), p_y(s), z(s), p_z(s))$ where $(p_x(s), p_y(s), p_z(s))$ are corresponding momentum coordinates. The set of coordinates $(x(s), p_x(s))$ and $(y(s), p_y(s))$ describe the transverse motion of particles whereas the $(z(s), p_z(s))$ coordinates describe the longitudinal motion. The independent variable s is path length along the reference trajectory. The momentum coordinates are in general scaled to the reference momentum p_0. This allows one to define new dimensionless momentum coordinates: $x'(s) \equiv p_x(s)/p_0, y'(s) \equiv p_y(s)/p_0$, and $\delta \equiv (p(s) - p_0)/p_0$. The prime denotes differentiation with respect to the s direction. In this dissertation, x' and y' are small angles, so the paraxial approximation applies. Also $p_z(s) \approx p(s)$ so $\delta(s) \approx (p_z(s) - p_0)/p_0$. The momentum deviation δ measures the fractional difference between the momentum of the particle and the momentum of a particle with the reference momentum p_0.

Each particle within a bunch now has six coordinates, $(x, x', y, y', z, \delta)$, that are coordinates in a six-dimensional phase space. If we neglect coupling, particle motion can be separated into transverse (horizontal and vertical) and longitudinal dimensions. The longitudinal dimension determines the length of a bunch, while the transverse dimensions determine the bunch height and width. The beam phase space description is useful in dealing with the distribution of particles. One can visualize a beam of particles at a particular time as a "cloud" of points in six-dimensional phase space.

2.2 LINEAR EQUATION OF MOTION

During beam transport, particles undergo both transverse and longitudinal oscillations around the reference trajectory or closed orbit. Transverse particle motion around the closed orbit is called betatron motion. Under the assumption that the amplitude of the betatron oscillation is small and there is no momentum deviation from the closed orbit, the transverse equation of motion of a particle in an accelerator is given by the linearized Hills's equation

$$u''(s) + K_{x,y}(s)u(s) = 0, \tag{2}$$

where u represents x or y for horizontal and vertical displacements relative to the ideal trajectory, and primes once again denote differentiation with respect to s. $K(s)$ is the focusing function along the beamline normally arranged to be periodic such that $K_{x,y}(s+L) = K_{x,y}(s)$, where L is the length of the periodic structure. If we assume that there is uncoupled motion in horizontal and vertical planes for the given dipole and quadrupole fields then the equations of motion in the horizontal and vertical planes can be solved independently.

There are three cases to consider: $K(s) = 0, K(s) > 0$ and $K(s) < 0$ corresponding to drift, quadrupole focusing, and quadrupole defocusing, respectively.

For $K(s) > 0$ constant over a distance s, the equation of motion is similar to that of harmonic oscillator and the solution to the Eq. (2) can be written as

$$\begin{aligned} u(s) &= A\cos\Big(\sqrt{K}s\Big) + B\sin\Big(\sqrt{K}s\Big), \\ u'(s) &= -\sqrt{K}A\sin\Big(\sqrt{K}s\Big) + \sqrt{K}B\cos\Big(\sqrt{K}s\Big), \end{aligned} \tag{3}$$

where A and B are integration constants to be determined by applying the initial conditions $s = 0, u(s) = u_0$ and $u'(s) = u'_0$. These give $A = u_0$, $B = u'_0/K$ and Eq. (3) can be expressed as

$$\begin{aligned} u(s) &= u_0\cos\Big(\sqrt{K}s\Big) + \frac{u'_0}{K}\sin\Big(\sqrt{K}s\Big), \\ u'(s) &= -u_0\sqrt{K}\sin\Big(\sqrt{K}s\Big) + u'_0\cos\Big(\sqrt{K}s\Big). \end{aligned} \tag{4}$$

In the matrix form, the above solutions can be expressed as

$$\begin{pmatrix} u(s) \\ u'(s) \end{pmatrix} = \begin{pmatrix} \cos\Big(\sqrt{K}s\Big) & \frac{1}{\sqrt{K}}\sin\Big(\sqrt{K}s\Big) \\ -\sqrt{K}\sin\Big(\sqrt{K}s\Big) & \cos\Big(\sqrt{K}s\Big) \end{pmatrix} \begin{pmatrix} u_0 \\ u'_0 \end{pmatrix}. \tag{5}$$

Hence, Eq. (5) can be expressed as

$$U(s) = M(s|s_0)U_0, \tag{6}$$

where $U(s) = \begin{pmatrix} u(s) \\ u'(s) \end{pmatrix}$ and $U_0 = \begin{pmatrix} u_0 \\ u'_0 \end{pmatrix}$ and $M(s|s_0)$ is the transfer matrix from s_0 to s defined by

$$M(s|s_0) = \begin{pmatrix} \cos\Big(\sqrt{K}l\Big) & \frac{1}{\sqrt{K}}\sin\Big(\sqrt{K}l\Big) \\ -\sqrt{K}\sin\Big(\sqrt{K}l\Big) & \cos\Big(\sqrt{K}l\Big) \end{pmatrix}, \tag{7}$$

with $l = s - s_0$.

Likewise, for $K(s) < 0$, the solution to Eq. (2) takes the form

$$\begin{pmatrix} u(s) \\ u'(s) \end{pmatrix} = \begin{pmatrix} \cosh\Big(\sqrt{|K|}s\Big) & \frac{1}{\sqrt{|K|}}\sinh\Big(\sqrt{|K|}s\Big) \\ \sqrt{|K|}\sinh\Big(\sqrt{|K|}s\Big) & \cosh\Big(\sqrt{|K|}s\Big) \end{pmatrix} \begin{pmatrix} u_0 \\ u'_0 \end{pmatrix} \tag{8}$$

and the transfer matrix from s_0 to s is represented by

$$M(s|s_0) = \begin{pmatrix} \cosh\Big(\sqrt{|K|}l\Big) & \frac{1}{\sqrt{|K|}}\sinh\Big(\sqrt{|K|}l\Big) \\ \sqrt{|K|}\sinh\Big(\sqrt{|K|}l\Big) & \cosh\Big(\sqrt{|K|}l\Big) \end{pmatrix}. \tag{9}$$

The last case is with $K = 0$ for a field free region, i.e. a drift space. Then the transfer matrix for a drift of length l takes the form

$$M(s|s_0) = \begin{pmatrix} 1 & l \\ 0 & 1 \end{pmatrix}. \tag{10}$$

If a particle traverses a series of n beam line elements with transfer matrices $M(s_1|s_0), \ldots, M(s_n|s_{n-1})$ starting from $s_0, s_1, \ldots s_{n-1}, s_n$, then the total one turn transfer map can be deduced by matrix multiplication of each transfer matrices for each of the elements in the following way

$$M(s_n|s_0) = M(s_n|s_{n-1}) \ldots M(s_2|s_1)M(s_1|s_0). \tag{11}$$

Thus the transfer matrix for any interval made up of sub-intervals is just the product of the transfer matrices of those sub-intervals, and this procedure allows one to track the particle motion through each accelerator element. In the thin-lens approximation with $l \to 0$, the transfer matrices defined by Eq. (7) and Eq. (9) for focusing and defocusing quadrupoles reduce to

$$M_{\text{focusing}} = \begin{pmatrix} 1 & 0 \\ -1/f & 1 \end{pmatrix}, M_{\text{defocusing}} = \begin{pmatrix} 1 & 0 \\ 1/f & 1 \end{pmatrix}, \tag{12}$$

where f is the focal length defined by $f \equiv \lim_{l\to 0} \to 1/|K|l$.

2.3 STABILITY CRITERIA

In a beam transport system going from a location s_1 to another location s_2, the matrix can be parameterized as

$$\begin{bmatrix} x_2 \\ x_2' \end{bmatrix}_{s_2} = \mathbf{M}(s_2|s_1) \begin{bmatrix} x_1 \\ x_1' \end{bmatrix}_{s_1}, \tag{13}$$

where the 2×2 transfer matrix $\mathbf{M}(s_2|s_1)$ is given by [6]

$$\mathbf{M}(s_2|s_1) = \begin{pmatrix} \sqrt{\frac{\beta_2}{\beta_1}}(\cos\Delta\psi + \alpha_1 \sin\Delta\psi) & \sqrt{\beta_1\beta_2}\sin\Delta\psi \\ -\frac{1+\alpha_1\alpha_2}{\sqrt{\beta_1\beta_2}}\sin\Delta\psi + \frac{\alpha_1-\alpha_2}{\sqrt{\beta_1\beta_2}}\cos\Delta\psi & \sqrt{\frac{\beta_1}{\beta_2}}(\cos\Delta\psi - \alpha_2\sin\Delta\psi) \end{pmatrix}. \tag{14}$$

We generally construct an accelerator with a repetitive period comprising n elements. Thus after one complete period we come to the starting point, i.e., $s_2 = s_1$. Under this periodic boundary condition, let us assume $\beta_2 = \beta_1 = \beta_0$, $\alpha_2 = \alpha_1 = \alpha_0$ and $\beta_0\gamma_0 - \alpha_0^2 = 1$. Hence Eq. (14) reduces to the form

$$\mathbf{M} = \begin{pmatrix} \cos\Delta\psi + \alpha_0\sin\Delta\psi & \beta_0\sin\Delta\psi \\ -\gamma_0\sin\Delta\psi & \cos\Delta\psi - \alpha_0\sin\Delta\psi \end{pmatrix}. \tag{15}$$

Let λ_1 and λ_2 be the eigenvalues and X_1, X_2 be the corresponding eigenvectors of the matrix $\mathbf{M}$. In such repetitive structures or modular machines, $\mathbf{M}$ has a unit determinant, and so the eigenvalues are the reciprocals of each other, i.e. $\lambda_1 = 1/\lambda_2$, and $\lambda_1 + \lambda_2 = \text{Trace } (\mathbf{M})$. To calculate the eigenvalues, we use the following eigenvalue equation

$$|\mathbf{M} - \lambda \mathbf{I}| = \lambda^2 - \text{Trace } (\mathbf{M})\lambda + 1 = 0. \tag{16}$$

With Trace $(\mathbf{M}) = 2\cos\Delta\psi$, we obtain the corresponding eigenvalues

$$\lambda_{1,2} = \cos\Delta\psi \pm i\sin\Delta\psi = e^{\pm i\Delta\psi}. \tag{17}$$

In order to have finite eigenvalues, the betatron phase advance $\Delta\psi$ must be real, guaranteed when $|\cos\Delta\psi| < 1$. We then obtain the general stability condition

$$\text{Trace } (\mathbf{M}) < 2. \tag{18}$$

In a circular machine, the above one turn transfer matrix $\mathbf{M}$ can be expressed in the following form

$$\mathbf{M} = \mathbf{I}\cos\Delta\psi + \mathbf{J}\sin\Delta\psi, \tag{19}$$

where $\mathbf{I}$ is the unit matrix, and $\mathbf{J}$ is defined by

$$\mathbf{J} = \begin{pmatrix} \alpha & \beta \\ -\gamma & -\alpha \end{pmatrix}, \mathbf{J}^2 = \begin{pmatrix} -1 & 0 \\ 0 & -1 \end{pmatrix}. \tag{20}$$

For N transits of the accelerator[1], the transfer matrix $\mathbf{M}$ can be expressed as

$$\mathbf{M}^N = (\mathbf{I}\cos\Delta\psi + \mathbf{J}\sin\Delta\psi)^N = \mathbf{I}\cos(N\Delta\psi) + \mathbf{J}\sin(N\Delta\psi). \tag{21}$$

Note that all matrix elements of the matrix $\mathbf{M}$ remain bounded as N increases. Furthermore, for a real betatron phase advance $\Delta\psi$, it is required that Eq. (18) holds. Thus Eq. (18) is a sufficient condition for stable transverse motion in an accelerator.

Now, we define the betatron tunes $Q_{x,y}$, some of the most important parameters in circular accelerators. The betatron tunes are defined as the number of transverse oscillations per revolution. Mathematically,

$$Q_{x,y} = \frac{\Delta\psi}{2\pi} = \frac{1}{2\pi}\oint \frac{ds}{\beta_{x,y}}. \tag{22}$$

During the design of the beam transport system, we have to be careful in choosing betatron tune values (especially the fractional values) to avoid transverse resonances which may cause particles loss.

[1]similar to De Moivre's formula, $(\cos x + i\sin x)^n = \cos nx + i\sin nx$.

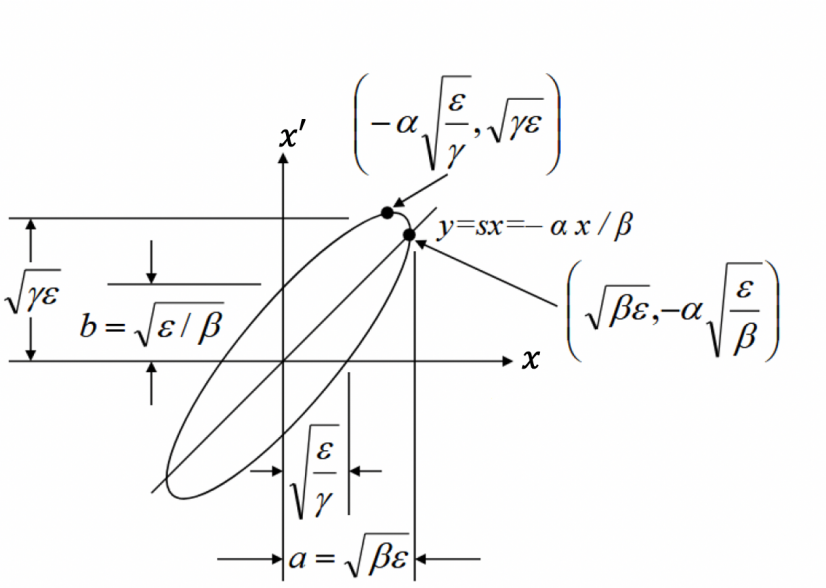

FIG. 2: Beam Phase Space Ellipse Characterized by the Twiss Parameters.

2.4 TRANSFORMATIONS IN PHASE SPACE

Particles in a beam can be represented by a statistical set of points in phase space. Phase space is a 6-dimensional space where each particle in the beam is represented by a point with coordinates (x, y, z, p_x, p_y, p_z) where (x, y, z) are the position coordinates and (p_x, p_y, p_z) are the momentum coordinates. Liouville's theorem allows one to characterize a beam of N particles by measuring the phase space volume it occupies. In conservative Hamiltonian systems, this volume is invariant. A good approximation for the beam shape in phase space is an ellipse. Any ellipse can be defined by specifying its shape, size, and orientation. Hence the particles of a beam in phase space can be represented by an ellipse called the phase space ellipse (Fig. 2) and described in [7] by

$$\gamma x^2 + 2\alpha x x' + \beta x'^2 = \epsilon, \tag{23}$$

where α, β, and γ are Twiss parameters or Courant-Snyder parameters. α is related to beam tilt, β is related to beam shape and size and γ is dependent on both α and β by the relation $\gamma = (1 + \alpha^2)/\beta$. ϵ is related to the beam size and is called the beam emittance. There are

horizontal, vertical, and longitudinal beam emittances. Referring to Fig. 2, the phase space area enclosed by the ellipse is

$$\int_{ellipse} dxdx' = \pi\epsilon. \tag{24}$$

Now it is time to apply the area theorem for linear optics. Since all particles enclosed by a phase ellipse stay within that ellipse, all that is needed is knowledge of initial ellipse parameters to describe the whole particle beam distribution along the transport line. Let the initial ellipse distribution at location $s = 0$ be defined by

$$\gamma_0 x_0^2 + 2\alpha_0 x_0 x_0' + \beta_0 x_0'^2 = \epsilon. \tag{25}$$

After traversing a certain distance along the beamline, the phase space ellipse at location $s \neq 0$ can be expressed in the form of Eq. (23). Now solving for x_0 and x_0' and inserting these values in Eq. (25), we get

$$\epsilon = (C'^2\beta_0 - 2S'C'\alpha_0 + S'^2\gamma_0)x^2 + 2(-CC'\beta_0 + S'C\alpha_0 + SC'\alpha_0 - SS'\gamma_0)xx' + (C^2\beta_0 - 2SC\alpha_0 + S^2\gamma_0)x'^2, \tag{26}$$

where C and S are cosine and sine "like" solutions of the equation of motion starting at $s = 0$, and C' and S' are their derivatives with respect to s. The above Eq. (26) is obtained by the method of matrix transformation described in the previous section 2.2. Under a general linear transformation, an ellipse at location $s = 0$ is transformed into another ellipse at $s \neq 0$. If the total transfer matrix has determinant 1, the area of the ellipse at location $s \neq 0$ after the transformation is the same as before the transformation at $s = 0$. In this case, emittance remains the same, and comparing Eq. (23) and Eq. (26), we get

$$\begin{aligned} \gamma &= C'^2\beta_0 - 2S'C'\alpha_0 + S'^2\gamma_0, \\ \alpha &= -CC'\beta_0 + S'C\alpha_0 + SC'\alpha_0 - SS'\gamma_0, \\ \beta &= C^2\beta_0 - 2SC\alpha_0 + S^2\gamma_0. \end{aligned} \tag{27}$$

The resulting new phase space ellipse at location $s \neq 0$ has the same area $\pi\epsilon$. However, the values of ellipse parameters change as defined by Eq. (27). It results in the new phase space ellipse with a different shape and orientation. Hence during the beam propagation along the beamline, the phase space continuously changes its shape and orientation, but the area remains constant. The transformation of ellipse or Twiss parameters (both are the same for the matched condition) in the matrix form can be represented as

$$\begin{pmatrix} \beta(s) \\ \gamma(s) \\ \alpha(s) \end{pmatrix} = \begin{pmatrix} C^2 & -2CS & S^2 \\ -CC' & CS' + C'S & -SS' \\ C'^2 & -2C'S' & S'^2 \end{pmatrix} \begin{pmatrix} \beta_0 \\ \gamma_0 \\ \alpha_0 \end{pmatrix}. \tag{28}$$

With the knowledge of initial values of parameters α_0, β_0, and γ_0, beam parameters anywhere along the beamline can be extrapolated using the above Eq. (28).

2.4.1 BEAM EMITTANCE

We have already defined one notion of the beam emittance in section 2.4 using Eq. (23). Since emittance is defined as the area occupied by the beam of particles, it gives the average spread of the particles in a beam phase space. Hence in uncoupled 6-dimensional beam phase space, we define three independent two-dimensional beam emittances. Another notion of the beam emittance, on the other hand, is as a measure of the transverse or longitudinal temperature of the beam and depends on the characteristics of a beam [7]. When the particle distribution is not uniform in phase space, the definition of emittance as the phase space area may not be very appropriate. The area occupied by the fraction of the total particles may not be perfectly equivalent to the beam emittance. In this case, we apply the statistical point of view to define the beam emittance. For electron beams, we can generally define the root-mean-square (RMS) emittance, $\epsilon_{rms,x}$, as

$$\epsilon_{rms,x} \equiv \sqrt{\langle x^2 \rangle \langle x'^2 \rangle - \langle x x' \rangle^2}. \tag{29}$$

For a given normalized distribution function $\rho(x, x')$ with $\int \rho(x, x') dx dx' = 1$, the moments of the beam distribution in Eq. (29) are

$$\begin{aligned} \langle x^2 \rangle &= \int \int x^2 \rho(x, x') dx dx' \\ \langle x'^2 \rangle &= \int \int x'^2 \rho(x, x') dx dx' \\ \langle x x' \rangle &= \int \int x x' \rho(x, x') dx dx'. \end{aligned} \tag{30}$$

The RMS emittance defined above based on statistical definition can be expressed in terms of beam width in the following way [8]

$$\epsilon_{rms,x} = \sqrt{\sigma_x^2 \sigma_{x'}^2 - \sigma_{xx'}^2} = \sigma_x \sigma'_x \sqrt{1 - r^2}, \tag{31}$$

where σ_x and $\sigma_{x'}$ are the rms beam size and beam divergence, $\sigma_{xx'}$ is the correlation, and r

is the correlation coefficient. These parameters are defined by the following relations

$$\begin{aligned}
\langle x\rangle &= \int x\rho(x,x')dxdx' \\
\langle x'\rangle &= \int x'\rho(x,x')dxdx' \\
\sigma_x^2 &= \int (x-\langle x\rangle)^2\rho(x,x')dxdx' \\
\sigma_{x'}^2 &= \int (x'-\langle x'\rangle)^2\rho(x,x')dxdx' \\
\sigma_{xx'} &= \int (x-\langle x\rangle)(x'-\langle x'\rangle)\rho(x,x')dxdx' = r\sigma_x\sigma_{x'}.
\end{aligned} \tag{32}$$

Beam emittance is usually expressed in the unit of [μm] or [nm] in an electron storage ring. The equilibrium beam emittance is determined by the combined effects of synchrotron radiation damping and quantum excitation. The details on how the synchrotron radiation damping and quantum excitation lead to the equilibrium emittances in an electron storage ring will be discussed later.

As the momentum of a particle increases, the value of $\beta\gamma$ also increases and the acceleration decreases the (unnormalized) emittance ϵ. Since the transverse relativistic momentum is conserved during a longitudinal acceleration, we also define the normalized beam emittance:

$$\epsilon_n \equiv \beta\gamma\epsilon, \tag{33}$$

where β and γ are Lorentz relativistic factors defined by $\beta \equiv v/c$ and $\gamma \equiv 1/\sqrt{(1-\beta^2)}$ respectively. The normalized emittance is invariant during acceleration.

2.5 DISPERSION AND CHROMATICITY

There is a finite spread of momentum of particles in a beam about the reference momentum p_0. This spread of momenta gives rise to a dispersion in the system. For the relative momentum deviation $\delta = \Delta p/p_0$, the inhomogeneous Hill's equations take the forms

$$\begin{aligned}
x''(s) + \left(\frac{1}{\rho(s)^2} - k(s)\right)x(s) &= \frac{1}{\rho(s)}\frac{\Delta p}{p_0} \\
y''(s) + k(s)y(s) &= 0,
\end{aligned} \tag{34}$$

where we assume that the dynamics of off-momentum particles is only affected in the horizontal plane, and there is no vertical dispersion. Since $\delta \neq 0$ is a particular case and the particular solution is given by $x_p = x_{\rm inh} = \rho(s)\delta$.

Next we solve Eq. (34) for the specific case of a uniform magnetic dipole without any focusing incorporated ($k(s) = 0$). In this case the solution of Eq. (34) can be written as

$$x(s) = x_h(s) + x_{inh} = A\cos\left(\frac{s}{\rho}\right) + B\sin\left(\frac{s}{\rho}\right) + \rho(s)\delta, \tag{35}$$

where $x_h(s)$ is a solution of homogeneous equation discussed in the previous section. The integration constants A and B are determined by applying the initial conditions at $s = 0$ which gives

$$\begin{aligned} x(s=0) &= A + \rho\delta = x_0, \\ x'(s=0) &= \frac{B}{\rho} = x_0'. \end{aligned} \tag{36}$$

Let us define the dipole bending angle $\theta = s/\rho$, then the solution in Eq. (35) can be expressed as

$$\begin{aligned} x(s=L) &= x_0\cos\theta + \rho x_0'\sin\theta + \rho\delta(1-\cos\theta) \\ x'(s=L) &= -\frac{x_0}{\rho}\sin\theta + x_0'\cos\theta + \delta\sin\theta. \end{aligned} \tag{37}$$

The above solution can be represented by the sum of two parts as follows

$$x(s) = x_\beta(s) + x_\delta(s), \tag{38}$$

where $x_\beta(s) = x_0\cos\theta + \rho x_0'\sin\theta$, and $x_\delta(s) = \rho\delta(1-\cos\theta)$ respectively. Thus the particle motion is the sum of betatron motion $x_\beta(s)$ plus a displacement due to the energy error $x_\delta(s)$. The solution given by Eq. (37) can be represented by 3×3 matrix as

$$\begin{bmatrix} x(s) \\ x'(s) \\ \delta \end{bmatrix} = \begin{bmatrix} \cos\theta & \rho\sin\theta & \rho(1-\cos\theta) \\ -\frac{1}{\rho}\sin\theta & \cos\theta & \sin\theta \\ 0 & 0 & 1 \end{bmatrix} \begin{bmatrix} x(s_0) \\ x'(s_0) \\ \delta \end{bmatrix}. \tag{39}$$

Since $x(s) = D(s)\delta$, where $D(s)$ is the dispersion function. Dividing by δ on both sides of Eq. (39), we get

$$\begin{bmatrix} D(s) \\ D'(s) \\ 1 \end{bmatrix} = \begin{bmatrix} C(s) & S(s) & D(s) \\ C'(s) & S'(s) & D'(s) \\ 0 & 0 & 1 \end{bmatrix} \begin{bmatrix} D(s_0) \\ D'(s_0) \\ 1 \end{bmatrix}, \tag{40}$$

where $C(s) = \cos\theta, \theta = s/\rho, S(s) = \rho\sin\theta, C'(s) = -\sin\theta/\rho, S'(s) = \cos\theta, D(s) = \rho(1-\cos\theta)$, and $D'(s) = \sin\theta$ respectively. If we know the 3×3 transport matrix and the value of the dispersion function and its derivative at the starting point s_0, we can calculate the

dispersion $D(s)$ at any downstream location s along the beamline. This simplified dipole calculation is presented for illustrative purposes only. When edge focusing in the dipole is included, a slightly different 3×3 transport matrix is obtained [7].

The RMS beam size at a given location is then defined by considering two terms, one from the betatron motion of the particles, and the other term from the finite momentum spread in the beam. The horizontal beam size is defined by

$$\sigma_x(s) = \sqrt{\epsilon_x \beta_x + D_x^2(s)\sigma_\delta^2}, \tag{41}$$

where ϵ_x is the horizontal beam emittance and σ_δ is the RMS relative momentum spread. Similarly, the angular beam divergence $\sigma_{x'}(s)$ is defined by

$$\sigma_{x'}(s) = \sqrt{\epsilon_x \gamma_x(s) + D_x'^2(s)\sigma_\delta^2}, \tag{42}$$

where $D_x'(s)$ is the dispersion derivative along the beamline. In a collider design, dispersion $D(s) = 0$ at the interaction point to maximize luminosity. Also, we construct dispersion-free straight sections along the beamline for RF cavities and other machine elements.

In addition to dispersion, a particle in a beam with finite momentum error δ sees a focusing strength for the quadrupoles slightly different from that of a particle at the design momentum. Hence off-momentum particles oscillate around the design orbit at frequencies different than a particle with the design momentum. The dependence of betatron tunes on fractional momentum deviation is called chromaticity. The horizontal and vertical chromaticities $\xi_{x,y}$ are defined by

$$\xi_{x,y} \equiv \frac{\Delta Q_{x,y}}{\Delta p/p}, \tag{43}$$

where $\Delta Q_{x,y}$ are the betatron tune shifts. The tune shifts $\Delta Q_{x,y}$ are defined by the following relation

$$\Delta Q_{x,y} = -\frac{1}{4\pi} \oint \beta_{x,y}(s) K_{x,y}(s)\, ds\, \frac{\Delta p}{p}, \tag{44}$$

where $K_{x,y}$ are quadrupole focusing strengths. Comparing Eq. (43) and Eq. (44), the horizontal and vertical chromaticities in terms of beta functions and quadrupole focusing strengths can be expressed as

$$\xi_{x,y} = -\frac{1}{4\pi} \oint \beta_{x,y}(s) K_{x,y}(s)\, ds. \tag{45}$$

The natural chromaticity in a storage ring depends on the lattice design and it arises solely from lattice quadrupoles. For higher energy particles, the focusing strength becomes weaker. In this case, betatron tune decreases, and the natural chromaticity becomes negative. For

large values of chromaticity and momentum spread, the betatron tunes may overlap low-order non-linear resonances, and eventually particle loss may occur [8].

We need to compensate for this chromatic aberration in a storage ring. This can be done by using sextupole magnets, whose focusing varies linearly with momentum. Special arrangement of sextupole families will be used to compensate the natural chromaticity.

2.6 LONGITUDINAL PARTICLE MOTION IN A STORAGE RING

Charged particle acceleration requires a nonvanishing force component in the direction of motion. Such fields are called longitudinal accelerating fields, which impart energy to the charged particles. The use of electrostatic high voltages to accelerate charged particles is limited due to electric breakdown above approximately 10 million volts. In a modern high-energy particle accelerators, radio frequency (RF) cavities resonating at microwave frequencies are widely used to accelerate the charged particles to higher energy. In this section, we will discuss the interaction of the longitudinal electric field with charged particles to explain the process of particle acceleration.

2.6.1 LONGITUDINAL EQUATION OF MOTION

The concept of generating the accelerating fields in resonating RF cavities was introduced by R. Wideroe [9]. Traveling electromagnetic waves are to fed into RF cavities, creating a longitudinal electric field that accelerates charged particles. The rate of change of energy for the given particle per passage through SRF cavity is

$$\frac{d}{dt}(\gamma mc^2) = -e\vec{E}(\vec{x}(t), t) \cdot \vec{v}, \tag{46}$$

where $\vec{E}(x,t)$ is the electric field, and $\vec{v}$ is the velocity of the particle. For velocity of light particles moving the the z direction, the total energy gain per passage is given by

$$\begin{aligned} \Delta(\gamma mc^2) &= -e\int_{-\infty}^{\infty} E_z(0,0,z)\sin\left(2\pi z/\lambda_{RF} + \psi\right) dz \\ &= \frac{e\tilde{E}_z\left(2\pi/\lambda_{RF}\right)e^{-i\psi} + \text{complexconjugate}}{2}, \end{aligned} \tag{47}$$

where $\tilde{E}_z$ is the Fourier transformation of electric field $E(x,t)$, λ_{RF} is the RF wavelength, and ψ is the phase of the particle passing through the cavity with respect to the crest[2]

[2]For sin function, the crest phase is 90^0 and for cos function, crest phase is 0^0. Harmonic cavity section uses cos function to denote the crest phase.

(maximum) phase when the field pattern is placed with even symmetry on the z axis. Let us consider a SRF cavity of length L. The RF voltage is defined by

$$V_C = |e\tilde{E}_z(2\pi/\lambda_{RF})|. \tag{48}$$

The accelerating field E_{acc} is defined by

$$E_{acc} = \frac{V_C}{L}, \tag{49}$$

and the energy gain of a particle at phase ψ is

$$V_C \sin\psi. \tag{50}$$

The accelerating gradient E_{acc} is normalized by the cavity length L and is expressed in the unit of [MV/m].

A particle synchronized with rf phase $\psi = \psi_s$ at revolution period T_0 and momentum p_0 is called a synchronous particle. Let the longitudinal electric field be defined by

$$E = E_0 \sin(\psi_{\rm rf}(t) + \psi_s). \tag{51}$$

where $\psi_{\rm rf} = h\omega_0 t$ is the rf phase, $\omega_0 = \beta_0 c/R_0$ is the angular revolution frequency of a reference particle, E_0 is the amplitude of the electric field, $\beta_0 c$ and R_0 are respectively the speed and the average radius of the circular orbit, h is an integer called the harmonic number, and ψ_s is the phase angle for a synchronous particle with respect to the rf wave.

A synchronous particle synchronizes with the rf wave with rf frequency $\omega_{\rm rf} = h\omega_0$. Hence synchronous particle experiences an rf voltage given by $V\sin\psi_s$. Then the acceleration rate is defined by

$$\frac{dE}{dt} = \frac{\omega_0}{2\pi}\ eV\sin\psi_s, \tag{52}$$

where $eV\sin\psi_s$ is the energy gain per revolution for this synchronous particle. If we consider a non-synchronous particle then it will have rf parameters with small deviations from the synchronous particle,

$$\omega = \omega_0 + \Delta\omega, \psi = \psi_0 + \Delta\psi, \theta = \theta_s + \Delta\theta,$$
$$p = p_0 + \Delta p, E = E_0 + \Delta E.$$

The parameters $\psi_s, \theta_s, \omega_0, p_0, E_0$ are respectively the rf phase angle, azimuthal orbital angle, angular revolution frequency, momentum, and energy of a synchronous particle, and $\psi, \theta, \omega, p, E$ are the corresponding parameters for an off-momentum particle. Now the rf

phase coordinate and azimuthal orbital angle are related by $\Delta\psi = \psi - \psi_s = -h\Delta\theta$ and the change in angular revolution frequency is defined by

$$\Delta\omega = \frac{d}{dt}\Delta\theta = -\frac{1}{h}\frac{d}{dt}\Delta\psi = -\frac{1}{h}\frac{d\psi}{dt}. \tag{53}$$

In the linear approximation, the change in angular revolution frequency is given by

$$\Delta\omega = -\eta\omega_0\delta, \tag{54}$$

where δ is the fractional off-momentum variable defined by

$$\delta = \frac{\Delta p}{p_0} = \frac{\omega_0}{\beta^2 E}\frac{\Delta E}{\omega_0}. \tag{55}$$

The time variation of δ is given by

$$\dot{\delta} = \frac{\omega_0}{2\pi\beta^2 E}eV(\sin\psi - \sin\psi_s), \tag{56}$$

where $\Delta E = eV(\sin\psi - \sin\psi_s)$. Now using Eq. (53), Eq. (54) and Eq. (55), the phase equation can be written as

$$\dot{\psi} = h\omega_0\eta\delta = \frac{h\omega_0^2\eta}{\beta^2 E}\left(\frac{\Delta E}{\omega_0}\right). \tag{57}$$

Similarly, using Eq. (55) and Eq. (56), we get another equation of motion for the energy difference between synchronous and non-synchronous particles as

$$\frac{d}{dt}\left(\frac{\Delta E}{\omega_0}\right) = \frac{1}{2\pi}eV(\sin\psi - \sin\psi_s). \tag{58}$$

The pair $(\psi, \Delta E/\omega_0)$ are pair of conjugate phase space coordinates and hence Eq. (57) and Eq. (58) form the "synchrotron equation of motion".

2.6.2 EVOLUTION OF SYNCHROTRON PHASE SPACE ELLIPSE

To get the beam phase space area during the particle tracking simulation, the following phase space mapping equations are used with phase space coordinates $(\psi, \Delta E)$

$$\begin{aligned} \Delta E_{\mathrm{n+1}} &= \Delta E_n + eV(\sin\psi_n - \sin\psi_s) \\ \psi_{\mathrm{n+1}} &= \psi_n + \frac{2\pi h\eta}{\beta^2 E}\Delta E_{\mathrm{n+1}}. \end{aligned} \tag{59}$$

The quantity $\eta/\beta^2 E$ depends on the acceleration rate of beam energy according to $E = E_{0,\mathrm{n+1}} + eV\sin\psi_s$. The factor $h\eta/\beta^2 E$ is nearly constant for the low acceleration rate, and

a closed curve can represent the beam phase space (separatrix). When the acceleration rate is high, separatrix is not a closed curve anymore.

2.6.3 PATH LENGTH AND MOMENTUM COMPACTION

The path length of a particle in a circular machine is affected by the curved sections of the beam transport line. The total path length is given by

$$L = \int (1 + \kappa(s) x_D(s)) ds, \tag{60}$$

where $x_D(s)$ is the horizontal orbit displacement and $\kappa(s) = 1/\rho(s)$ in the dipole magnet while being zero elsewhere. With a relative momentum deviation $\delta = \Delta p/p$, and the horizontal dispersion function $D(s)$, we get $x_D(s) = D(s)\delta$. Now, Eq. (60) takes the form

$$L = L_0 + \delta \int_{s_0}^{s} \frac{D(s)}{\rho(s)} ds. \tag{61}$$

The path length $L_0 = \int dz$, for $\delta = 0$ is the ideal design length of the beamline. The deviation from the ideal path length is

$$\Delta L = L - L_0 = \int_{s_0}^{s} \frac{D(s)}{\rho(s)} ds. \tag{62}$$

The variation in path length is caused by different momenta of particles within a beam. Hence this variation of the path length with momentum is determined by the momentum compaction factor α_c, defined by

$$\alpha_c \equiv \frac{\Delta L/L_0}{\Delta p/p_0} = \frac{1}{L_0} \oint_{L_0} \frac{D(s)}{\rho(s)} ds. \tag{63}$$

For a given path length L, the travel time is given by

$$\tau = \frac{L}{\beta c}, \tag{64}$$

where $\beta = v/c$ is the velocity of the particle. Using the logarithmic differentiation on both sides of above Eq. (64), we get

$$\frac{\Delta \tau}{\tau} = \frac{\Delta L}{L} - \frac{\Delta \beta}{\beta}. \tag{65}$$

The first term $\Delta L/L$ is defined by the momentum compaction α_c, and $cp = \beta E$ which can be differentiated to get $dp/p = d\beta/\beta + dE/E$. And with $dE/E = \beta^2 dp/p$, we can solve for $d\beta/\beta$ and we get $d\beta/\beta = (1/\gamma^2) dp/p$. Now, Eq. (65) takes the form

$$\frac{\Delta \tau}{\tau} = -\left(\frac{1}{\gamma^2} - \alpha_c\right) \frac{dp}{p} = -\eta_c \frac{dp}{p}, \tag{66}$$

and the phase slip factor η_c is defined by

$$\eta_c \equiv -\left(\frac{1}{\gamma^2} - \alpha_c\right). \tag{67}$$

The momentum compaction factor characterizes a critical energy called transition energy defined by

$$\gamma_t \equiv \frac{1}{\sqrt{\alpha_c}}. \tag{68}$$

The transition energy plays a vital role in phase focusing in a storage ring. Above the transition energy, a particle with higher energy needs a longer time for one revolution than a particle with lower energy. There is also a particular case, when momentum compaction η_c vanishes for $\gamma = \gamma_{tr}$. In this case, the revolution period becomes independent of the particle momentum, and the storage ring would be isochronous.

2.6.4 PHASE STABILITY

In an electron storage ring, particles emit synchrotron radiation, and lose energy by a certain average amount in each revolution. RF cavities are used to compensate for this energy loss and to provide longitudinal focusing; particles execute longitudinal oscillations around the synchronous phase. A synchronous particle travels along the design orbit with reference momentum p_0 with revolution period T_0. A synchronous particle arrives at the rf cavity at a constant rf phase angle ψ_s. The energy gained by a synchronous particle through the rf cavity is $eV_0 \sin\psi_s$, where V_0 is the effective rf voltage. The acceleration rate is then defined by $\dot{E} = f_0 eV_0 \sin\psi_s$, where f_0 is the revolution frequency. An off-momentum particle might see a phase slightly shifted from ψ_s and thus gain a different amount of energy. Hence the arrival time and the energy gain for each particle will be different. The rate of change of energy deviation is given by

$$\frac{\mathrm{d}}{\mathrm{dt}}\left(\frac{\Delta E}{\omega_0}\right) = eV_0(\sin\psi - \sin\psi_s), \tag{69}$$

where $\Delta E = E - E_0$ is the energy difference between non-synchronous and synchronous particles and ψ is the rf phase for the non-synchronous particles. Similarly the equation of motion for rf phase angle ψ is given by

$$\frac{\mathrm{d}}{\mathrm{dt}}(\psi - \psi_s) = \frac{\eta h \omega_0^2}{\beta^2 E_0}\left(\frac{\Delta E}{\omega_0}\right), \tag{70}$$

where h is the harmonic number and η is the phase slip factor. Here, ψ and $\Delta E/\omega_0$ are conjugate phase space coordinates and Eq. (69) and Eq. (70) form the basic synchrotron

equation of motion. The differential equation of motion for the small amplitude phase oscillation is

$$\frac{\mathrm{d}^2}{\mathrm{dt}^2}(\psi - \psi_s) = \frac{heV_0\omega_0^2\eta\cos\psi_s}{2\pi\beta^2 E_0}(\psi - \psi_s) = \omega_\mathrm{s}^2(\psi - \psi_s), \tag{71}$$

where ω_s is the small-amplitude angular synchrotron frequency. The stable phase is chosen by considering the synchrotron oscillation frequency ω_s must be real and stable condition is given by

$$\eta\cos\psi_s < 0. \tag{72}$$

The angular synchrotron frequency is given by

$$\omega_\mathrm{s} = \omega_0\sqrt{\frac{heV_0|\eta\cos\psi_s|}{2\pi\beta^2 E_0}}. \tag{73}$$

The synchrotron tune Q_s is defined as the number of synchrotron oscillation per revolution:

$$Q_\mathrm{s} \equiv \frac{\omega_\mathrm{s}}{\omega_0}\sqrt{\frac{heV_0|\eta\cos\psi_s|}{2\pi\beta^2 E_0}}. \tag{74}$$

The rf phase should be chosen depending on the particle energy being either below or above the transition energy to satisfy the condition given by Eq. (72). For stable phase focusing, the rf-synchronous phase should be chosen as follows

$$\begin{aligned} 0 < \psi_s < \frac{\pi}{2}, \text{ for } \gamma < \gamma_{tr} \\ \frac{\pi}{2} < \psi_s < \pi, \text{ for } \gamma > \gamma_{tr}. \end{aligned} \tag{75}$$

In the electron storage ring, the particle energy is generally above the transition energy, and rf phase is chosen as $\pi/2 < \psi_\mathrm{s} < \pi$. Above transition energy ($\gamma > \gamma_\mathrm{tr}$), higher energy particles arrive at the rf later and receives more energy from the rf cavity. On the other hand, a low energy particle arrives sooner and gains less energy from rf cavity. This process gives rise to the phase stability of the synchrotron motion.

2.7 SYNCHROTRON RADIATION

2.7.1 RADIATION DAMPING AND QUANTUM EXCITATION

Particle dynamics is affected by the emission of synchrotron radiation in an electron storage ring. This emission of radiation is strongly dependent on the beam energy. The radiation is emitted in quanta of discrete energy. The photon emission time is short and

thus the synchrotron radiation process can be considered to be as instantaneous. Emission of photons into synchrotron radiation is a statistical process that leads towards the quantum fluctuation of electron beam parameters in a storage ring. Finally, the equilibrium beam parameters are achieved through the combined effect of radiation damping and quantum excitation.

Damping of the beam phase space occurs due to average energy loss into synchrotron radiation. Beam oscillation takes place both in transverse and longitudinal dimensions and the transverse oscillation damps from the loss of transverse momentum with the emission of photons. The loss in the longitudinal momentum is replenished by the rf system installed in the storage ring. The transverse betatron oscillations and the longitudinal synchrotron oscillation amplitudes are damped like

$$A_i = A_{i,0} e^{-\alpha_i t} \tag{76}$$

where $i = x, y, z$ denotes the horizontal, vertical and the longitudinal dimensions respectively. The damping decrements are defined by

$$\begin{aligned}
\alpha_x &= \frac{C_\alpha}{C} E^3 \big(1 - \frac{I_{4\mathrm{x}}}{I_2}\big) = \frac{C_\alpha}{C} E^3 J_x \\
\alpha_y &= \frac{C_\alpha}{C} E^3 \big(1 - \frac{I_{4\mathrm{y}}}{I_2}\big) = \frac{C_\alpha}{C} E^3 J_y \\
\alpha_z &= \frac{C_\alpha}{C} E^3 \big(2 + \frac{I_{4\mathrm{x}} + I_{4\mathrm{y}}}{I_2}\big) = \frac{C_\alpha}{C} E^3 J_z,
\end{aligned} \tag{77}$$

where $C_\alpha = cr_c/3(mc^2)^3 = 2113.1$ m^2/GeV^3/sec, E is the beam energy, J_x, J_y, and J_z are damping partition numbers along the horizontal, vertical, and longitudinal dimensions, and C is the ring circumference. The radiation integrals are defined by

$$\begin{aligned}
I_1[m] &= \oint (\kappa_x D_x + \kappa_y D_y) ds \\
I_2[m^{-1}] &= \oint \kappa^2 ds \\
I_3[m^{-2}] &= \oint |\kappa|^3 ds \\
I_{4\mathrm{x}}[m^{-1}] &= \oint [\kappa^2 \kappa_x D_x + 2\kappa_x (k D_x + k' D_y)] ds \\
I_{4\mathrm{y}}[m^{-1}] &= \oint [\kappa^2 \kappa_y D_y + 2\kappa_y (k' D_x - k D_y)] ds \\
I_{5\mathrm{u}}[m^{-1}] &= \oint |\kappa|^3 \mathcal{H}_u ds,
\end{aligned} \tag{78}$$

where k, k' are the strengths for normal and skew quadrupoles, respectively, $u = x$ or y, D_u are the dispersion functions, $I_{4\mathrm{u}}$ are for a sector magnet, $\mathcal{H}_u(s) = \beta_u D_u'^2 + 2\alpha_u D_u D_u' + \gamma_u D_u^2$

is the invariant emittance, $\kappa_u = 1/\rho_u$ denote the inverse local curvatures, and $\kappa^2 = \kappa_x^2 + \kappa_y^2$ for dipoles. The damping partition numbers J_x, J_y and J_z are defined by

$$\begin{aligned} J_x &= 1 - \frac{I_{4\mathrm{x}}}{I_2} \\ J_y &= 1 - \frac{I_{4\mathrm{y}}}{I_2} \\ J_z &= 2 + \frac{I_{4\mathrm{x}} + I_{4\mathrm{y}}}{I_2}. \end{aligned} \tag{79}$$

In general, there is no vertical dispersion included in optics design and hence $J_y = 1$. The sum of the damping partition numbers is an invariant quantity and

$$J_x + J_y + J_z = 4. \tag{80}$$

This relation is called the Robinson criteria [10]. The damping constants defined in Eq. (77) can be expressed in terms of energy loss per turn U_0, beam energy E, and revolution time T_0 as

$$\begin{aligned} \alpha_x &= \frac{U_0}{2ET_0}(1-\xi) = \frac{U_0}{2ET_0} J_x \text{ with} \quad J_x = 1 - \xi \\ \alpha_y &= \frac{U_0}{2ET_0} = \frac{U_0}{2ET_0} J_y \text{ with} \quad J_y = 1 \\ \alpha_z &= \frac{U_0}{2ET_0}(2+\xi) = \frac{U_0}{2ET_0} J_z \text{ with} \quad J_z = 2 + \xi. \end{aligned} \tag{81}$$

So the damping partition numbers J_x, J_y and J_z depend on the radiation integrals. The parameter ξ at a given beam energy is related to the dispersion function, which is entirely determined by the magnet lattice.

2.7.2 EQUILIBRIUM EMITTANCE AND ENERGY SPREAD

Following the usual textbook arguments, we derived the formula for the damped emittance and energy spread in a single energy storage ring. Later, we re-derived the formula in a dual energy storage ring case based on the single energy storage ring result. The average change in synchrotron oscillation amplitude A is given by [7]

$$\langle \Delta A^2 \rangle = \langle A'^2 - A^2 \rangle = \varepsilon^2, \tag{82}$$

where ε is the energy emitted by the photon and the averaging is over the synchrotron oscillation phase. If the emission rate for photons from a single electron is $\dot{N}_{\mathrm{ph}}$, then a statistical argument gives that the growth rate in amplitude is

$$\frac{d\langle \Delta A^2 \rangle}{dt} = \dot{N}_{ph} \langle \varepsilon^2 \rangle. \tag{83}$$

The average on the right-hand side of Eq. (83) is over the photon emission distribution, and $\dot{N}_{\rm ph}\langle\varepsilon^2\rangle$ is defined by

$$\dot{N}_{\rm ph}\langle\varepsilon^2\rangle = \frac{55}{24\sqrt{3}}P_\gamma\varepsilon_c. \tag{84}$$

The average power radiated during the radiation is

$$\langle P_\gamma\rangle = \frac{U_0}{T_0} = C_\gamma\frac{c}{2\pi}\frac{E^4}{\rho^2}, \tag{85}$$

In Eq. (85), U_0 is the total energy radiated in synchrotron radiation, T_0 is the total revolution time in a storage ring and $C_\gamma = 4\pi r_e/3(mc^2)^3 = 8.8463\times10^{-5}\mathrm{m}/GeV^3$. The synchrotron radiation power depends on the beam energy E and the bend radius ρ. The critical photon energy $\varepsilon_{\rm c}$ used in Eq. (84) can be defined as

$$\varepsilon_c = \hbar\omega_c = \frac{3\hbar c}{2(mc^2)^3}\frac{E^3}{\rho}. \tag{86}$$

In equilibrium, the oscillation damping balances this growth rate, and $\langle A^2\rangle = \tau_{\rm z}\dot{N}_{\rm ph}\langle\varepsilon^2\rangle/2$. Now the energy distribution caused by the statistical emission of photons assumes a Gaussian distribution with the standard root mean squared energy spread given by $\sigma_\varepsilon^2 = \langle A^2\rangle/2$, because the square of the rms energy displacement of a particle undergoing sinusoidal energy motion is one-half of the amplitude squared. The quantity $\tau_{\rm z}$ is the damping time in the longitudinal dimension.

In the case of a ring with bend radiation only, the damped energy spread is given by [11]

$$\frac{\sigma_E^2}{E^2} = C_{\rm q}\frac{\gamma^2}{(2+\xi)}\frac{\langle 1/\rho^3\rangle}{\langle 1/\rho^2\rangle} = \frac{\tau_z}{4E^2}\dot{N}_{\rm ph}\langle\varepsilon^2\rangle, \tag{87}$$

where $C_{\rm q} = 55\hbar c/33\sqrt{3}mc^2 = 3.84\times10^{-13}$ m for electrons, γ is the relativistic energy factor and $(2+\xi)$ is the damping partition in the longitudinal dimension. Finally, substituting the values of $\dot{N}_{\rm ph}\langle\varepsilon^2\rangle$ and $\tau_{\rm z}$ [12] in Eq. (87), the damped energy spread becomes

$$\frac{\sigma_E^2}{E^2} = \frac{\tau_z}{4E^2}\dot{N}_{ph}\langle\varepsilon^2\rangle = \frac{C_q}{\gamma^2}\frac{\gamma^7\langle 1/\rho^3\rangle}{[(2+\xi)\gamma^3\langle 1/\rho^2\rangle]}. \tag{88}$$

Similarly to the discussion leading to the equilibrium energy spread, we consider the perturbation to the transverse motion caused by photon emission. Since the photon emission will not change the particle position and direction [7], we can write

$$\delta x = 0 = \delta x_\beta + D\frac{\varepsilon}{E} \rightarrow \delta x_\beta = -D\frac{\varepsilon}{E}, \tag{89}$$

$$\delta x' = 0 = \delta x'_\beta + D'\frac{\varepsilon}{E} \rightarrow \delta x'_\beta = -D'\frac{\varepsilon}{E}, \tag{90}$$

where D and D' are dispersion and the derivative of dispersion respectively. This phenomenon of photon emission will modify the phase-space ellipse and the variation of Courant-Snyder invariant is given by

$$\delta a^2 = \frac{2}{\beta_x}[Dx_\beta + (\beta_x D' - \frac{\beta_x'}{2}D)(\beta_x x' - \frac{\beta_x'}{2})x]\frac{\varepsilon}{E} + \frac{1}{\beta_x}[D^2 + (\beta_x D' - \frac{\beta_x'}{2}D)^2](\frac{\varepsilon}{E})^2. \quad (91)$$

In Eq. (91), the first term inside the bracket will vanish due to betatron oscillation. The average variation of the oscillation amplitude a due to the emission of photon energy ε becomes

$$\delta\langle a^2\rangle = \mathcal{H}(z)(\frac{\varepsilon}{E})^2, \quad (92)$$

where $\mathcal{H}(z) = \beta D'^2 + 2\alpha DD' + \gamma D^2$ is the chromatic invariant of the ring [8]. To get the variation of the oscillation amplitude per turn, we average again over all photon energies, multiply by the total number of photons emitted per unit time, and the integration is carried out over the whole ring

$$\Delta\langle a^2\rangle = \frac{1}{cE_0^2}\oint \dot{N}_{\rm ph}\langle\varepsilon^2\rangle\mathcal{H}(z)dz. \quad (93)$$

The rate of change of this oscillation amplitude is given by

$$\frac{\mathrm{d}\langle\Delta a^2\rangle}{\mathrm{dt}} = \frac{1}{E_0^2}\langle\dot{N}_{\rm ph}\langle\varepsilon^2\rangle\mathcal{H}(z)\rangle_z, \quad (94)$$

where the index z indicates averaging along the ring. Since the equilibrium is reached when the average quantum excitation rate around the ring is equal to the damping rate. This leads to the following condition

$$\frac{\sigma_u^2}{\beta_u} = \frac{\tau_{\rm u}}{4E^2}\langle\dot{N}_{\rm ph}\langle\varepsilon^2\rangle\mathcal{H}(z)\rangle_z, \quad (95)$$

where $\sigma_u^2 = \langle u^2(z)\rangle = \langle a^2\beta_u/2\rangle$ is the standard width of a Gaussian particle distribution with betatron function β_u, where $u = x, y$ for both horizontal and vertical dimensions. Now, the equilibrium beam emittance of a relativistic electron in a storage ring is given by

$$\epsilon_u = \frac{\sigma_u^2}{\beta_u} = C_{\rm q}\frac{\gamma^2}{J_{\rm u}}\frac{\langle\mathcal{H}_u/\rho^3\rangle}{\langle 1/\rho^2\rangle} = \frac{\tau_u}{4E^2}\langle\dot{N}_{\rm ph}\langle\varepsilon^2\rangle\mathcal{H}(z)\rangle_z. \quad (96)$$

Substituting the values of $\tau_x, \dot{N}_{\rm ph}\langle\varepsilon^2\rangle$ and $\mathcal{H}_x(z)$ in Eq. (96), the damped equilibrium emittance in a single energy storage ring becomes

$$\epsilon_x = \frac{\tau_x}{4E^2}\langle\dot{N}_{\rm ph}\langle\varepsilon^2\rangle\mathcal{H}(z)\rangle_z = \frac{C_{\rm q}}{\hat{\gamma}^2}\frac{\gamma^7\langle\mathcal{H}_x/\rho^3\rangle}{[(1-\xi)\gamma^3\langle 1/\rho^2\rangle]}, \quad (97)$$

where $(1-\xi)$ is the horizontal damping partition number.

CHAPTER 3

STORAGE RING BASED ELECTRON COOLER DESIGN

In this chapter we will discuss beam cooling requirements in high energy physics research and briefly discuss different cooling methods used to cool charged particles. Then we will further discuss the principles of electron cooling and explain cooling based on a storage ring. We introduce a novel concept for a ring cooler: a dual energy storage ring cooler.

3.1 BEAM COOLING REQUIREMENT IN A COLLIDER

The main consideration underlying beam cooling is the "beam quality". Cooling methods enhance the beam quality by compensating for various phenomena related to beam size and loss of stored beam particles. Cooling provides the sharply collimated beams required for precise high energy physics experiments. Beam cooling aims at reducing the size and energy spread of a particle beam circulating in a storage ring, and leads to enhanced luminosity. The luminosity in a collider is defined by [13]

$$L = \frac{N_1 N_2 f_0}{4\pi\sigma_x^*\sigma_y^*} \approxeq \frac{N_1 N_2 f_0}{\epsilon\beta_y^*}, \tag{98}$$

where N_1 and N_2 are particle densities, f_0 is revolution frequency, ϵ is the RMS emittance of the beam, σ_x^*, σ_y^* are the horizontal and vertical beam sizes, and β_y^* is the Twiss beta value at the interaction point respectively. The luminosity L will be higher if $\epsilon\beta_y^*$ or the corresponding beam sizes are smaller and N_1, N_2 have larger values. Hence the goal is to '*compress*' the same number of particles into a beam of smaller size and energy spread, i. e., to increase the particle density. The phase space density is a general figure of merit of a particle beam. Cooling significantly improves this figure of merit.

3.1.1 COOLING METHODS

In the case of light charged particles, e.g. electrons or positrons, there is a natural synchrotron radiation effect. But the energy radiated decreases strongly with the rest mass of the particles. Hence for heavier particles, radiation damping is negligible even at high energies of the order of few hundred GeV. Artificial damping needs to be introduced to enhance the damping effect in heavier particles.

There are different beam cooling methods adopted to cool the heavy charged particle beams. The four main cooling methods are: stochastic cooling, electron cooling, laser cooling, and ionisation cooling. In this subsection, we will discuss these four different cooling methods briefly.

The method of stochastic cooling was invented by Simon van der Meer [14] at CERN at the beginning of the 1970s, for which he was awarded the Nobel prize in 1984. This method was used to collect and cool antiproton beams. Stochastic cooling uses a feedback system that operates on and reduces individual particle oscillation amplitudes, not the motion of the beam as a whole [15]. There are two steps repeated every turn in stochastic cooling: a pick-up measures individual particle oscillation deviations, and a kicker corrects the angular error of the oscillation downstream, reducing the oscillation amplitude. A comprehensive description of stochastic cooling has been given in the references [16–18].

Electron cooling has become a convenient tool to increase the phase space density of heavy charged particle (proton, ion, antiproton) beams in storage rings. The initial idea of electron cooling was introduced by G.I. Budker in 1966 [19]. It was first tested in 1974 with a 68 MeV proton beam at the NAP-M storage ring. In electron cooling, the circulating ion beam and an intense electron beam share the same orbit on a small fraction of a circular accelerator. In a straight cooler section, the interaction between electron beam and heavy particle beam introduces friction when the average velocities of the heavy particles and electrons coincide in magnitude and direction. During the interaction, the heavy particles are damped and the electrons are heated. This method is highly adapted to decrease the beam heating and increase the damping in a heavy particle storage ring.

Laser cooling, on the other hand, is a very powerful technique that takes place mainly in the longitudinal plane, and it works for particular ions that have a closed transition between a stable lower state and a short-lived higher state. In laser cooling [20], an ion is excited by a photon's absorption and returns to the ground state by the spontaneous emission of a photon. This technique has been successfully applied for trapping ions and cooling them to a temperature below 1 mK [21].

In ionization cooling, particles pass through a material medium and lose energy (momentum) through ionization interactions, followed by beam reacceleration in rf cavities [22]. The momentum losses occur in both longitudinal and transverse dimensions. Reacceleration using rf cavities restores only longitudinal momentum; there is no restoration of transverse momentum loss resulting in the transverse cooling of the particle beams. This cooling method is mainly used for particles like muons and is generally not applicable for cooling charged

particles like electrons and protons.

Next, we will briefly review the principles of electron cooling. Some concepts on storage ring based electron cooler design will be provided.

3.1.2 PRINCIPLE OF ELECTRON COOLING

It is challenging to reduce the charged particles beam phase space volume without losing particles. The main goal of an electron cooler is to increase the intensity of the heavy-charged particle beams [23]. Cooled heavy particle beams have smaller beam sizes and divergence, providing a means for focusing particle beams with a small energy spread. So, how can this electron cooling technique be applied to get the quality beam in a collider experiment?

Liouville's theorem states that the phase space volume occupied by the particles can not be reduced further by applying conservative forces. It means the phase space volume of beam particles can be treated like a balloon filled with air, and compressing the balloon in one region makes it expand elsewhere. The only way to reduce the volume of the balloon is by cooling the gas inside it [24]. We use an electron beam at a lower temperature to cool the heavy charged particles beam at higher temperatures. To accomplish this heat exchange, we mix the heavy charged particles beam at the higher temperature with a colder electron beam which cools it through direct interaction between electron beam and heavy charged particles beam via Coulomb scattering. In this phenomenon, the force involved is velocity-dependent, and it depends on the relative velocity of the electron beam and the charged particle beams that need to be cooled. Beam cooling techniques are non-Liouvillian processes.

Effective cooling requires the ion and electron beams' average longitudinal velocities to be equal, and the two beams to overlap transversely, thus creating electron-ion plasma. The ions, while traveling with electrons, undergo Coulomb scattering and, under certain conditions, transfer some of their thermal energy to the electrons. In equilibrium, the ion beam temperature in the beam frame of reference becomes equal to the effective electron temperature, i.e.,

$$T_p = T_e, m_e v_e^2 = m_p v_p^2, \tag{99}$$

where T_p and T_e are the transverse temperatures, m_p and m_e are the masses, and v_p and v_e are the transverse velocities for proton and electron beam respectively. Since the proton's mass is about 2000 times larger than the mass of an electron, the ratio of their transverse velocities becomes $v_{e\perp}/v_{p\perp} \approx 40$. Hence due to the cooling effect, the angular divergence $\theta_{p\perp} = v_{p\perp}/\beta c$ of the proton beam is reduced by the factor of 40 compared to the electron beam. This provides the smaller transverse beam size and beam divergence for the proton beam which

is required at the beam interaction point in the collider to enhance the luminosity.

3.2 ELECTRON STORAGE RING BASED COOLER

Electron cooling is an effectual technique to shrink the size and momentum spread of the stored ion beams for high-precision collider experiments. The technique of electron cooling has opened up new possibilities in high-energy collider experiments, especially in many newly constructed ion storage rings by providing cooled ion beams for collider experiments. This technique has been widely applied and developed in many heavy ion accelerators worldwide [23–25]. The main objective of the electron cooler is to increase of the intensity of heavy charged particles beam and finally increase the luminosity in a collider using the cooled heavy charged particles beam.

Electron storage rings have been considered as coolers since the late 1970s. However, none has been built as a cooler as of this writing. An electron storage ring has the great advantage that the electron beam cools by emitting synchrotron radiation in bending magnets in the arc sections of the storage ring. So the electron beam can be re-used as long as the beam lifetime is long enough [26]. At electron beam energy less than 50 MeV, the intrabeam-scattering (IBS) effect is dominant which may create a large equilibrium emittance. Further, the Touschek effect plays the dominant role, reducing the beam lifetime. It means the storage ring-based cooler concepts only apply to more than 50 MeV electron beam energies. At such an energy or higher, the energy loss due to synchrotron radiation is more significant, and radiation damping times are inversely proportional to the energy loss per turn. Hence the electron beam reaches equilibrium in a short time. During beam storage for long hours, the hadron beam emittance in a collider deteriorates for various reasons. The main reason for emittance growth during hadron beam storage is IBS. In order to improve the luminosity in a collider, we need to apply some cooling technique that either keeps constant or further lowers the hadron beam emittance.

3.3 MODEL FOR COOLING RATE

We consider the following highly simplified model to calculate the heat transfer rate between an electron beam and an ion beam. Based on the law of thermodynamics, one can define a total transverse internal energy of an electron beam as

$$U_e = N_e k T_e, \tag{100}$$

where N_e is the total number of electrons in a bunch, T_e is the transverse temperature of

the electron beam, and k is the Boltzmann constant. Similarly for an ion beam, the total transverse internal energy is given by

$$U_i = N_i k T_i. \tag{101}$$

An electron beam is brought into thermal contact with an ion beam and Coulomb interactions between the particles happen. When the ions are at higher temperature than the electrons, heat in the transverse degree of freedom is transferred from the ion beam to the electron beam leading to the ion beam cooling. We assume a phenomenological model for the cooling per pass, and for simplicity, we will assume that every ion bunch is cooled once per pass by an electron bunch with the bunches at the same frequency. Now the change in the transverse internal energy of the ion beam is given by

$$\Delta U = U_{i,k} - U_{i,k+1} = U_{e,k+1} - U_{e,k} = \eta(kT_{i,k} - kT_{e,k}), \tag{102}$$

where k and $k+1$ represent the consecutive beam passes respectively and η is a parameter that accounts for the cooling interaction. Equating the change of transverse internal energy for each case for an electron beam and an ion beam, we get the following equations

$$\begin{aligned} U_{e,k+1} - U_{e,k} &= \eta(kT_{i,k} - kT_{e,k}) \\ T_{e,k+1} &= (1 - \eta/N_e)T_{e,k} + (\eta/N_e)T_{i,k}. \end{aligned} \tag{103}$$

Similarly, the equation for the temperature of the ion beam becomes

$$\begin{aligned} U_{i,k} - U_{i,k+1} &= \eta(T_{i,k} - T_{\mathrm{e,k}}) \\ T_{i,k+1} &= (1 - \eta/N_i)T_{i,k} + (\eta/N_i)T_{e,k}. \end{aligned} \tag{104}$$

Because the electron beam undergoes synchrotron radiation damping, the electron beam temperature is lowered after each pass. Let R denote the effect of the synchrotron radiation in electron beam, then the above Eq. (103) and Eq. (104) can be combined and put into the following difference equation as

$$\begin{pmatrix} T_e \\ T_i \end{pmatrix}_{k+1} = \begin{pmatrix} 1 - \eta/N_e - R & \eta/N_e \\ \eta/N_i & 1 - \eta/N_i \end{pmatrix} \begin{pmatrix} T_e \\ T_i \end{pmatrix}_k + \begin{pmatrix} RT_{e,equ} \\ 0 \end{pmatrix}, \tag{105}$$

where $T_{e,equ}$ is the equilibrium temperature of the electron beam.

First, consider the case when there is no cooling interaction, i.e., $\eta = 0$. The solution to this first-order linear difference equation is

$$\begin{aligned} T_{e,l} &= (T_{e,0} - T_{e,equ})(1 - R)^l + T_{e,equ}, \\ T_{i,l} &= T_{i,0}, \end{aligned} \tag{106}$$

where the subscript 0 indicates the initial condition, and l indicated the state after pass l. In this uncoupled case the ion temperature does not change and the electron temperature approaches the equilibrium temperature of the electrons (determined by the ring radiation damping) with a damping decrement given by $1 - R$.

Now include the cooling interaction with $\eta \neq 0$, and consider the evolution equation with $R = 0$ [27]. To analytically derive a cooling time note

$$T_{i,k+1} - T_{e,k+1} - (T_{i,k} - T_{e,k}) = -\eta \frac{N_e + N_i}{N_e N_i}(T_{i,k} - T_{e,k}), \tag{107}$$

This difference equation is solved by

$$T_{i,l} - T_{e,l} = \left(1 - \eta \frac{N_e + N_i}{N_e N_i}\right)^l (T_{i,0} - T_{e,0}) \tag{108}$$

showing the temperature difference between the ions and electrons damps away by a factor $1 - \eta(N_e + N_i)/(N_e N_i)$ each revolution of the ring. In the usual case the cooling time is much greater than the revolution time. Then we can define a time to equilibrium of $t_{eq} = t_{rev} N_e N_i/(\eta(N_e + N_i))$.

When $\eta \neq 0$ and $R \neq 0$, there is a fixed point for the combined evolution equations given by

$$T_e = T_i = T_{e,equ}. \tag{109}$$

An equilibrium solution exists where both the electron and ion beam have the same temperature defined by $T_{e,equ}$. Note that this equilibrium temperature is independent of the strength of the cooling interaction. In practice within this model, the electron distribution evolves to the same temperature regardless of the presence of ion cooling or not. Furthermore, with the cooling on, the ions evolve to the same temperature as the electrons.

To get the cooling rate in the combined system, investigate the linear stability of the system including the cooling interaction. The interaction matrix defined in Eq. (105) is

$$\begin{pmatrix} 1 - \eta/N_e - R & \eta/N_e \\ \eta/N_i & 1 - \eta/N_i \end{pmatrix}. \tag{110}$$

For stability, this matrix should have both eigenvalues with absolute value less than 1, because then as in the solution in Equations (106) and (108), the higher powers of the matrix cause any initial temperature differences to eventually converge to zero. The damping fraction per revolution, as in the above solutions, will be λ where λ is a matrix eigenvalue, one for each mode. The eigenvalue equation takes the form,

$$(\lambda - 1)^2 + \left(\frac{\eta}{N_i} + \frac{\eta}{N_e} + R\right)(\lambda - 1) + \frac{\eta}{N_i} R = 0. \tag{111}$$

Solving the above equation, the corresponding eigenvalues are given by

$$\lambda_{\pm} = 1 - \left(\frac{\eta}{2N_i} + \frac{\eta}{2N_e} + \frac{R}{2}\right) \pm \sqrt{\left(\frac{\eta}{2N_i} + \frac{\eta}{2N_e} + \frac{R}{2}\right)^2 - \frac{\eta}{N_i}R}. \tag{112}$$

For the positive η and R values, both eigenvalues are clearly less than one.

The stability limit is achieved when $\lambda_{-} = -1$ or

$$2 = \left(\frac{\eta}{2N_i} + \frac{\eta}{2N_e} + \frac{R}{2}\right) + \sqrt{\left(\frac{\eta}{2N_i} + \frac{\eta}{2N_e} + \frac{R}{2}\right)^2 - \frac{\eta}{N_i}R}. \tag{113}$$

Getting this condition in practical reality requires high cooling efficiency with a cooling time comparable to the revolution time. So in all realistic conditions where the cooling time is much longer than the revolution time, the eigenvalue with the minus sign remains stable.

When the net cooling time, the time to equilibrium, and the radiation cooling time are much longer than the revolution time the net cooling time can be estimated from λ_{+} as $t_{rev}/(1-\lambda_{+})$, leading to

$$\begin{aligned} t_{\text{net,cooling}} &= \frac{t_{\text{rev}}}{\left[\left(\frac{\eta}{2N_i} + \frac{\eta}{2N_e} + \frac{R}{2}\right) - \sqrt{\left(\frac{\eta}{2N_i} + \frac{\eta}{2N_e} + \frac{R}{2}\right)^2 - \frac{\eta}{N_i}R}\right]} \\ &\approx \frac{t_{\text{rev}}}{(\eta/N_i)} = \frac{t_{eq}(N_e + N_i)}{N_e}, \quad \text{for } \eta/N << R, \end{aligned} \tag{114}$$

where it is assumed that there is one cooling region per ion revolution. We choose this sign in the solution to the quadratic equation because this eigenvalue is closest to one. This mode is damped away to zero slowest in applying repeated powers of the matrix. The approximate formula applies when the cooling process is limited by the time it takes to transfer transverse energy from ions to electrons through the cooling rate, i.e., the cooling time is much greater than the electron radiation damping time. The solution has the correct scaling. Better cooling efficiency leads to shorter cooling times and a more significant numbers of ions (possessing more significant heat) will cool more slowly for a constant electron radiation rate.

Now, going through the definitions and comparing to the standard definitions of the cooling time [28], the cooling time assuming an infinite electron reservoir is

$$t_{\text{cooling}} = \frac{3m_i/m_e}{8(2\pi)^{1/2} n_e r_e^2 c L Z^2} \left(\frac{kT_e}{mc^2} + \frac{kT_i}{mc^2}\right)^{3/2}. \tag{115}$$

One obtains

$$t_{\text{cooling}} = t_{\text{eq}} \frac{N_e + N_i}{N_e} \tag{116}$$

in the limit when the electron radiation damping time $t_{\rm rad} = t_{\rm rev}/R$ is much shorter than the ion cooling time. Note, $t_{eq} = t_{cooling}$ exactly when $N_i << N_e$.

In a dual energy storage ring-based loop accelerator being used in a cooling application, the cooling ring or cooling section needs to be at the same gamma as the ions to be cooled. In this case, synchrotron radiation damping is dominated by the high energy ring and the high energy ring energy, which will provide an overall cooling rate not too much different than in usual ERL cooling. Then the complete quadratic formula described above can be solved for the overall damping time as a function of $t_{\rm rad}/t_{\rm eq}$ for several values of the ratio of ion and electron densities N_i/N_e. The overall damping time is then defined by

$$t_{\pm} = \frac{t_{\rm rad}}{\left[\left(\frac{1+N_i/N_e}{2} + \frac{t_{\rm rad}}{2t_{\rm eq}}\right) \mp \sqrt{\left(\frac{1+N_i/N_e}{2} + \frac{t_{\rm rad}}{2t_{\rm eq}}\right)^2 - \frac{t_{\rm rad}}{t_{\rm eq}}}\right]}. \tag{117}$$

The more compelling case happens when the intensity of electron beam dominates the ion beam intensity, i.e., $N_e >> N_i$ and is exactly solvable. The damping times for two different modes are

$$t_{\pm} = t_{\rm rad}, t_{\rm eq}. \tag{118}$$

For the short damping time, i.e., $t_{\rm rad} < t_{\rm eq}$, the overall cooling rate is dominated by the heat transfer efficiency between the ion beam and electron beam and is independent of the radiation rate yielding $t_{\rm cooling} = t_{\rm eq}$. Once $t_{\rm rad} > t_{\rm eq}$, the overall cooling rate is dominated by the rate at which the heat may be dissipated by radiation, and $t_{\rm cooling} = t_{\rm rad}$. It means the radiation damping rate of the electron beam determines the heat dissipation no matter how great the heat transfer rate into the electron beams. The second case is $t_{\rm rad} < t_{\rm eq}$, when one should lower the energy of the high energy loop to that value where the damped radiation emittance is low enough. The quadratic Eq. (117) can be solved numerically by taking different ion and electron densities ratios. The curves shown in Fig. 3 are the cooling time for the slowest-cooling mode. The sign of the square root changes to positive beyond the value of $t_{\rm rad}/t_{\rm eq}$ which causes the discriminant to vanish. The graph in Fig. 3 explains the general procedure for the loop accelerator design from both qualitative and quantitative perspectives. The best cooling rate possible is under the assumption that the high energy loop is at energy such that $t_{\rm rad} << t_{\rm eq}$ is given by the condition $t_{\rm cooling} = (1+N_i/N_e)t_{\rm eq}$. The second thing is to choose a cooling rate somewhat beyond this limit, say 50% or higher, and increase the radiation damping time by lowering the high energy loop energy to the value indicated by the graph.

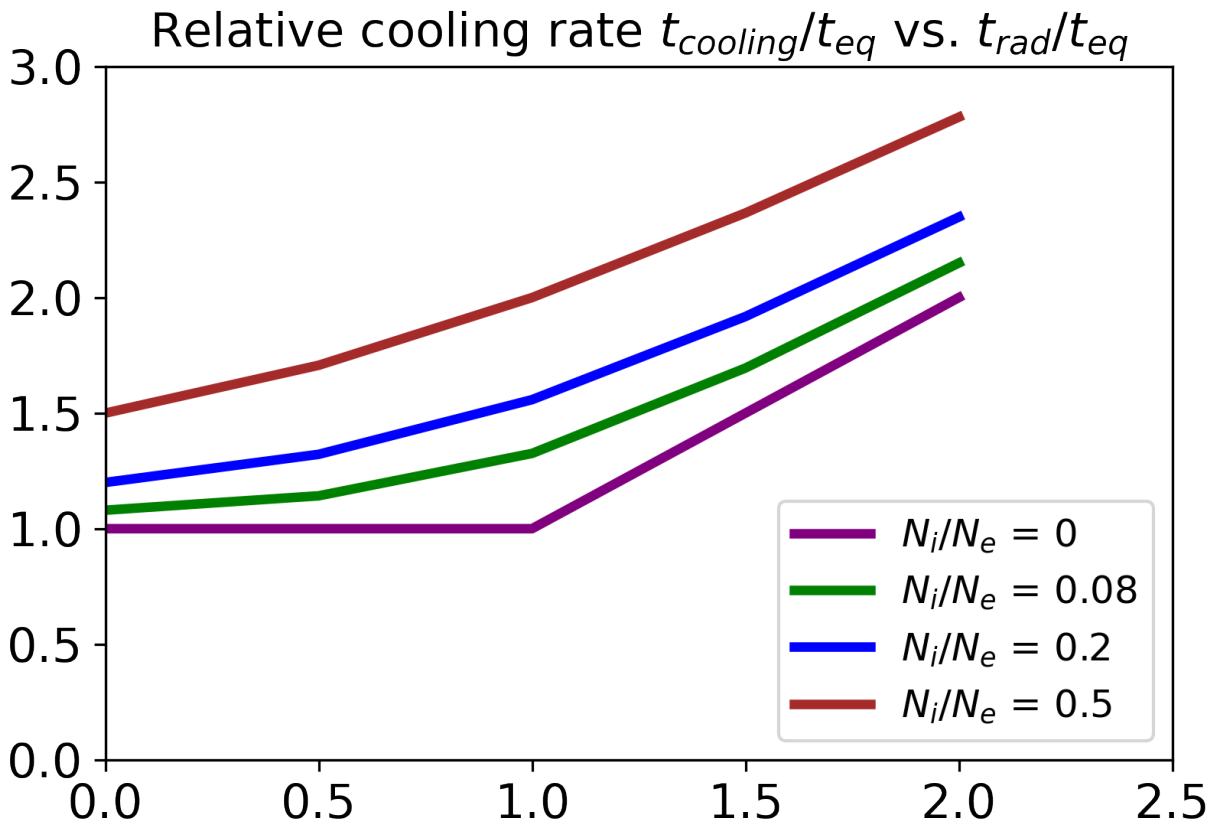

FIG. 3: Relative Cooling Time for N_i/N_e.

3.4 DUAL ENERGY ELECTRON STORAGE RING

The concept of an accelerator with different energies was initiated in Ref. [29]. This type of accelerator arrangement is called an energy recovered loop accelerator. Such a design consists of two loops with significantly different energies: the low energy loop and the high energy loop connected by an energy recovered linac (ERL). There are two possible configurations. The "dog-bone" configuration is shown in Fig. 4, where the electron beam is accelerated moving left to right and decelerated moving right to left.

The "traditional" configuration is shown in Fig. 5. Unlike the "dog-bone" configuration, where two beams propagate in opposite directions in the ERL, the beams in "traditional" configuration move along the same direction in the ERL.

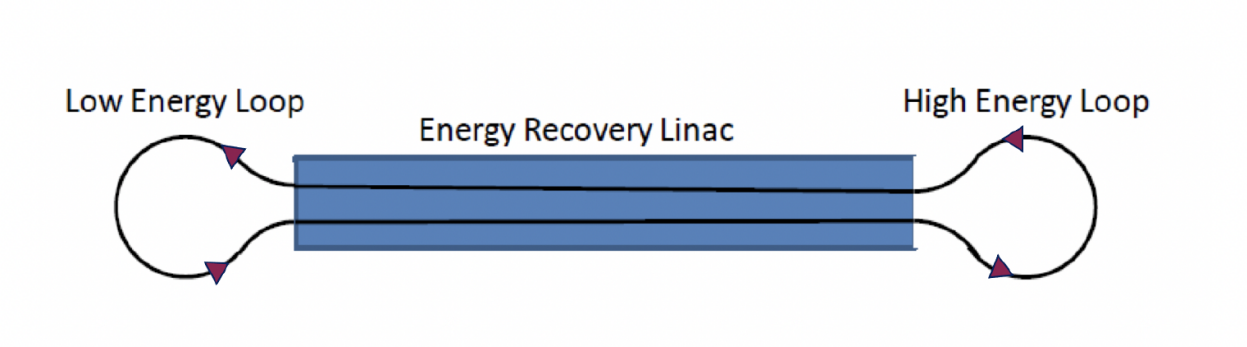

FIG. 4: "Dog-bone" Configuration of an Energy Recovered Loop Accelerator.

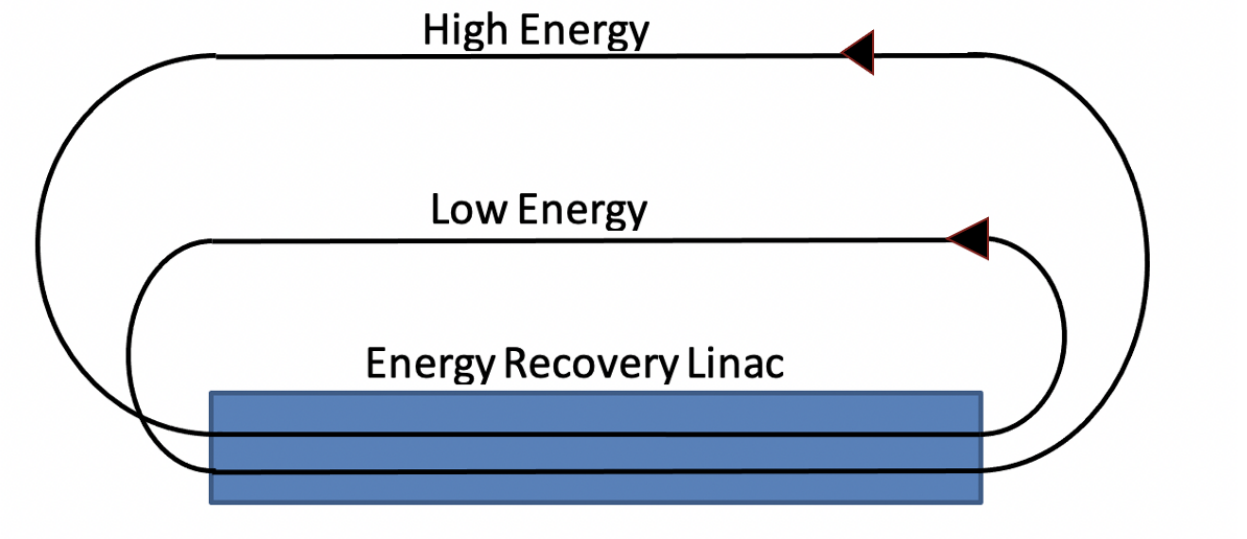

FIG. 5: "Traditional" Configuration of an Energy Recovered Loop Accelerator.

Our dual energy storage ring design is based on the traditional configuration, where both accelerating and decelerating beams move left to right. As the common beamline, an energy

recovery linac (ERL) accelerates the beam from the low energy E_L to the high energy E_H and then decelerates the beam from E_H to E_L in the subsequent pass. This idea can be extended to more than two loops through the accelerator, and indeed multiple different closed orbit sets are possible through the same accelerator, as long as the energy differences in the loops agree with the energy change provided by the linac [29, 30]. This new design concept may have many potential applications, including as a beam cooler.

3.5 DUAL ENERGY ELECTRON STORAGE RING COOLER

One possible application based on a dual-energy electron storage ring is as an electron cooler that decreases the beam heating and increases the damping in a ion storage ring. A dual energy storage ring-based cooler design uses electron cooling methodology to achieve the best possible solution to the emittance degradation due to all heating effects in the ion storage ring and colliders.

Applying electron cooling at ion energies above a few GeV has been limited due to the unfavorable reduction of electron cooling efficiency with energy and the consequent difficulty in producing and accelerating a high-current high-quality electron beam [31, 32]. A high-current electron storage ring cooler can offer a solution to both of these problems by allowing high cooling beam quality to be maintained by naturally occurring synchrotron radiation damping of the electron beam. We propose a new concept of a storage ring cooler, i.e., a dual energy storage ring cooler, that expands the range of applicability of storage-ring based electron cooling of ion beams by allowing the cooling electrons and ions to share the same relativistic gamma in a tunable way, while simultaneously taking advantage of strong synchrotron radiation damping allowed by high electron energies. Such a storage ring electron cooler will benefit any ion storage ring or EIC by significantly enhancing the quality of their beams and therefore improving their performance and scientific and industrial capabilities.

3.5.1 MOTIVATION

Strong cooling of the hadron beam in EIC or in a hadron collider can be used to mitigate IBS and other effects. It can reduce the beam emittance or preserve the emittance of the hadron beam. For the strong cooling of a hadron beam in the energy range of a few tens - several hundred GeV, a cooled electron beam in the energy range of a few tens - several hundred MeV is required. In such a low-energy electron beam, the IBS effect is powerful, giving short IBS lifetimes of the order of a millisecond. Furthermore, synchrotron radiation energy loss is proportional to the fourth power of beam energy. For such a low energy range,

the radiation damping effect is very weak giving long damping times of the order of seconds up to a minute.

To get better balance between IBS and radiation damping, we propose a high-energy ring to enhance the synchrotron radiation and a low-energy ring for cooling. This is the motivation behind the dual energy storage ring cooler design.

3.5.2 DESIGN CONCEPT

The schematic drawing of a dual energy storage ring cooler is shown in Fig. 6. In the

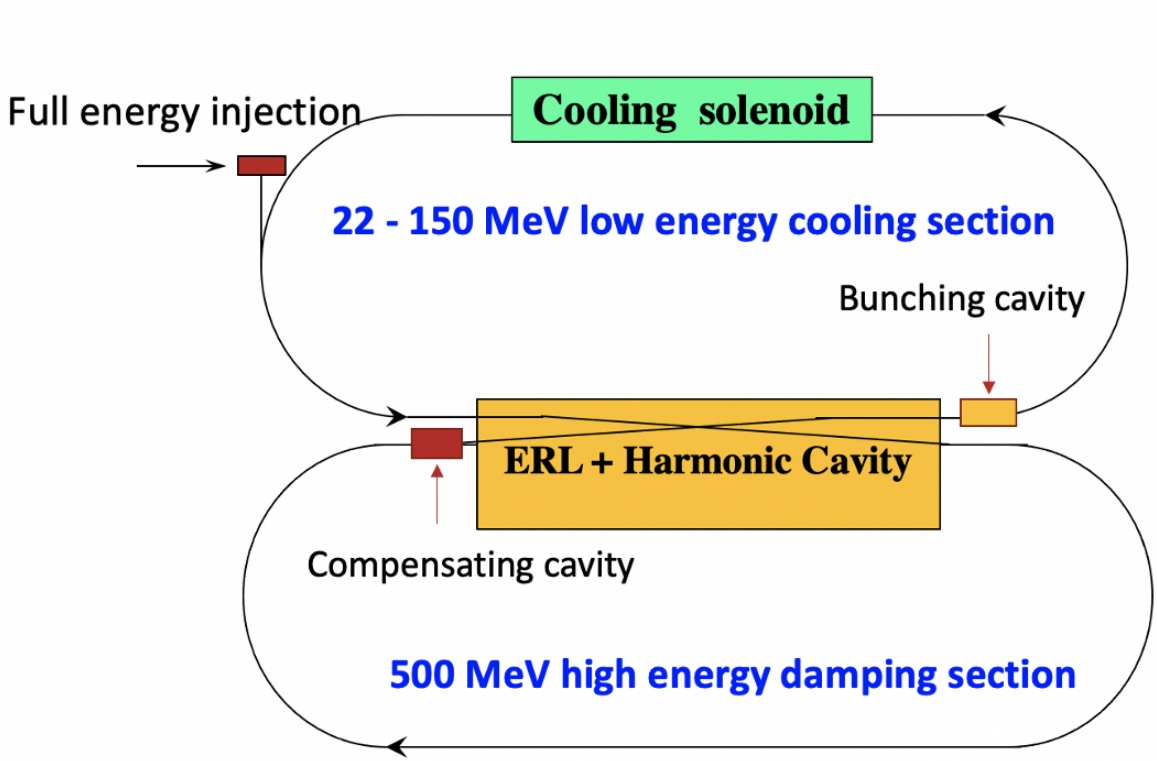

FIG. 6: Schematic Drawing of a Dual Energy Storage Ring Cooler.

low-energy cooling section, the electron beam moves with the same velocity as the ion beam and cooling interaction occurs via Coulomb scattering as in traditional electron cooling. The cooling section provides efficient cooling, whereas the damping section is designed to reach the required equilibrium beam parameters. These two rings are connected by superconducting radio-frequency (SRF) structures, which provide the necessary energy difference.

In our design, the SRF system consists of main cavities and harmonic cavities next to each other. The main cavities are running at crest that accelerates the beam from low energy E_{L} to high energy E_{H} and then decelerates the beam from E_{H} to E_{L} in the next pass. The harmonic cavities run in opposite phases to the main cavities in both accelerating and decelerating passes. Harmonic cavities among the main cavities extend the bunch length, which helps to get the longer bunch length required for a cooling application. Here, we use a third harmonic cavity which provides the desirable bunch length of the order of a centimeter for better cooling. A bunching cavity runs at a zero-crossing phase outside the common beam line provides the necessary longitudinal focusing for the system. Another compensating RF cavity used to compenstate the synchrotron radiation energy loss.

Initially, we investigated using wigglers in the high-energy ring to enhance the radiation damping. Later our calculations showed that increasing the energy in the high energy section may be a good option to get enough synchrotron radiation damping effect without using wigglers. Although we may need to use larger numbers of cryomodules to boost the energy of the electron beam going from a low energy ring to a high energy ring, wigglers magnets with relatively high field strength are costly. So, it is more cost effective to use SRF cavities to boost the electron beam energy than using wigglers to get shorter damping times. Hence our final design consists of set of SRF cavities to boost the energy as shown in Fig. 6.

CHAPTER 4

DUAL ENERGY ELECTRON STORAGE RING COOLER

In this chapter we discuss the dual energy storage ring cooler in detail. We explore the longitudinal and transverse stability in a dual energy storage ring. The linear optics design and beam dynamics study will be presented. We estimate the damping times and IBS times in a dual energy storage ring for the first time. We also derive the formulas for damped equilibrium emittance and energy spread and compare to the results of simulations. Finally, dynamic aperture, momentum aperture, and Touschek lifetime in a dual energy storage ring will be discussed.

4.1 LINEAR OPTICS DESIGN

The guiding and focusing of a charged particle beam in a circular accelerator rely on a series of magnetic elements, separated by field-free drift spaces, that form the accelerator lattice. A dual energy storage ring cooler has a figure-8 configuration, with the low energy ring having a cooling section and the high energy ring is designed to enhance the synchrotron radiation damping as shown in Fig. 6. The optics of the dual energy storage ring cooler is shown in Fig. 7. This ring optics is used for the stability studies of electron beams and exploration of cooling beam parameters. The arcs are composed of standard FODO cells with a 90^0 phase advance that provide an opportunity of compensating chromaticities using properly arranged sextupoles without creating high-order sextupole-induced resonances. Two families of sextupoles are used to compensate for the chromaticities equally distributed in both low and high-energy rings. Dispersion is suppressed at the ends of the arcs to create dispersion-free straights for machine elements, such as SRF structures and the cooling solenoid. However, the evaluation of cooling performance shows that an appropriate dispersion in the solenoid may be needed to produce a sufficient cooling of ion beams. The optics can be further optimized to satisfy this requirement.

In addition, we design the ring optics to match the beta functions before and after the RF systems placed in between the two rings for the acceleration and deceleration of electron beams. This provides the fixed beam size which ensures the transverse stability exists in the system. In the absence of dispersions, the Root-Mean Square (RMS) beam

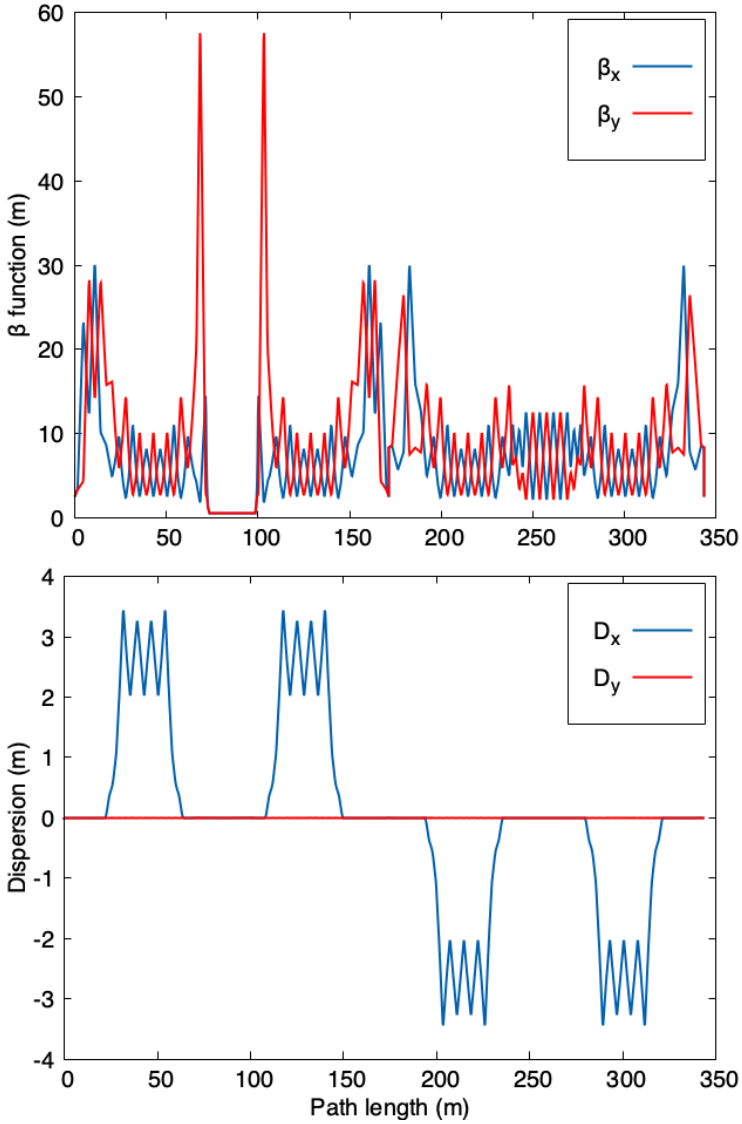

FIG. 7: Optics of a Dual Energy Storage Ring.

sizes are defined by $\sigma_{x,y} = \sqrt{\beta_{x,y}\epsilon_{x,y}}$, where $\beta_{x,y}$ and $\epsilon_{x,y}$ are the transverse beta functions and emittances respectively. In the accelerating pass, the emittance value decreases due to adiabatic damping [8]. In order to keep the beam size fixed, we adjust the beta ratio of the two rings to the momentum ratio and that assures the transverse stability in the system as seen in the next section. We need to match the beta functions in the cooler as well. The beta function in the cooling solenoid with the solenoidal magnetic field B_s is given by

$\beta_s = 2p/eB_s$, where p, and e are the momentum and a charge of the particle respectively. If we do not match the beta functions, then the beam size will grow in the transverse direction.

After the ring optics design was completed, single and multi-particle tracking were carried out using the ELEGANT particle tracking code. Initially, we observed particle instability and careful studies showed a considerable change in the longitudinal position of a particle during tracking due to a large value of arc M_{56}. After the arc M_{56} value was reduced to -0.17 m, particle stability is obtained in the dual energy ring system.

4.2 STABILITY

It is challenging and essential to keep beam current constant with minimum fluctuation in a storage ring. For the dual energy storage ring design, we performed both longitudinal and transverse beam stability studies analytically and using the ELEGANT [33] particle tracking code.

4.2.1 EQUILIBRIA AND SYNCHROTRON STABILITY

In this section, we derive the longitudinal stability conditions that need to be obtained in a dual energy electron storage ring. There are two basic solutions to the equilibrium problem possible. These solutions will be called "storage ring mode" because it more resembles the usual single loop storage ring with strong synchrotron motion, and "ERL mode" because, in this case, the RF in the two beam passes nearly cancels the longitudinal focusing. One remarkable conclusion from this analysis: even in the ERL mode it is possible to obtain stable small amplitude synchrotron oscillations. We also explore the effects of synchrotron radiation in the dual energy electron storage ring.

In the design, two rings share a common beam-line where the SRF structure accelerates the beam from low energy E_{L} to high energy E_{H} and then decelerates the beam from E_{H} to E_{L} in the next pass. The right choice of RF voltage is necessary for the beam acceleration and deceleration. The phasor diagram for the beam accelerating and decelerating voltage is shown as in Fig. 8, where we choose the phase stable solution when both rings are above the transition energy. Referring to Fig. 8, an equilibrium can exist if an acceleration followed by deceleration leads back to the same energy. In the absence of synchrotron radiation, there are two possible solutions for the equilibrium condition defined by

$$\phi_{\mathrm{s,d}} = \pi \pm \phi_{\mathrm{s,a}}, \tag{119}$$

where $\phi_{\mathrm{s,d}}$, and $\phi_{\mathrm{s,a}}$ are the synchrotron phases of the decelerating and accelerating beam

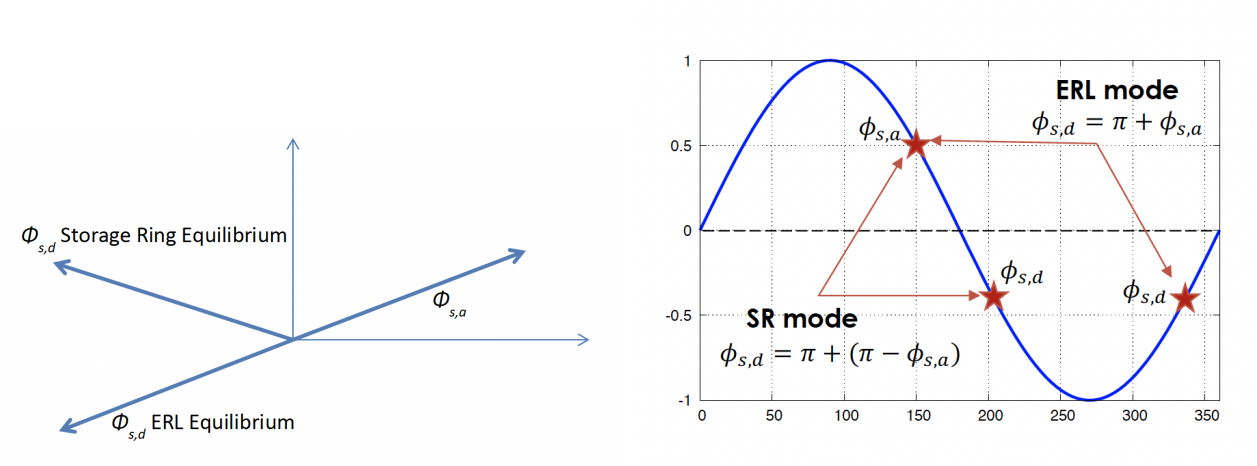

FIG. 8: RF Voltage Phasors for the Phase Stable Case When Both Rings Are Above Transition Energy.

passes. In Eq. (119), the plus sign solution is the most used in energy recovered linacs and is called the "ERL equilibrium". The minus sign solution has strong synchrotron phase stability as in a storage ring and is called the "storage ring equilibrium".

Consider an initial slight deviation ΔE_0 in the beam energy E_0 and the phase $\Delta\phi_0$ away from the synchronous phase ϕ_0 of the storage ring equilibrium. The total one-turn transfer matrix in phase space $(\Delta\phi, \Delta E)$, starting from the end of the low energy ring, is given by

$$\begin{pmatrix} 1 & -h_{\rm L}/E_{\rm L} \\ 0 & 1 \end{pmatrix} \begin{pmatrix} 1 & 0 \\ -V\sin\phi_{\rm s,d} & 1 \end{pmatrix} \begin{pmatrix} 1 & -h_{\rm H}/E_{\rm H} \\ 0 & 1 \end{pmatrix} \begin{pmatrix} 1 & 0 \\ -V\sin\phi_{\rm s,a} & 1 \end{pmatrix}, \qquad (120)$$

where transfer matrices starting from the left end of Eq. (120) are for the accelerating beam pass, after passing the high energy ring, after the decelerating pass, and finally, after the low energy ring. The parameter $h_{\rm H} = 2\pi h f_0 L_{\rm H}\eta_{\rm H}/\beta_{\rm H}^3 c$ is a dimensionless combination of parameters proportional to the frequency slip factor for the high energy ring. $h_{\rm L}$ is defined similarly to $h_{\rm H}$ using the parameters from the low energy ring. In this combination, h is the harmonic number including both rings, f_0 is the total revolution frequency, c is the speed of light in a vacuum, $\beta_{\rm H}$ is the normalized velocity, $L_{\rm H}$ is the path length, and $\eta_{\rm H}$ is the phase slip factor [7], all in the high energy ring. Therefore, the phase advance μ for the synchrotron

motion is

$$\begin{aligned}\cos\mu = 1 + h_L V \sin\phi_{s,a}/E_{\rm L} + h_H V \sin\phi_{\rm s,a}/E_{\rm H} + \\ h_L h_H V^2 \sin^2\phi_{\rm s,a}/(2E_{\rm L}E_{\rm H}),\\ \mu = \cos^{-1}[1 + h_L V \sin\phi_{s,a}/E_{\rm L} + h_H V \sin\phi_{\rm s,a}/E_{\rm H} + \\ h_L h_H V^2 \sin^2\phi_{\rm s,a}/(2E_{\rm L}E_{\rm H})].\end{aligned} \tag{121}$$

The synchrotron tune is then defined by

$$Q_s = \frac{\mu}{2\pi} = \frac{1}{2\pi}\cos^{-1}[1 + h_L V \sin\phi_{s,a}/E_{\rm L} + h_H V \sin\phi_{\rm s,a}/E_{\rm H} + h_L h_H V^2 \sin^2\phi_{\rm s,a}/(2E_{\rm L}E_{\rm H})]. \tag{122}$$

The following argument shows this functional form for the solution is correct. In the specific case that the linac (RF cavity) runs on zero-crossing and the beam energy and h values are identical in the two rings, the situation is the same physically as a single storage ring with two beam passes. The total phase advance is just twice the single circuit result, computed using half the harmonic number for two rings.

In storage ring language, the synchrotron phase is usually referenced to the positive going zero-crossing phase in the cavity. To make the transition in the above formulas, simply add ninety degrees ($\pi/2$) to $\phi_{\rm s,a}$ such that $\phi^{SR}_{\rm s,a} = \phi_{\rm s,a} + \pi/2$. The net result is then $\sin\phi_{\rm s,a} \to -\cos\phi^{SR}_{\rm s,a}$, as is more standard in textbooks. Then Eq. (122) can be re-rewritten as

$$Q_s = \frac{\mu}{2\pi} = \frac{1}{2\pi}\cos^{-1}[1 - h_L V \cos\phi^{SR}_{s,a}/E_{\rm L} - h_H V \cos\phi^{SR}_{\rm s,a}/E_{\rm H} + h_L h_H V^2 \cos^2\phi^{SR}_{\rm s,a}/(2E_{\rm L}E_{\rm H})]. \tag{123}$$

Following the same argument for the ERL equilibrium, the total one turn transfer matrix in phase space $(\Delta\phi, \Delta E)$ is given by

$$\begin{pmatrix} 1 & -h_L/E_{\rm L} \\ 0 & 1 \end{pmatrix}\begin{pmatrix} 1 & 0 \\ V\sin\phi_{\rm s,a} & 1 \end{pmatrix}\begin{pmatrix} 1 & -h_H/E_{\rm H} \\ 0 & 1 \end{pmatrix}\begin{pmatrix} 1 & 0 \\ -V\sin\phi_{\rm s,a} & 1 \end{pmatrix}. \tag{124}$$

Therefore, in storage ring language, the phase advance for the synchrotron motion is

$$\begin{aligned}\cos\mu = 1 - h_L h_H V^2 \cos^2\phi^{SR}_{\rm s,a}/(2E_{\rm L}E_{\rm H}),\\ \mu = \cos^{-1}[1 - h_L h_H V^2 \cos^2\phi^{SR}_{\rm s,a}/(2E_{\rm L}E_{\rm H})].\end{aligned} \tag{125}$$

The synchrotron tune is then defined by

$$Q_s = \frac{\mu}{2\pi} = \frac{1}{2\pi}\cos^{-1}[1 - h_L h_H V^2 \cos^2\phi^{SR}_{\rm s,a}/(2E_{\rm L}E_{\rm H})]. \tag{126}$$

It is a remarkable conclusion that in an ERL equilibrium, the electron is synchrotron stable as long as both rings are either above or below the transition energy. Because of the synchrotron motion in the two-energy ring, the positive and negative slopes are not completely cancelled, yielding net phase focusing. As these calculations are made, one must impose the consistency condition on the revolution frequency

$$f_0 = \frac{1}{t_{\rm H} + t_{\rm L}} = \frac{c}{(L_{\rm H}/\beta_{\rm H}) + L_{\rm L}/\beta_{\rm L}}, \tag{127}$$

where t_H, and t_L are revolution times for the high and low energy rings, respectively. Now, we consider the effect of synchrotron radiation in the system. The total energy loss due to synchrotron radiation is given by the sum of energy loss in each ring due to radiation effects. A compensating cavity running at the crest is used to compensate for the total energy loss.

4.2.2 TRANSVERSE STABILITY

Using the one loop transfer map, we describe the transverse stability in a dual energy storage ring. Matrix parameterization in a ring moving from one point to another takes the form [6]:

$$\begin{bmatrix} x_2 \\ x_2' \end{bmatrix} = M(s_1, s_2) \begin{bmatrix} x_1 \\ x_1' \end{bmatrix}, \tag{128}$$

where $M(s_1, s_2) = \begin{pmatrix} m_{11} & m_{12} \\ m_{21} & m_{22} \end{pmatrix}$ is a transfer matrix from point s_1 to another point s_2 in a storage ring. The elements of matrix are defined by

$$\begin{aligned} m_{11} &= \sqrt{\frac{\beta_2}{\beta_1}}(\cos\mu + \alpha_1 \sin\mu) \\ m_{12} &= \sqrt{\beta_1\beta_2}\sin\mu \\ m_{21} &= -\frac{(1+\alpha_1\alpha_2)}{\sqrt{\beta_1\beta_2}}\sin\mu + \frac{(\alpha_1 - \alpha_2)}{\sqrt{\beta_1\beta_2}}\cos\mu \\ m_{22} &= \sqrt{\frac{\beta_1}{\beta_2}}(\cos\mu - \alpha_2 \sin\mu). \end{aligned} \tag{129}$$

Here, α_i, β_i are the Twiss parameters in the ring at different locations. In our simplified model the Low Energy Ring (LER) and High Energy Ring (HER) are connected by zero-length RF cavities, which accelerate the beam going from the LER to the HER and decelerate the beam going from the HER to the LER. The transfer matrix for the LER, the HER, the accelerating cavity and the decelerating cavity are denoted by $M_{LER}, M_{HER}, M_{cav}^{acc}$, and M_{cav}^{dec}

respectively and defined by

$$\begin{aligned} M_{LER} &= \begin{pmatrix} \cos\psi_L + \alpha_L \sin\psi_L & \beta_L \sin\psi_L \\ -(1+\alpha_L^2)\sin\psi_L/\beta_L & \cos\psi_L - \alpha_L \sin\psi_L \end{pmatrix}, \\ M_{HER} &= \begin{pmatrix} \cos\psi_H + \alpha_H \sin\psi_H & \beta_H \sin\psi_H \\ -(1+\alpha_H^2)\sin\psi_H/\beta_H & \cos\psi_H - \alpha_H \sin\psi_H \end{pmatrix}, \\ M_{cav}^{acc} &= \begin{pmatrix} 1 & 0 \\ 0 & p_L/p_H \end{pmatrix}, \\ M_{cav}^{dec} &= \begin{pmatrix} 1 & 0 \\ 0 & p_H/p_L \end{pmatrix}. \end{aligned} \tag{130}$$

Now, the total one-turn transfer map is given by

$$M = M_{cav}^{dec} M_{HER} M_{cav}^{acc} M_{LER}. \tag{131}$$

Let us assume that the beam optics design has vanishing α before and after the acceleration and deceleration. Then $\alpha_L = \alpha_H = 0$ in the above Eq. 130. The trace of the total transfer matrix M is calculated and takes the form

$$\text{Trace } M = 2\cos\psi_L \cos\psi_H - \sin\psi_L \sin\psi_H \, (p_L\beta_H/p_H\beta_L + p_H\beta_L/p_L\beta_H) \tag{132}$$

The stability criteria is defined by $|$ Trace $M/2$ $|< 1$.

$$|\text{ Trace } M/2 \,| = |\cos\psi_L \cos\psi_H - \frac{1}{2}\sin\psi_L \sin\psi_H (p_L\beta_H/p_H\beta_L + p_H\beta_L/p_L\beta_H)\,| < 1. \tag{133}$$

Next, further assume that the optics design has the same beam size before and after acceleration and deceleration because if this condition is not satisfied, the beam will not be matched [34]. In this case the ratio of beta functions at the cavities in the two rings is equal to the ratio of the momentum on either side of the cavities since going through a RF cavity changes the emittance in the ratio of p_L/p_H on acceleration. Thus $p_L\beta_H/p_H\beta_L = 1$ and hence the stability criteria defined by Eq. 133 takes the form

$$|\text{ Trace } M/2 \,| = |\cos\psi_L \cos\psi_H - \sin\psi_L \sin\psi_H \,| < 1. \tag{134}$$

From the stability criteria one concludes that when the beta ratios are equal to the momentum ratios, then, indeed, the situation is always transversely stable. Not only that, the phase advance for the whole ring is the sum of the phase advances for the individual rings because

$$\cos\psi_{tot} = \cos(\psi_L + \psi_H). \tag{135}$$

4.3 SRF CAVITIES

A Superconducting Radio Frequency (SRF) structure encloses a volume and can sustain an infinite number of resonant electromagnetic modes. These cavities play an important role in CW particle accelerators and are primarily used to impart energy to the particle traveling through it. An accelerating cavity is provided with a longitudinal electric field. The proper phasing with the particle bunches is required to impart momentum to the particles. Since the cavity is a structure with an electromagnetic field in it, a magnetic field, on the other hand, provides deflection to the particle beam but no acceleration. The fundamental theory on the RF cavity is presented in Appendix A.

The dual-energy storage ring design has a set of SRF cavities: the main cavity to accelerate or decelerate the beam, the harmonic cavity to lengthen the bunch length, the compensating cavity to compensate for the energy loss due to synchrotron radiation, and the bunching cavity to provide additional longitudinal focusing in the system.

4.3.1 BUNCH LENGTHENING USING THE HARMONIC CAVITY

Higher harmonic cavities are used to modify the slope and shape of RF voltage together with the main cavities so the the bunch length can be controlled in storage rings. Harmonic cavities have been widely used in storage rings to increase the beam lifetime and Landau damping by lengthening the bunch [35]. The total longitudinal voltage gain V_g experienced by the beam can be written as

$$V_g = V_m \cos(\omega_{\rm rf} t + \psi_s) + V_{\rm th} \cos\big(\omega_{\rm rf}^{th} t + \psi_s^{th}\big), \tag{136}$$

where V_m, and $V_{\rm th}$ are the main, and harmonic cavity voltages, ψ_s, and ψ_s^{th} are RF phases for the main and the harmonic cavities respectively. We use a third harmonic cavity next to the main cavity, so the harmonic angular rf $\omega_{\rm rf}^{th} = 3\omega_{\rm rf}$. Then we have the following boundary conditions to evaluate the voltage amplitudes for each cavities:

$$i)\ \ V_g\Big|_{t=0} = V_m \cos(\omega_{\rm rf} t + \psi_s) + V_{\rm th} \cos\big(\omega_{\rm rf}^{th} t + \psi_s^{th}\big) = 350, \tag{137}$$

$$ii)\ \ \frac{dV_g}{dt}\Big|_{t=0} = 0, \tag{138}$$

$$iii)\ \ \frac{d^2V_g}{dt}\Big|_{t=0} = 0. \tag{139}$$

The voltage amplitudes V_m, and $V_{\rm th}$ are evaluated using the above initial boundary conditions at $t = 0$. The low energy ring is at 150 MeV, and the high energy ring is at 500 MeV. The

total gain in the energy is 350 MeV as given by the first boundary condition. The main cavity is running in the crest ($\psi_s = 0°$), and the third harmonic cavity is running with the decelerating phase ($\psi_s^{th} = 180°$). Then we get the following relationships

$$\begin{aligned} V_m &= \frac{9}{8} V_g \\ V_{\text{th}} &= \frac{V_g}{8}. \end{aligned} \tag{140}$$

During the particle tracking simulation, proper RF phases and voltages should be applied by the rf cavities for beam stability. The harmonic cavity voltage is added to the main cavity

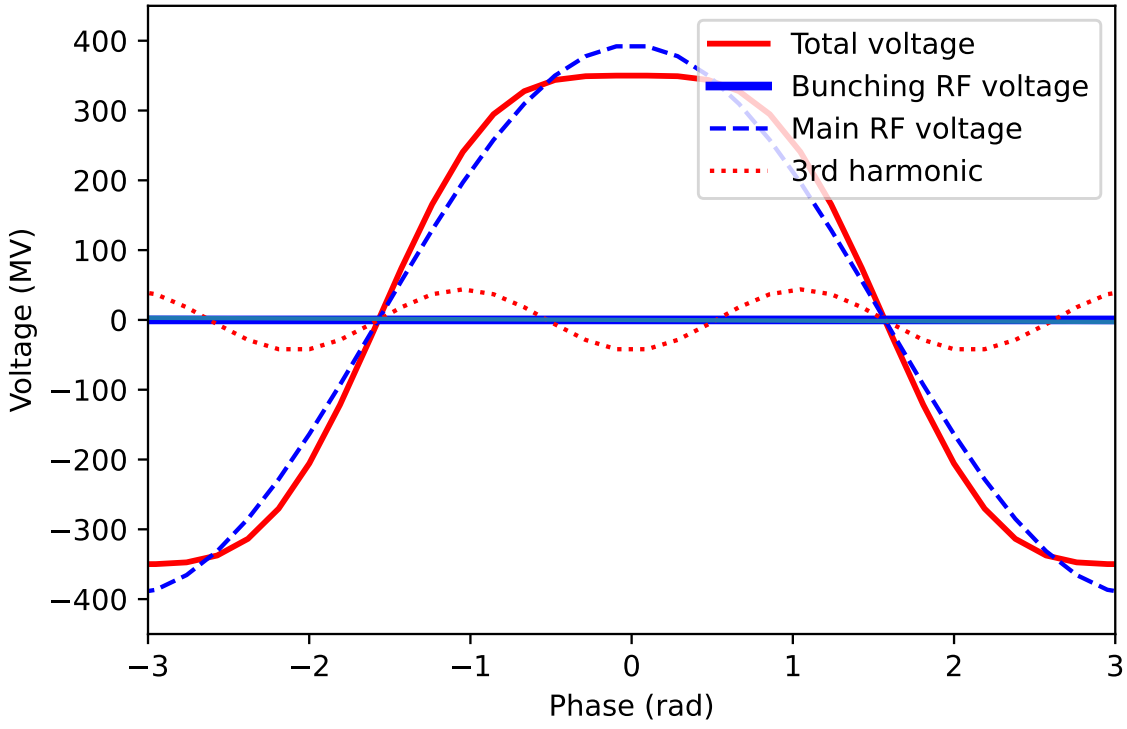

FIG. 9: Main and the Third Harmonic Cavities Voltages to Reach the Desired 'Flat-Top'.

voltage with an amplitude and the phase as defined earlier such that the slope at the bunch center is zero. As shown in Fig. 9, there is a flat-top total voltage.

In our baseline design, the total energy gain during the accelerating pass is exactly cancelled by the total energy loss during the decelerating pass. Hence it is desirable to enhance the longitudinal focusing in the system by providing a bunching cavity. The bunching cavity is situated outside the common beamline. Since the bunch length is depends inversely on the rf voltage, the bunching cavity voltage plays an important role in determining the possible bunch length. The final equilibrium bunch length in electron storage ring is determined by the combined effect of synchrotron radiation, quantum excitation, and the IBS effect.

When particles pass through the bending arcs, synchrotron radiation takes place and the energy loss is present. In this case, a compensating RF cavity running on the RF crest is used with the proper voltage to compensate the energy loss. This compensating cavity is required; otherwise, energy loss accumulates each turns and eventually the particles get lost.

4.3.2 ENERGY FLUCTUATION IN SRF CAVITIES

In a storage ring based cooler design, fluctuation in the beam energy affects the cooling rates. So, it is important to understand the energy fluctuations due to voltage fluctuations especially when beam passes through the RF cavities.

In our cooler design, we have a system of RF cavities: the main cavity, harmonic cavity, bunching cavity, and compensating cavity. The main cavity is used to accelerate or decelerate the beam, the harmonic cavity to lengthen the bunch length, the bunching cavity to provide the longitudinal focusing, and the compensating cavity to compensate for the energy loss due to synchrotron radiation. When the beam passes through these cavities, voltage fluctuation results in energy fluctuation of the beam. During the accelerating pass, the total gain through the RF system is about 350 MeV. The maximum voltage gain occurs through the main cavity given by Eq. (140). The peak main cavity voltage becomes $V_m = 9 * 350/8 =$ 393.75 MeV. To calculate the energy fluctuation due to the voltage fluctuation, we alter the main cavity voltage by 0.1% keeping the voltage of all remaining cavities constant. With 0.1% voltage fluctuation in the main cavity, the main cavity peak voltage becomes 393.75 - 0.1% of 393.75 = 393.36 MeV. With the bunch length of 13.5 cm, we run ELEGANT particle tracking and calculate the average momentum of the particle. The relative change in the particle momentum is given by

$$\%(\Delta p) = \frac{|p_{\text{cen}} - p_{\text{ave}}|}{p_{\text{cen}}}, \tag{141}$$

where $p = \beta\gamma$ is particle's momentum in units of MeV/c, $p_{\rm cen} = 293.54$ MeV/c is particle's central momentum, and $p_{\rm ave} = 294.47$ MeV/c is the particle's average momentum. Now, substituting the values in Eq. (141), the change in particle's momentum $\beta\gamma = 0.7924$ MeV/c. Furthermore, $\gamma = \sqrt{1 + (\beta\gamma)^2} = 1.275$, and the energy fluctuation is given by $\Delta E = \gamma \times m_0 c^2$ = 0.69 MeV.

4.4 BEAM DYNAMICS

4.4.1 DAMPING TIMES AND IBS TIMES

In this sub-section, we first estimate the damping time in a dual energy storage ring, beginning by recalling the analysis of the single energy ring case. The transfer matrix for the accelerating pass, with longitudinal phase space variables $(\Delta z, \Delta E)$, is given by

$$\begin{pmatrix} \Delta z' \\ \Delta E' \end{pmatrix} = \begin{pmatrix} 1 & 0 \\ 2\pi e V \cos\phi_s/\lambda_{\rm rf} & 1 \end{pmatrix} \begin{pmatrix} \Delta z \\ \Delta E \end{pmatrix}. \tag{142}$$

When one includes the synchrotron radiation, because for the off-energy particle and the synchronous particle have energy updates

$$\begin{aligned} E' &= E - W(E) \\ E'_s &= E_s - W(E_s), \end{aligned} \tag{143}$$

the linearized model for the ring becomes

$$\begin{pmatrix} \Delta z' \\ \Delta E' \end{pmatrix} = \begin{pmatrix} 1 & M_{56}/E \\ 0 & 1 - \frac{dW}{dE}\Big|_{E_s} \end{pmatrix} \begin{pmatrix} \Delta z \\ \Delta E \end{pmatrix}. \tag{144}$$

Here, the function $W(E)$ gives the total radiated energy per pass as a function of energy. When $0 < dW/dE < 1$ (this is essentially always the case), the determinant of the product matrix is less than one. The origin of the phase space with $\Delta z = 0$ and $\Delta E = 0$ is a fixed point of the product map. Because the non-linear energy equation for a full turn at the synchronous phase is $E'_s = E_s + eV\sin\phi_s - W(E_s)$, an equilibrium with $eV\sin\phi_s = W(E_s)$ must be established. If a ring electron radiates on average energy of $\Delta E_{\rm rad}$ per pass, then the deviation in a synchrotron oscillation damps exponentially at a rate given by

$$\frac{1}{\tau_{z,rad}} = \frac{1}{2t_{\rm rev}} \frac{\Delta E_{\rm rad}}{E} (2 + \xi), \tag{145}$$

where τ_{rad} is the exponential decay time of the deviation, $t_{\rm rev}$ is the revolution time, E is the ring energy, and ξ is the focusing lattice radiation partition integral [36]. Consistent

with Robinson's radiation partition theorem, the damping rates for the deviations in the horizontal and vertical betatron oscillations are

$$\begin{aligned}\frac{1}{\tau_{x,rad}} &= \frac{1}{2\tau_{\rm rev}}\frac{\Delta E_{rad}}{E}(1-\xi)\\ \frac{1}{\tau_{y,rad}} &= \frac{1}{2\tau_{\rm rev}}\frac{\Delta E}{E},\end{aligned} \tag{146}$$

respectively. Here $\tau_{x,rad}$ and $\tau_{y,rad}$ are horizontal and vertical damping times respectively. Note that the energy dependence of the result is entirely captured in the ratio $\Delta E_{\rm rad}/E$.

In a dual energy storage ring, we need to consider the low energy ring and the high energy ring separately to calculate the damping time. The total damping time for the whole ring is then the proper summation of damping times for the low energy ring and the high energy ring. Consider first the damping of synchrotron oscillation. A simple analysis of this problem is that after traversing the high energy ring the oscillation deviation is damped by $\exp[-\Delta E_{\rm H}(2+\xi_{\rm H})/2E_{\rm H}]$. After traversing both the high energy ring and low energy ring, the deviation is damped by $\exp[-\Delta E_{\rm L}(2+\xi_L)/2E_{\rm L}]\exp[-\Delta E_{\rm H}(2+\xi_{\rm H})/2E_{\rm H}] = \exp[-\Delta E_{\rm L}(2+\xi_L)/2E_{\rm L} - \Delta E_{\rm H}(2+\xi_H)/2E_{\rm H}]$, where subscripts L and H stand for the low energy ring and the high energy ring respectively. The combined damping rate is therefore given by $1/(t_{\rm rev,L}+t_{\rm rev,H})\times[-\Delta E_{\rm L}(2+\xi_{\rm L})/2E_{\rm L} - \Delta E_{\rm H}(2+\xi_{\rm H})/2E_{\rm H}]$, where $t_{\rm rev,L}+t_{\rm rev,H}$ is the total revolution time for a single transit of both rings. The ratio $t_{\rm rev}/\tau_{\rm rad}$ simply adds for each loop, i.e.

$$\frac{t_{\rm rev,\ tot}}{\tau_{\rm rad,tot}} = \frac{t_{\rm rev,\ L}}{\tau_{\rm rad,L}} + \frac{t_{\rm rev,\ H}}{\tau_{\rm rad,H}}, \tag{147}$$

where $t_{\rm rev,\ L} = C_{\rm L}/c\beta_{\rm L}$, and $t_{\rm rev,\ H} = C_{\rm H}/c\beta_{\rm H}$ are the revolution time for each ring respectively. Here $C_{\rm L}$ and $C_{\rm H}$ are the circumferences for the low energy ring and high energy ring such that total circumference of the storage ring $C = C_{\rm L} + C_{\rm H}$. $\beta_{\rm L}$, and $\beta_{\rm H}$ are the relativistic beta values for the corresponding beam energies at low energy and high energy, and c is the velocity of light. In our design, both rings have the same circumference, i.e., $C_{\rm L} = C_{\rm H} = C/2$. For the relativistic electron beam, we can assume that $\beta_{\rm L} = \beta_{\rm H} \approx 1$. Under this condition, Eq. (147) becomes

$$\frac{1}{\tau_{\rm rad,tot}} = \frac{1}{2\tau_{\rm rad,L}} + \frac{1}{2\tau_{\rm rad,H}}. \tag{148}$$

The same idea applies to each degree of freedom in turn.

To see that this analysis is more or less correct, consider a model where the two different energy rings are connected by a zero-length accelerator. Follow the argument through one

full circuit of the ring performing all calculations to linear order. The total one turn transfer matrix is

$$\begin{pmatrix} 1 & 0 \\ 2\pi eV\cos\phi_{s,a}/\lambda_{\rm rf} & 1 \end{pmatrix} \begin{pmatrix} 1 & M_{56,L}/E_L \\ 0 & 1-dW/dE\Big|_{E_{s,L}} \end{pmatrix} \begin{pmatrix} 1 & 0 \\ 2\pi eV\cos\phi_{s,d}/\lambda_{\rm rf} & 1 \end{pmatrix} \begin{pmatrix} 1 & M_{56,H}/E_H \\ 0 & 1-dW/dE\Big|_{E_{s,H}} \end{pmatrix}. \tag{149}$$

The determinant of the matrix is simply the product of the determinants, which is

$$\left(1-dW/dE\Big|_{E_{s,L}}\right)\left(1-dW/dE\Big|_{E_{s,H}}\right) \approx 1-dW/dE\Big|_{E_{s,L}} - dW/dE\Big|_{E_{s,H}}, \tag{150}$$

yielding the same combination principle in the evidence above.

In a dual energy storage ring, accelerating and decelerating passes cancel. A compensating cavity is used to compensate for the energy loss due to synchrotron radiation. In this case, the equilibrium condition for the synchronous particle is

$$eV_c\sin\phi_{s,c} = W(E_{s,L}) + W(E_{s,H}), \tag{151}$$

where V_c and $\phi_{s,c}$ are the RF voltage and phase angle for the compensating cavity. This shows that the equilibrium tends to be dominated by the higher energy radiation.

The damping times calculations in a dual energy storage ring are presented in Appendix F. The damping times depend on beam energy and lattice design. Since the energy loss per turn due to synchrotron radiation is directly proportional to fourth power of the beam energy, the corresponding damping time is inversely proportional to the third power of the beam energy for the given lattice. In dual energy storage ring case, two rings are at markedly different energies, the damping effect is dominated by high energy ring. The total damping rate is calculated using the formula given by Eq. (148) and the damping time is the reciprocal of the damping rate.

The theory of intra-beam scattering (IBS) is described well in a number of publications [37–40]. The IBS is the multiple small-angle Coulomb scattering of charged particles within an accelerator beam. This scattering process couples the beam emittances in all three dimensions and eventually leads to emittance growth. Electron storage rings have strong radiation damping, and the equilibrium emittance is determined by a balance between radiation damping, quantum excitation, and IBS. This balance process also determines the equilibrium bunch length [41].

In our dual energy storage ring, we calculate the IBS rates for each ring using ELEGANT. For the given optics design and equilibrium beam parameters, ELEGANT uses an IBS

model [39] to calculate the IBS rates in each ring. Similarly to the total damping rate calculation defined by Eq. (148), the total IBS rate is calculated using the formula

$$\frac{1}{\tau_{\mathrm{IBS,tot}}} = \frac{1}{2\tau_{\mathrm{IBS,L}}} + \frac{1}{2\tau_{\mathrm{IBS,H}}}, \tag{152}$$

where $\tau_{\mathrm{IBS,L}}$, and $\tau_{\mathrm{IBS,H}}$ are the IBS times for low energy ring and high energy ring respectively and $\tau_{\mathrm{IBS,tot}}$ is the total IBS time for the whole ring. We determine the damping times and IBS times in each dimension separately for the low energy ring and the high energy ring. The total damping times and the total IBS times are then calculated using the formula given by Eq. (148), and Eq. (152), respectively. Table 1 lists the damping times and IBS times for individual rings and for the whole ring. The damping times in all three-dimensions are shorter than the corresponding IBS times. An electron storage ring with shorter damping time compared to the IBS time is highly required by design to mitigate the emittance growth due to the IBS effect.

TABLE 1: Damping Times and IBS Times in a Dual Energy Storage Ring.

Parameters	LER (s)	HER (s)	Total (s)
$\tau_{\mathrm{rad,x}}$	60.7	1.64	3.19
$\tau_{\mathrm{rad,y}}$	13.03	0.35	0.68
$\tau_{\mathrm{rad,z}}$	4.68	0.13	0.25
$\tau_{\mathrm{IBS,x}}$	4.11	6.62	5.07
$\tau_{\mathrm{IBS,y}}$	6.6E03	3.9E05	1.30E4
$\tau_{\mathrm{IBS,z}}$	0.79	0.35	0.49

4.4.2 DAMPED EQUILIBRIUM EMITTANCE AND ENERGY SPREAD

We have already discussed the effects of radiation damping and damping times in a dual

energy storage ring. We derive the new formula for damped equilibrium energy spread and the emittance in a dual energy storage ring. Our calculation shows that these equilibrium parameters tend to be dominated by the radiation in the high-energy ring. The equilibrium beam parameters in the cooling section at the low energy ring are determined by the damped equilibrium parameters at the high energy ring.

As in a single-energy storage ring, the linear optics design may be used to control the damped equilibrium emittance and energy spread. Because the individual radiation events in the two rings are different and independent, we can provide analytical estimates of the damping times in a dual energy storage ring. The damped energy spread, and emittance can be determined for various parameters related to lattice design and the ring energies. We present analytical calculations and simulation results to estimate damped energy spread and emittance values in a dual energy storage ring. We also note that these quantities tend to be dominated by the radiation in the high-energy ring

In the case of a dual energy storage ring, one determines the equilibrium energy spread by adding total photon flux $\dot{N}_{ph}\langle\varepsilon^2\rangle$ from all sources in the two rings passes and utilizes the two-ring damping time τ_z determined elsewhere [12]. Therefore, the equilibrium energy spread in a dual energy storage ring is given by

$$\frac{\sigma_E^2}{E^2} = \frac{\tau_{\rm z}}{4E^2}\dot{N}_{\rm ph}\langle\varepsilon^2\rangle = \frac{C_{\rm q}}{\hat{\gamma}^2}\frac{\gamma_H^7\langle 1/\rho_H^3\rangle + \gamma_L^7\langle 1/\rho_L^3\rangle}{[(2+\xi_H)\gamma_H^3\langle 1/\rho_H^2\rangle + (2+\xi_L)\gamma_L^3\langle 1/\rho_L^2\rangle]}, \tag{153}$$

where $\hat{\gamma}^2$ in the denominator scales with the corresponding ring energy, and L and H stand for low and high energy rings, respectively

However, $\delta\langle a^2\rangle$ is energy dependent (geometric emittance). As we know, the normalized emittance is a constant parameter in a dual energy storage ring, we should get

$$\delta\langle\gamma a^2\rangle = \gamma\mathcal{H}(z)\left(\frac{\varepsilon}{E}\right)^2. \tag{154}$$

Then,

$$\begin{aligned}
\frac{{\rm d}\langle\gamma a^2\rangle}{{\rm dt}} &= G_x^N = \frac{\gamma}{E^2}\oint \dot{N}_{\rm ph}\langle\varepsilon^2\rangle\mathcal{H}(z)dz, \\
\frac{{\rm d}\langle\gamma a^2\rangle}{{\rm dt}} &= \frac{\langle\dot{N}_{\rm ph}\langle\varepsilon_L^2\rangle\mathcal{H}_x^L(z)}{m^2c^4\gamma_L} + \frac{\langle\dot{N}_{\rm ph}\langle\varepsilon_H^2\rangle\mathcal{H}_x^H(z)}{m^2c^4\gamma_H}.
\end{aligned} \tag{155}$$

The quantity $N\langle\varepsilon^2\rangle$ is defined by

$$N\langle\varepsilon^2\rangle = \frac{3}{2}C_{\rm u}\hbar c\frac{\gamma^3}{\rho^3}\frac{\langle P_\gamma\rangle}{\langle 1/\rho^2\rangle}, \tag{156}$$

where $C_{\rm u} = 55/24\sqrt{3}$. Substituting the value of average power loss due to synchrotron radiation, Eq. (155) takes the form

$$G_{\rm x}^{N} = \frac{3}{4\pi T_{tot}} C_{\rm u} C_{\gamma} \hbar m^2 c^5 (\gamma_H^6 \langle \mathcal{H}_x^H / \rho_H^3 \rangle + \gamma_L^6 \langle \mathcal{H}_x^L / \rho_L^3 \rangle). \tag{157}$$

Then equilibrium is reached with $\langle \gamma a^2 \rangle = \tau_{\rm x}^t G_{\rm x}^N/2$, and $\sigma_{\rm x}^2 = \tau_{\rm x}^t G_{\rm x}^N/2$. The geometric emittance is defined by

$$\epsilon_x = \frac{\sigma_x^2}{\beta_x} = \frac{1}{2}\frac{\langle \gamma a^2 \rangle}{\gamma} = \frac{1}{4\gamma}\tau_{\rm x}^t G_{\rm x}^N. \tag{158}$$

Substituting the values of $\tau_{\rm x}^t$ and $G_{\rm x}^N$ in the above Eq. (158), the damped equilibrium emittance in a dual energy storage ring is given by

$$\epsilon_{\rm x} = \frac{C_{\rm q}}{\hat{\gamma}} \frac{\gamma_H^6 \langle \mathcal{H}_{\rm x}^H / \rho_{\rm H}^3 \rangle + \gamma_L^6 \langle \mathcal{H}_{\rm x}^L / \rho_L^3 \rangle}{[(1-\xi_H)\gamma_H^3 \langle 1/\rho_H^2 \rangle + (1-\xi_L)\gamma_L^3 \langle 1/\rho_L^2 \rangle]}, \tag{159}$$

where $\mathcal{H}_{\rm x}^L$ and $\mathcal{H}_{\rm x}^H$ are chromatic invariants for the low energy ring and the high energy ring respectively. $(1-\xi_L)$ and $(1-\xi_H)$ are the horizontal damping partition numbers for the low energy ring and the high energy ring, respectively.

Using Eq. (153) and Eq. (159), we calculate the damped equilibrium energy spread and the emittance values for each rings in a dual energy ring. Our calculations show that the damped equilibrium parameters are dominated by the high energy ring. The damped equilibrium energy spread values at low energy ring and high energy ring are related by the following condition

$$\left(\frac{\sigma_E}{E}\right)_L \approx \left(\frac{\sigma_E}{E}\right)_H \times \frac{\gamma_H}{\gamma_L}. \tag{160}$$

The similar relationship is valid in the case of damped equilibrium emittance, i.e.,

$$\epsilon_x^L \approx \epsilon_x^H \times \frac{\gamma_H}{\gamma_L}, \tag{161}$$

where ϵ_x^L and ϵ_x^H are the horizontal damped equilibrium emittances for the low energy ring and the high energy ring, respectively. Hence damped equilibrium parameters in a dual energy ring is dominated by the high energy ring such that the low energy ring parameters are approximately equal to the high energy ring parameters multiplied by the energy ratio of the high energy ring to the low energy ring. Further, damped equilibrium emittance and energy spread values are obtained from ELEGANT particle tracking simulations and compared with the analytical calculations. Table 2 lists the values of equilibrium parameters with the beam energies of 150 MeV in the low energy ring and 1000 MeV in the high energy ring. Overall, the results show an agreement with 100 particles being used to extract the

TABLE 2: Equilibrium Parameters for LER = 150 MeV and HER = 1000 MeV.

	LER		HER	
Parameter	Analytical	Tracking	Analytical	Tracking
$\epsilon_x(\mu m)$	18.20	19.99	2.73	2.55
% Difference	9.83		6.59	
$\frac{\sigma_E}{E}(\times 10^{-3})$	3.03	3.28	0.454	0.509
% Difference	8.25		12.11	

damped parameters. The discrepancy is expected to be further reduced with more particles statistically. Here, the high energy ring energy is chosen to be 1000 MeV to increase the damping effect and hence save simulation time.

Further, we calculate the damped equilibrium emittance and energy spread in a dual energy storage ring with the low energy ring at 150 MeV and the high energy ring at 500 MeV. Table 3 lists the equilibrium parameters. Due to the limitation in simulation time, we calculate equilibrium parameters analytically.

4.4.3 DYNAMIC APERTURE

The dynamic or physical aperture is defined as the largest betatron oscillation amplitude, which is still stable in the presence of non-linear fields in a storage ring [7]. The Dynamic Aperture (DA) plays a significant role in the design of a storage ring which eventually determines the injection efficiency and beam lifetime. The strong focusing quadruples are used to design the ring optics that introduce chromatic aberrations. To compensate for these chromatic aberrations, we require strong sextupoles to be installed in the ring's dispersive region [42]. These strong sextupoles result in a small DA. Further explorations on the DA with different sextupoles distributions in a dual energy storage ring system were carried out. The maximum DA is obtained with sextupoles placed in both the low and high-energy rings to compensate for chromaticity [43]. The DA in a dual energy storage ring is calculated using numerically intensive procedures in ELEGANT. The DA for the LER at 150 MeV and the HER at 500 MeV is shown in Fig. 10.

TABLE 3: Equilibrium Parameters for LER = 150 MeV and HER = 500 MeV.

Parameter	Unit	LER	HER
Energy	MeV	150	500
Normalized horizontal emittance	μm	622	622
Normalized vertical emittance	μm	31	31
Un-normalized horizontal emittance ϵ_x	μm	2.12	0.635
Un-normalized vertical emittance ϵ_y	μm	0.106	0.0317
Energy spread σ_E/E	10^{-4}	7.4	2.2

The maximum DA possible is $\pm 8\sigma_x$ in the horizontal plane, and $35\sigma_y$ in the vertical plane for on-momentum particle, where σ_x and σ_y are the root means square (RMS) beam sizes in two planes, respectively.

4.4.4 MOMENTUM APERTURE AND TOUSCHEK LIFETIME

The Momentum Aperture (MA) is defined as the maximum momentum deviation that a particle can have without becoming unstable and being lost by colliding with the vacuum chamber of the storage ring [44]. The MA in a storage ring is determined by the complex 6-dimensional dynamics of the particle. In our dual energy storage ring, the MA is calculated using ELEGANT starting at the beginning of the Low Energy Ring (LER) and going to the end of the High Energy Ring (HER), as shown in Fig. 11. From Fig. 11, we can see that the LER momentum acceptance is bigger than the HER momentum acceptance. The reduction in MA for HER is due to the damping of beam phase-space through the RF acceleration from the LER [8], with the ratio of two energies [34]. In our design, both LER and HER are of equal length in circumference.

Touschek scattering is a phenomenon describing the collision of two electrons in a bunch with transferring a small momentum in the transverse direction into a large momentum in the longitudinal direction, leading to the loss of particles [45]. Based on the MA of the ring, Touschek lifetime is calculated both analytically and in simulation using ELEGANT. The

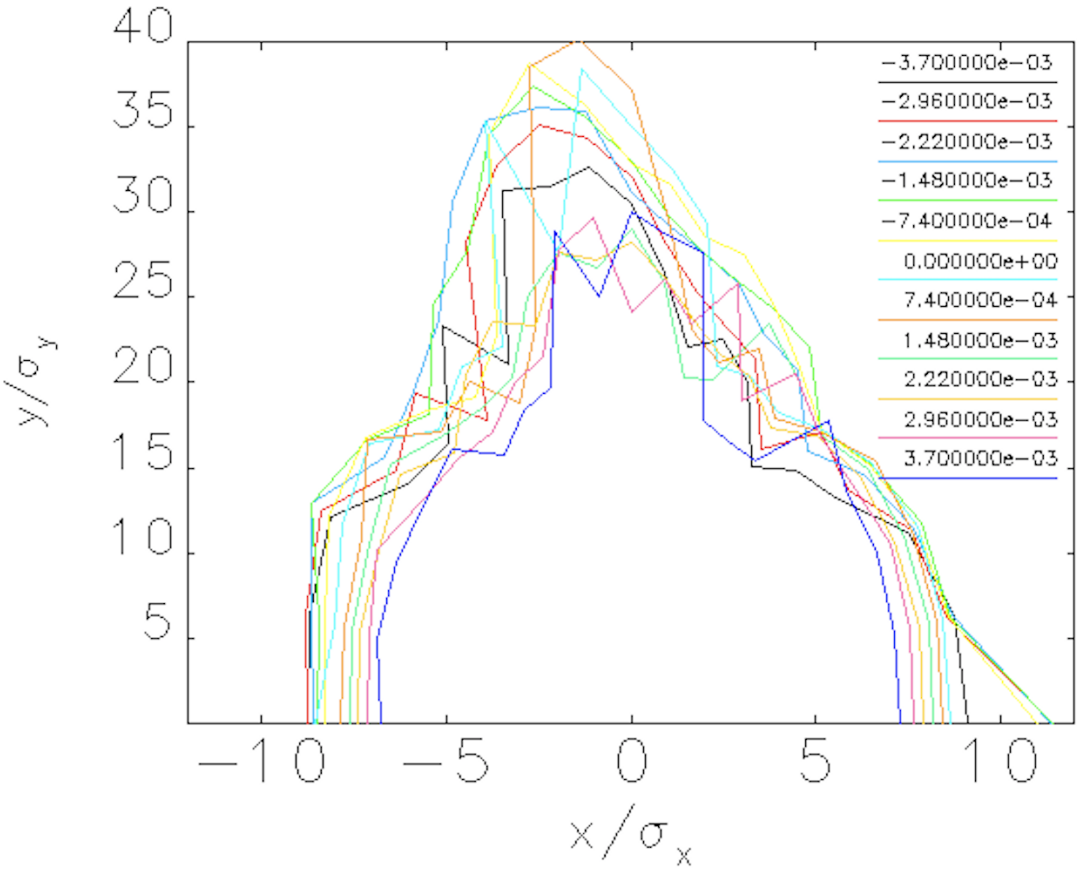

FIG. 10: DA for Low Energy Ring at 150 MeV and High Energy Ring at 500 MeV.

Touschek scattering rate α and the lifetime τ (where the lifetime is defined for the beam intensity to decay down half of its initial value) is given by [46]

$$\alpha = \frac{1}{\tau} = \frac{r_e^2 cq}{8\pi e\gamma^3 \sigma_s} \frac{1}{C} \oint \frac{F([\delta_{acc}(s)/\gamma\sigma_{x'}(s)]^2)}{\sigma_x(s)\sigma'_x(s)\sigma_y(s)\delta^2_{acc}} ds. \tag{162}$$

The integration in the formula above is along the circumference of the ring, where r_e is the classical electron radius, q is the bunch charge, σ_s is the RMS bunch length, C is the circumference of the ring, $\sigma_x(s)$ and $\sigma_y(s)$ are the RMS horizontal and vertical beam sizes including the dispersion terms, c is the speed of the light, e is the electronic charge, γ is the relativistic Lorentz factor of the beam, and $\delta_{acc}(s)$ is the local relative momentum acceptance along the ring respectively. The beam sizes $\sigma_x(s)$ and $\sigma_y(s)$ can be calculated

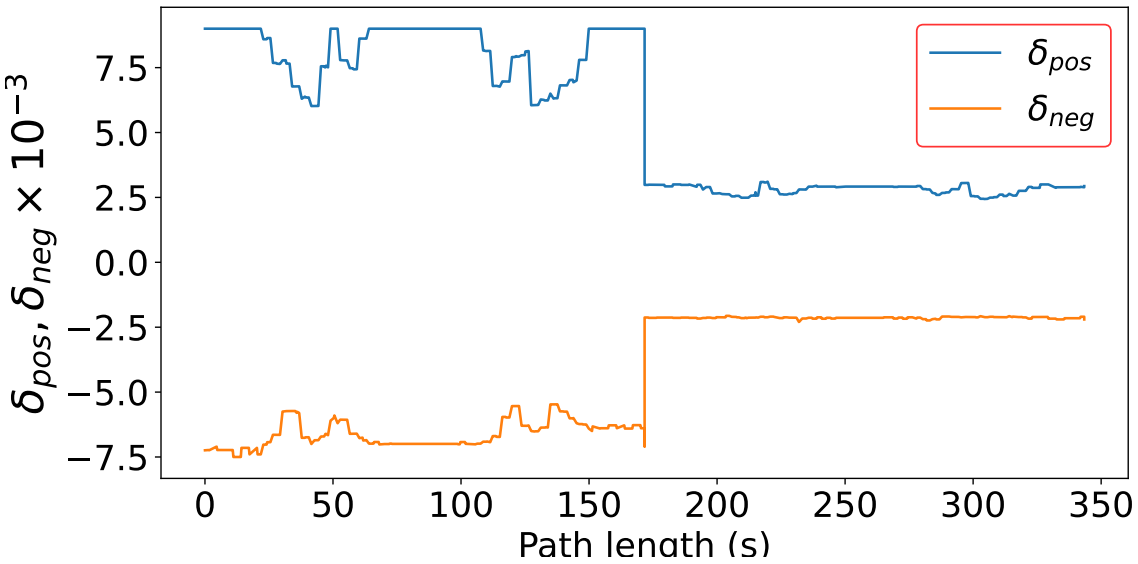

FIG. 11: Momentum Aperture for Low Energy Ring at 150 MeV and High Energy Ring at 500 MeV.

using the formula

$$\sigma_x(s) = \sqrt{\epsilon_x \beta_x(s) + (\sigma_\delta \eta(s))^2}, \tag{163}$$

$$\sigma_y(s) = \sqrt{\epsilon_y \beta_y(s)}, \tag{164}$$

with $\epsilon_x = \epsilon_{x0}/(1+\kappa), \epsilon_y = \kappa\epsilon_{x0}/(1+\kappa)$ and there is no vertical dispersion. Here ϵ_{x0} is the natural horizontal emittance, κ is the emittance coupling factor, η and η' are the horizontal dispersion and the slope of the horizontal dispersion respectively. The quantity $\sigma_{x'}(s)$ is the beam divergence which can be calculated using the formula

$$\sigma_{x'}(s) = \frac{\epsilon_x}{\sigma_x(s)} \sqrt{1 + \frac{\mathcal{H}(s)\sigma_\delta^2}{\epsilon_x}}, \tag{165}$$

where $\mathcal{H}(s)$ is the chromatic invariant given by

$$\mathcal{H}(s) = \gamma_x \eta^2 + 2\alpha_x \eta\eta' + \beta_x \eta'^2. \tag{166}$$

The special function $F(x)$ is defined by

$$F(x) = \int_0^1 (\frac{1}{u} - \frac{1}{2}\ln\left(\frac{1}{u}\right) - 1) \exp\left(-\frac{x}{u}\right) du. \tag{167}$$

The Touschek lifetime in a dual energy storage ring is obtained through $1/\tau = 1/(2\tau_{LER}) + 1/(2\tau_{HER})$, where τ_{LER} and τ_{HER} are the corresponding Touschek lifetimes for the LER and HER, respectively. Based on our calculation, the Touschek lifetime in a dual energy storage ring is dominated by the high energy ring. The Touschek lifetimes are presented in Table 4. Touschek lifetimes are calculated in a dual energy storage ring for the low energy ring at

TABLE 4: Touschek Lifetime in a Dual Energy Storage Ring.

Method	Touschek Lifetime (h)		
	τ_{LER}	τ_{HER}	Total
ELEGANT	0.67	0.43	0.42
Formula	0.68	0.34	0.34

150 MeV and the high energy ring at 500 MeV using ELEGANT and analytical formula. The lifetime values obtained from the analytical calculations and simulations, agree well. The number of particles in the bunch is 6.9 $\times 10^{10}$ and the RMS bunch length (σ_s) used in this calculation is 2.5 cm. The damped equilibrium emittance and energy spread values are used with the emittance coupling factor $\kappa = 0.05$. Touschek lifetime values obtained in a dual energy storage ring are shorter than expected. Further exploration on increasing the momentum acceptance to extend the Touschek lifetime is in progress.

4.4.5 LASLETT TUNE SHIFTS

This sub-section uses derivations to calculate the Laslett tune shift in a dual energy storage ring. The Laslett space-charge tune shift is the betatron tune shift for particles with small betatron amplitudes. Particles with large betatron amplitudes have a smaller space-charge tune shift; the small-amplitude tune shift dominates the large-amplitude one.

The following estimate shows that the small-amplitude tune shift is small. The equation of motion, including space charge, following reference [7] is

$$u\text{”} + \Big[k_0 - \frac{2r_c}{\beta^2\gamma^3}\frac{\lambda}{\sigma_x(\sigma_x+\sigma_y)}f_{\rm corr}\Big]u = 0, \tag{168}$$

where k_0 is the unperturbed focusing from the magnet lattice, and the second term is the space charge defocusing. $f_{\rm corr}$ is the correction factor due to image fields, and is defined by

$$f_{\rm corr} = 1 + \frac{2\sigma_y(\sigma_x+\sigma_y)}{b^2}\epsilon_1[1+(\gamma^2-1)B] + \epsilon_2(\gamma^2-1)\frac{b^2}{g^2}B, \tag{169}$$

where σ_x, σ_y are the RMS beam sizes, γ is the relativistic factor, B is the magnetic field, b, and g are the metallic and ferromagentic boundaries, respectively. The coefficients ϵ_1 and ϵ_2 are the Laslett form factors which are for infinite parallel plate vacuum chambers and magnetic poles defined by

$$\epsilon_1 = \pi^2/48, \qquad \epsilon_2 = \pi^2/24. \tag{170}$$

In the case of constant focusing and constant space charge defocusing, the total phase advance in radians is

$$\Delta\psi = \Big[k_0 - \frac{2r_c}{\beta^2\gamma^3}\frac{\lambda}{\sigma_x(\sigma_x+\sigma_y)}f_{\rm corr}\Big]^{1/2}L \cong \sqrt{k_0}L - \frac{r_c}{\beta^2\gamma^3\sqrt{k_0}}\frac{\lambda}{\sigma_x(\sigma_x+\sigma_y)}f_{\rm corr}L. \tag{171}$$

In the usual analysis of a single energy storage ring, tune is defined as $Q = L\times\sqrt{k_0}/2\pi$, and tune shift is given by

$$\Delta Q = -\frac{r_c}{2\pi\beta^2\gamma^3\sqrt{k_0}}\frac{\lambda}{\sigma_x(\sigma_x+\sigma_y)}f_{\rm corr}. \tag{172}$$

This result is derived for a single energy storage ring case. In a dual-energy storage ring, the total phase advance change is the sum of those over the low and high-energy rings. Hence the total change in phase advance is

$$\begin{aligned}\Delta\psi_{\rm tot} &= \Delta\psi_L + \Delta\psi_H = \sqrt{k_{\rm oL}}L_L + \sqrt{k_{\rm oH}}L_H \\ &- \frac{r_c}{\beta_L^2\gamma_L^3\sqrt{k_{0\rm L}}}\frac{\lambda_L}{\sigma_{\rm xL}(\sigma_{\rm xL}+\sigma_{\rm yL})}f_{\rm corr}L_L - \frac{r_c}{\beta_H^2\gamma_H^3\sqrt{k_{0\rm H}}}\frac{\lambda_H}{\sigma_{\rm xH}(\sigma_{\rm xH}+\sigma_{\rm yH})}f_{\rm corr}L_H.\end{aligned} \tag{173}$$

The unperturbed tune for the model is $Q = (\sqrt{k_{0\rm L}}L_L + \sqrt{k_{0\rm H}}L_H)/2\pi$, and the tune shift for one complete revolution is

$$\Delta Q = -\frac{r_c}{2\pi\beta_L^2\gamma_L^3\sqrt{k_{0\rm L}}}\frac{\lambda_L}{\sigma_{\rm xL}(\sigma_{\rm xL}+\sigma_{\rm yL})}f_{\rm corr}L_L - \frac{r_c}{2\pi\beta_H^2\gamma_H^3\sqrt{k_{0\rm H}}}\frac{\lambda_H}{\sigma_{\rm xH}(\sigma_{\rm xH}+\sigma_{\rm yH})}f_{\rm corr}L_H. \tag{174}$$

After performing a proper perturbation calculation, and following the results in Wiedemann 21.63 [7],

$$\Delta Q_{x,y} = -\frac{r_c}{2\pi}\oint\frac{\beta_{x,y}\lambda_L}{\beta_L^2\gamma_L^3\sigma_{\rm xL}(\sigma_{\rm xL}+\sigma_{\rm yL})}f_{\rm corr}dz - \frac{r_c}{2\pi}\oint\frac{\beta_{x,y}\lambda_H}{\beta_H^2\gamma_H^3\sigma_{\rm xH}(\sigma_{\rm xH}+\sigma_{\rm yH})}f_{\rm corr}dz, \tag{175}$$

where $\beta_{x,y}$ are the values of the beta-function for the unperturbed solution to Hill's equation for the ring. This calculation re-enforces the conclusion that the vertical emittance in the low energy ring should not be allowed to become too small. The linear particle density is defined by $\lambda_L = N_{\rm tot}/n_b\sqrt{2\pi}\sigma_z$, where $N_{\rm tot}$ is the total number of particles in the circulating beam, n_b is the number of bunches ($n_b = 1$), and σ_z is the standard bunch length for Gaussian distribution. The beam sizes are defined by $\sigma_{x,y} = \sqrt{\beta_{x,y}\epsilon_{x,y}}$, where $\epsilon_{x,y}$ represents the transverse emittances. Then the normalized beam emittance is defined by $\epsilon^N_{x,y} = \gamma\beta_{x,y}\epsilon^{rms}_{x,y}$, where γ is the relativistic energy factor.

Taking the first part of the above integral in Eq. (175) and solving, we get

$$-\frac{r_c}{2\pi}\int_0^{2\pi R}\frac{\beta_{x,y}\lambda_L}{\beta_L^2\gamma_L^3\sigma_{\rm xL}(\sigma_{\rm xL}+\sigma_{\rm yL})}f_{\rm corr}dz \approx -\frac{r_c}{2\pi\beta_L\gamma_L^2}\frac{N_b}{\sqrt{2\pi}\sigma_{\rm zL}}\frac{C_L}{\epsilon_y^N(1+\sqrt{\frac{\epsilon_x}{\epsilon_y}})}. \tag{176}$$

The total tune shift given by Eq. (175) is

$$\Delta Q_{x,y} \approx -\frac{r_c}{2\pi\beta_L\gamma_L^2}\frac{N_b}{\sqrt{2\pi}\sigma_{\rm zL}}\frac{C_L}{\epsilon_y^N(1+\sqrt{\frac{\epsilon_x}{\epsilon_y}})} - \frac{r_c}{2\pi\beta_H\gamma_H^2}\frac{N_b}{\sqrt{2\pi}\sigma_{\rm zH}}\frac{C_H}{\epsilon_y^N(1+\sqrt{\frac{\epsilon_x}{\epsilon_y}})}, \tag{177}$$

where CL and CH are the circumferences for the low and high energy rings, respectively. The Laslett tune shifts are estimated for each ring separately and the total tune shift is calculated which are presented in Table 5. These calculated values for the tune shifts are very minimal, and they are not significant enough to cause resonant detuning. We have used the standard RMS bunch length of 2.5 cm, and the number of particles used in this calculation is 6.9×10^{10}.

4.5 DUAL ENERGY STORAGE RING COOLER PARAMETERS

The cooling performance in a ring cooler highly depends on electron beam quality. The equilibrium electron beam parameters are calculated by considering the radiation damping and quantum excitation. Special care has been taken in lattice design to obtain the desired equilibrium electron beam to determine the cooling performance. The cooling simulation is performed with the electron beam parameters listed in Table 6.

The optics is designed for the low energy ring at 150 MeV and the high energy ring at 500 MeV. Both rings are identical, with the total circumference of 343.4 m. Table 6 has a ring circumference of 532.8 m after adding extra 60.0 m length in the cooling section at a low energy ring to run a cooling simulation. The average dipole bending radius is 2.55 m. The arcs are composed of standard FODO cells with a 90^0 phase advance. Chromaticities are

TABLE 5: Laslett Tune Shifts in a Dual Energy Storage Ring.

Energy (MeV)	150 (LER)	500 (HER)
Circumference C (m)	171.7	171.7
r_c	2.82e-15	2.82e-15
N_b	6.9e+10	6.9e+10
β	0.999	0.999
γ	293.54	978.47
RMS bunch length σ_z (m)	0.025	0.025
RMS Hori. Emittance ϵ_x (um)	2.12	0.635
RMS Vert. Emittance ϵ_y (um)	0.106	0.0317
Nor. Hori. Emittance ϵ_x^N (um)	622	622
Nor. Verti. Emittance ϵ_y^N (um)	31.1	31.1
ϵ_x/ϵ_y	20	20
Laslett tune shift	0.0057	0.00052
Laslett tune shift (whole ring)	0.0063	

corrected using two families of sextupoles distributed equally in both low and high-energy rings. A numerically intensive procedure in ELEGANT is used to calculate the dynamic aperture in a dual energy storage ring. The dynamic aperture is plotted in the horizontal and vertical planes in terms of beam sizes. The possible DA is $\pm 8\sigma$ in the horizontal, and 35σ in vertical, for on-momentum particle. These aperture values are good enough for the stability of charged particles. The Laslett space-charge tune shift value for the whole ring is 0.0063, which is a small value and is supposed not to alter the particles' betatron oscillation significantly. Based on the momentum aperture search, Touschek lifetime is calculated. The Touschek lifetime is less than an hour. To increase lifetime, we need to explore further the method of increasing momentum aperture in a dual energy storage ring. Intra-beam scattering (IBS) and synchrotron radiation (SR) damping times are calculated in all three dimensions. The damping times are shorter than the IBS times. It fulfills the requirement of an electron storage ring design to mitigate the emittance growth due to the IBS effect.

Table 6 and Table 7 lists the specific electron storage ring parameters, electron beam parameters, cooler parameters, RF parameters, and proton beam parameters. These parameters are used to calculate the ring parameters such as Touschek lifetime, IBS and SR damping times. The cooling section length has a 120 m solenoid magnet. For a 4.0 T solenoidal magnetic field, the matched β function in the cooler is 0.25 m. The RMS beam sizes are calculated taking matched β function and damped equilibrium emittance values obtained for the low energy ring. Transverse and longitudinal beam temperature at the cooler are calculated using the damped emittance and energy spread values. The details of the formulas used to calculate the beam temperatures are presented in Appendix B.

The RF parameters in a dual energy storage ring are calculated with high precision. First, the revolution time for each ring is calculated. The total revolution frequency is calculated taking the reciprocal of the sum of the revolution times for both rings. The RF frequency is 97.7 MHz, except in the third harmonic cavity which uses three times the RF frequency. A bunching cavity with a small voltage of 80 V running on 180^0 provides additional longitudinal focusing in the system. ELEGANT simulations show that smaller the bunching cavity voltage, the longer the bunch length possible. A compensating cavity running on 90^0 phase with RF voltage 1643 V is used to compensate for the energy loss due to synchrotron radiation.

TABLE 6: Parameters in a Dual Energy Electron Storage Ring Cooler.

Storage Ring Parameters	Value
Low energy ring energy [MeV]	150
High energy ring energy [MeV]	500
Total ring circumference [m]	532.8
Natural chromaticity h/v	-16.17/-24.70
Corrected chromaticity h/v	1.0/0.87
Dipole bending radius [m]	2.55
On-momentum dynamic aperture h/v	$\pm 8\sigma/35\sigma$
Betatron tune h/v	11.131/9.227
Phase advance of FODO arc [radians]	$\pi/2$
Space charge tune shift	0.0063
Touschek lifetime [hour]	0.68
IBS time h/v/l [s]	5.07/1.3E4/0.49
SR damping time h/v/l [s]	3.19/0.68/0.25
Electron Beam Parameters	
Bunch intensity	6.9×10^{10}
Bunch charge [nC]	11.1
Peak bunch current [A]	52.9
Average bunch current [A]	1.08
RMS bunch length [cm]	2.5
FWHM bunch length [cm]	5.8
Energy loss per turn [keV]	1.643
Synchrotron power [kW]	1.774
RF Parameters	
RF frequency [MHz]	97.7
Main cavity voltage, phase [MV, degree (a/d)]	393.75, 90/270
Harmonic cavity voltage, phase [MV, degree (a/d)]	43.75, 270/90
Compensating cavity voltage, phase [kV, degree]	1.643, 90
Bunching cavity voltage, phase [V, degree]	80, 180

h/v/l for horizontal, vertical and longitudinal dimensions.

a/d for accelerating/decelerating

TABLE 7: Proton and Electron Beam Parameters at Cooler.

Electron Beam Parameters @ Cooler	Value
Average β function in the cooling section h/v [m]	0.25/0.25
Normalized emittance h/v [μm]	622/31.1
Emittance coupling (κ)	0.05
Energy spread @ cooler [10^{-4}]	7.4
RMS beam size h/v @ cooler [mm]	0.74 /0.16
Transverse temperature @ cooler [eV]	9323.87
Longitudinal temperature @ cooler [eV]	0.2798
Cooling channel length [m]	120
Cooling solenoid [kG]	40
Proton Beam parameters	
Proton energy [GeV]	275
Relativistic factor γ	293.1
Bunch intensity	6.9×10^{10}
Bunch charge [nC]	11.1
Normalized emittance h/v [μm]	2.8/0.45
Energy spread [10^{-4}]	6.6
RMS bunch length [cm]	6.0
RMS beam sizes h/v [cm]	0.17/0.043
IBS time h/v/l [h]	2.6/3.7/4.1
Cooling time h/v/l [h]	0.65/1.38/1.5

CHAPTER 5

COOLING PERFORMANCE

Until now, we discussed the beam dynamics in a dual energy storage ring and explored the stability criteria. This chapter mainly discusses the cooling performance in a dual energy storage ring cooler. The cooling performance is simulated using Jefferson Lab Simulation Package for Electron Cooling (JSPEC) for proton beams at the top energy of 275 GeV for the Electron-Ion Collider.

5.1 INTRODUCTION

A collider experiment requires high density and low energy spread particle beams to obtain high luminosity. Light particle beams, for example, those of electrons undergo synchrotron radiation damping. However, heavy particle beams like the proton and heavy ions do not have a significant radiation damping effect and they need some mechanism to get compressed. *Electron cooling* is an established method that can suppress or reverse the beam emittance growth and increase both peak and average luminosity [47].

The theory of electron cooling is based on the friction force that results from the relative motion of ions immersed in an electron beam. In a straight cooling section, the ion and electron beams co-propagate with the same average velocities. The cooled electron beam and the hot ion beam can be considered as two thermodynamics systems. According to the second law of thermodynamics, heat transfer occurs between a system at a higher temperature to a system at lower temperature till there exists an equilibrium temperature. In the end, the cooled ion beam is extracted and directed toward the collision point or interaction point in a collider where it collides with other particles. In a dual-energy ring cooler, the electron beam in the electron storage ring is reused after it completes the cooling interaction with the ion beam.

5.2 CONCEPT OF BEAM TEMPERATURE

According to thermodynamics, the temperature measures the average kinetic energy of the atoms or molecules in the system. The distribution of particles in a beam can be explained by thermodynamic-like velocity distribution. Hence, one can assign a temperature to the

ensemble of beam particles and relate them to the velocity fields of phase-space coordinates. To cool means to reduce the beam temperature.

A velocity-dependent drag force is involved during the cooling process; hence, the process is non-Liouvillean. There are many factors to heat the beam in an accelerator. Some factors are beam mismatch, space charge, intra-beam scattering, residual gas, and external noise. In general, the transverse beam temperature $T_\perp$ and the longitudinal beam temperature $T_\parallel$ in the beam rest frame are defined by [27]

$$\begin{aligned} T_\perp &= m_e V_\perp^2 \gamma^2 = m_e c^2 \frac{\varepsilon_L}{\beta_s}\gamma^2, \qquad V_\perp^2 = V_x^2 + V_y^2. \\ T_\parallel &= m_e c^2 \left(\frac{\Delta p}{p}\right)^2, \end{aligned} \tag{178}$$

where γ is the relativistic energy factor, $m_e c^2$ is the rest mass energy of an electron, β_s is matched Twiss beta function in the cooler, $V_\perp$ is the transverse velocity, ε_L is the un-normalized Larmor emittance defined by $\varepsilon_L = V_\perp^2 \beta_s / c^2$, and $\Delta p/p$ is the equilibrium energy spread. The above temperatures are defined in the case of magnetized electron cooling.

5.3 BEAM COOLING

5.3.1 COOLING RATES

The heat exchange between the electron beam and ion beam occurs until they reach to the same equilibrium temperature. This heat exchange via Coulomb's scattering occurs continuously, defined by the cooling rates. In the case of non-magnetized cooling, the cooling rate is defined by [48]

$$\frac{1}{\tau_{\text{cool}}} = \frac{3\pi Z^2 r_i r_e c n_e \Lambda_c}{\sqrt{2}\gamma^2 \left[2\left(kT_e/m_e c^2\right)^{3/2} + \left(kT_i/m_i c^2\right)^{3/2}\right]} \times \frac{L_c}{C_i}, \tag{179}$$

where m_i, Z, r_i and T_i are the mass, charge, classical radius, and temperature of the ions, and m_e, r_e, T_e, and n_e are the mass, classical radius, temperature, and the density of cooling electrons. The quantity Λ_c is the Coulomb logarithmic cut-off term, and chosen to be $\Lambda_c = 20$ in the cooling simulation in a dual energy storage ring cooler. The ratio of cooling channel length to the total circumference of the ion ring is given by the term L_c/C_i and the total cooling rate is affected by this ratio. From Eq. (179), it is clear that the cooling rate has a linear dependence on electron beam intensity n_e, and cooler length L_c/C_i, favorable for highly charged ions Z^2, slow for hot ion beams, and decreases with energy as γ^2.

To get best cooling rates, it is important that the transverse cross-sections of the electron beam and ion beam completely overlap with each other. Partial overlapping results in reduced cooling. The energy term γ^2 in the denominator comes from the cooling force formula, which is based on the exchanges of momenta in all directions in the rest frame of the electron and ion beams. Taking laboratory frame as a reference frame, the cooling rate receives one γ from time dilation and another one from the electron density as a result of Lorentz transformation. This γ^2 term being in the denominator highly affects the cooling rates and it takes significantly longer to cool the ion beams with electron beams at high energy. Even so, reasonable cooling rates can be achieved by increasing the electron-beam density n_e to a great extent.

5.3.2 COOLING FORCES

Several friction forces are proposed to explain the kinetics of electron cooling of beams in the heavy particle storage ring [49–51]. The effectiveness of the friction force increases if the relative velocity between electron beam and ion beam is small. The drag force between electron and ion beams are based on the binary collision model. Due to Coulomb interaction between ion and electron beam the momentum and energy exchange takes place which is logarithmically divergent in the region of large impact parameter. The calculation of non-magnetized friction force experienced by an ion moving with electron beam in the cooler section is explained in reference [51].

A strong magnetic field is applied along the longitudinal direction inside the cooler in magnetized cooling. This causes the electron motion to follow a spiral trajectory around the magnetic field line. In the magnetized electron beam, when the maximum impact parameter is larger than the radius of the electron Larmor rotation, so-called "magnetized collisions" between the ion and electron take place. In this case, the electron beam is attracted by the ion, which pulls it along the magnetic field line. Depending on the different ranges of the ion velocity and impact parameter compared with the radius of electron Larmor rotation, the collisions can be classified into three categories: fast, adiabatic, and magnetized [49, 50].

5.3.3 INTRABEAM SCATTERING

Intrabeam scattering (IBS) in the ion beam enhances diffusion growth of 6D phase space volume of the ion beam. The IBS calculation is based on the momentum variation due to Coulomb interactions with other particles in the beam. There are several models for IBS calculation. Besides the Martini model [52], the Bjorken-Mtingwa (BM) model [39] is another

widely used model for the IBS expansion rate calculation. During the cooling simulation in the case of magnetized cooling, we use BM model for the IBS expansion rate calculation in a dual energy storage ring cooler. Using BM model, the IBS expansion rate of a beam with Gaussian distribution can be calculated using the following formula

$$\frac{1}{\tau_d} = A\Big\langle \int_0^\infty \frac{d\lambda\lambda^{1/2}}{[|L+\lambda I|]^{1/2}} \Big\{ \mathrm{Tr}L^d \mathrm{Tr}\Big(\frac{1}{L+\lambda I}\Big) - 3\mathrm{Tr}L^d\Big(\frac{1}{L+\lambda I}\Big)\Big\}\Big\rangle, \tag{180}$$

where $d = x, y, l$, I is the identity matrix, the angle bracket as a whole is taken to average over the storage ring. For a bunched beam the term A is defined as

$$A = \frac{cr^2 N L_c}{8\pi\beta^3\gamma^4\epsilon_x\epsilon_y\sigma_p\sigma_s}, \tag{181}$$

where c is the speed of the light, r is the classical radius of the ion, N is the number of ions, β, γ the relativistic Lorentz factor, ϵ_x, ϵ_y the horizontal and vertical emittance, σ_p is the rms momentum spread, and σ_s the rms bunch length. L is defined by

$$L = L^{(x)} + L^{(y)} + L^{(z)}, \tag{182}$$

with

$$\begin{aligned} L^{(x)} &= \frac{\beta_x}{\epsilon_x}\begin{pmatrix} 1 & 0 & -\gamma\phi_x \\ 0 & 0 & 0 \\ -\gamma\phi_x & 0 & \gamma^2 H_x/\beta_x \end{pmatrix} \\ L^{(y)} &= \frac{\beta_y}{\epsilon_y}\begin{pmatrix} 0 & 0 & 0 \\ 0 & 1 & -\gamma\phi_y \\ 0 & -\gamma\phi_y & \gamma^2 H_y/\beta_y \end{pmatrix} \\ L^{(z)} &= \frac{\gamma^2}{\sigma_p^2}\begin{pmatrix} 0 & 0 & 0 \\ 0 & 0 & 0 \\ 0 & 0 & 1 \end{pmatrix}, \end{aligned} \tag{183}$$

where $\beta_{x,y}$ is the horizontal or vertical Twiss functions and $\phi_{x,y}$ and $H_{x,y}$ are defined as

$$\phi_{x,y} = D'_{x,y} - \frac{\beta'_{x,y} D_{x,y}}{2\beta_{x,y}}, \text{and} \quad H_{x,y} = \frac{D^2_{x,y} + \beta^2_{x,y}\phi^2_{x,y}}{\beta_{x,y}}. \tag{184}$$

In the above expression $D_{x,y}$ and $D'_{x,y}$ are dispersion and dispersion slope in horizontal and vertical directions respectively.

5.3.4 PROTON BEAM PARAMETERS

Similarly to the electron ring lattice, the hadron ring lattice design is carried out to get the desired hadron beam parameters in a collider experiment. After the hadron ring lattice is designed, beam dynamics studies provide the emittance, dynamic aperture, beam lifetime, and stability. In particular, the beam size and intensity at the location of the electron cooler are obtained. The cooling simulation is carried out for 275 GeV proton beam at the Relativistic Heavy Ion Collider (RHIC) ring. Its Twiss parameters are used to run the JSPEC simulation. The proton beam parameters are listed in Table 8, taken from reference [1].

TABLE 8: Proton Beam Parameters.

Proton energy [GeV]	275
Relativistic factor γ	293.1
Bunch intensity	6.9×10^{10}
Bunch charge [nC]	11.1
Normalized emittance h/v [μm]	2.8/0.45
Energy spread [10^{-4}]	6.6
RMS bunch length [cm]	6.0
RMS beam sizes h/v [cm]	0.17/0.043
Cooling channel [m]	120
Cooling solenoid [kG]	40

5.4 COOLING PERFORMANCE

This section presents the summary of the cooling performance to cool a 275 GeV proton

beam in EIC, as determined using the JSPEC simulation code. Cases both with and without dispersion at the cooler have been calculated. The asymptotic formula by Meshkov [53] is used to calculate the friction force between electron and proton beams. The details of the theory of interactions of heavy particles with magnetized electron beam are presented in [49–51, 53].

5.4.1 COOLING SIMULATION

In the absence of cooling, the IBS heating effect for the proton beam is very large in both horizontal and longitudinal planes, as shown in Fig. 12. The need to keep control of the proton horizontal emittance and energy spread against this IBS heating demonstrates the need for strong cooling at EIC both in the horizontal and longitudinal planes.

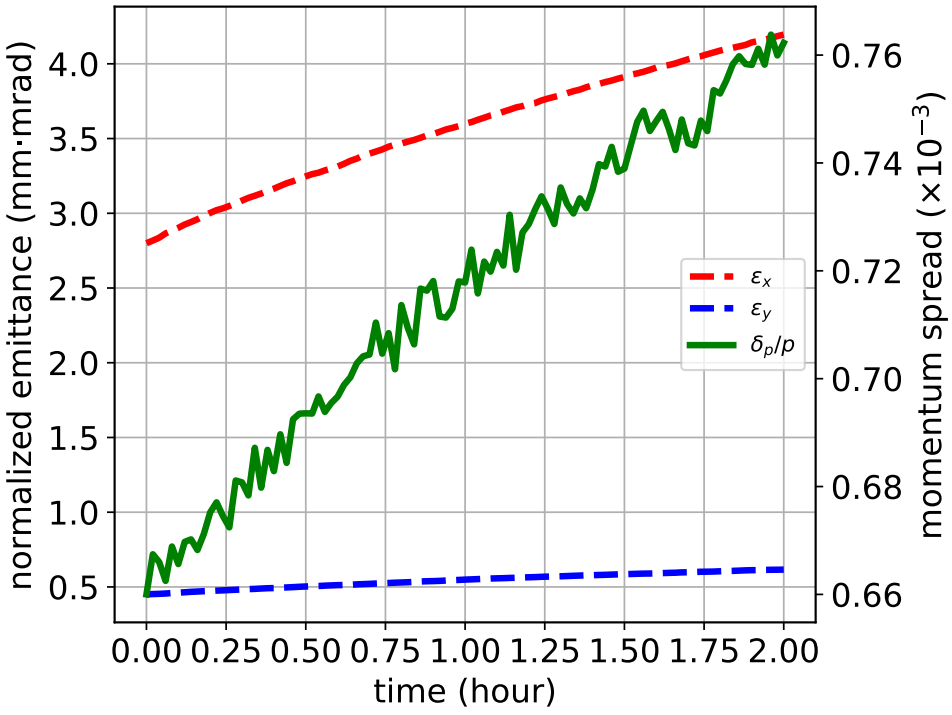

FIG. 12: Emittance Growth of 275 GeV Proton Beam Caused by the IBS Effect in the Absence of Cooling.

Simulations show that almost no transverse cooling is observed in the absence of dispersion in the cooling section. However, strong longitudinal cooling is observed due to the large difference in cooling gradients. When a horizontal dispersion $D_x = 2.5$ m and vertical dispersion $D_y = 0.5$ m are included in the cooling section for the ion beam, the cooling rates between the horizontal and longitudinal direction [49, 54] are redistributed. The introduction of dispersion in the cooling section greatly enhances transverse cooling.

Table 8 shows the proton beam parameters used to run JSPEC simulation. Table 9 lists electron cooling times and proton IBS times. Cooling times in all three dimensions are shorter than the IBS times. The simulation calculations show that a 275 GeV proton beam can be cooled with a 150 MeV electron beam with in the given cooling times presented in Table 9. Figure 13 shows the evolution of the proton beam transverse and longitudinal emittance with cooling. In the absence of dispersion, there is no cooling effect in the horizontal but a strong cooling in the longitudinal direction. When we introduce the dispersion $D_x = 2.5$ m and $D_y = 0.5$ m in the cooler, there exists a strong cooling both in transverse and longitudinal directions.

5.4.2 PROTON BEAM PHASE SPACE

To see the cooling effect more clearly, we plot the initial and final proton beam phase-space as simulated by JSPEC. Figure 14 shows clearly that the proton beam phase-space density is increased after the cooling effect in all six-dimensions.

5.4.3 RATES CALCULATION

JSPEC simulation calculates the initial IBS rate, electron cooling rate, and total expansion rate. These rates are listed in Table 9. Initial IBS rates are smaller compared to the initial electron cooling rates in all three directions. It means electron cooling times are shorter than proton IBS times. The total expansion rate is negative. It indicates that the electron cooling effect dominates the proton IBS growth rate. The variation of IBS, electron cooling, and total expansion rates during JSPEC simulation is plotted in Fig. 15.

5.5 COOLING OF LOW ENERGY PROTON BEAMS

We further run the JSPEC cooling simulation for a 100 GeV proton beam, which requires cooler ring energy to be 55 MeV. Damped equilibrium emittance and energy spread values are calculated for 55 MeV electron beam energy in the cooler ring. Electron beam sizes,

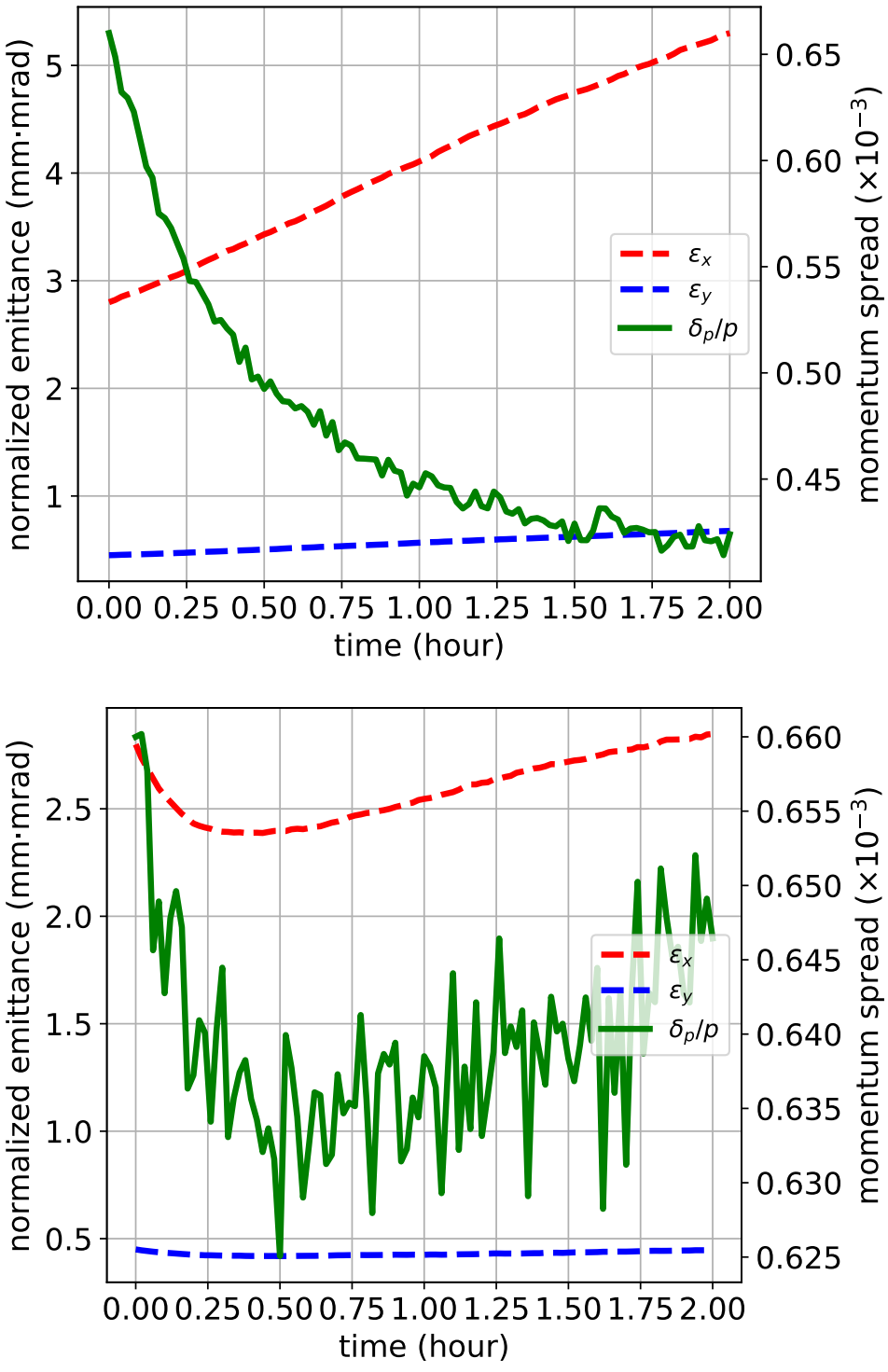

FIG. 13: The Evolution of the Horizontal (ε_x), Vertical (ε_y) and Longitudinal (δ_p/p) Proton Beam Emittance During Cooling. Upper Plot: $D_i = 0$ m; Bottom Plot: $D_x = 2.5$ m, $D_y = 0.5$ m and IBS Coupling Factor = 0.2.

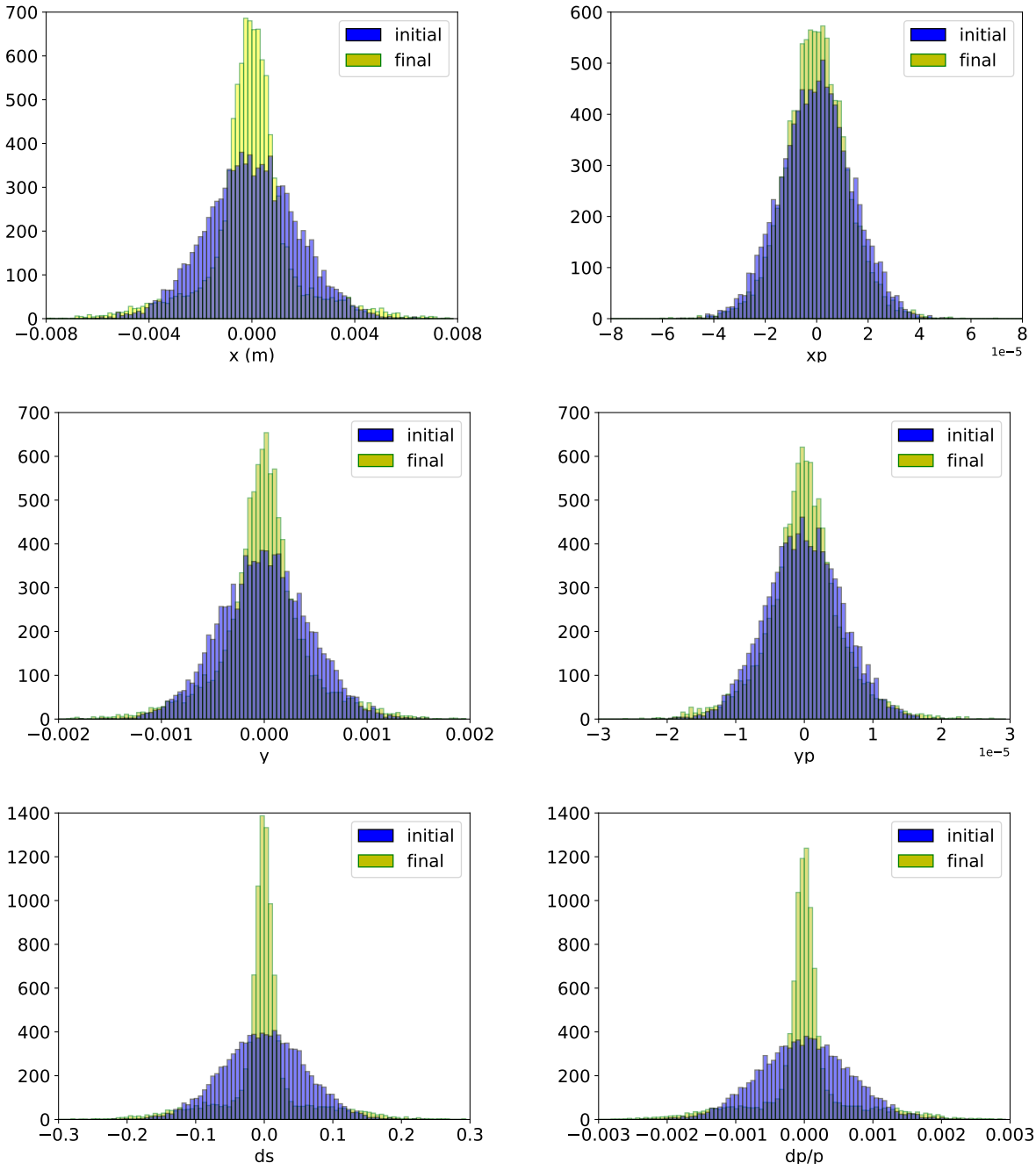

FIG. 14: Initial and Final Proton Beam Phase-space.

TABLE 9: Rates and Time Calculations.

Parameter	Horizontal	Vertical	Longitudinal
IBS rate (1/s)	1.063E-04	7.437E-05	6.810E-05
Electron cooling rate (1/s)	-4.076E-04	-2.016E-04	-1.897E-04
Total expansion rate (1/s)	-3.012E-04	-1.272E-04	-1.216E-04
IBS time (h)	2.6	3.7	4.1
Cooling time (h)	0.65	1.38	1.5

transverse, and longitudinal temperatures are calculated based on those damped equilibria parameters. Proton beam parameters for a 100 GeV case are taken from EIC-CDR [1]. Simulations show that no cooling is observed and the proton beam emittance growth takes place in all three dimensions. It requires further studies to understand the hadron beam cooling at lower energies.

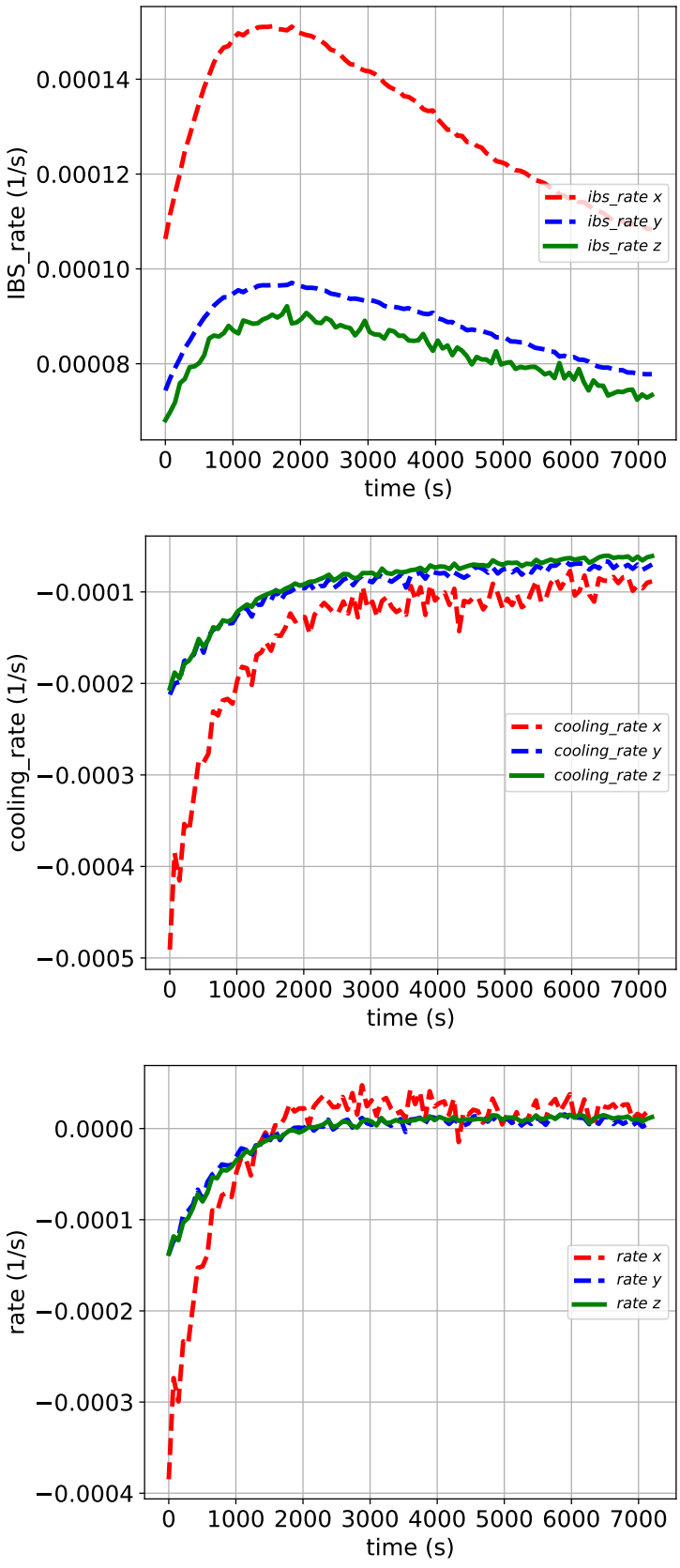

FIG. 15: IBS, Cooling, and Total Expansion Rates.

CHAPTER 6

CONCLUSIONS

The main goal of studying a dual energy storage ring cooler design was to explore the possibilities on storage ring based cooler design to cool the hadron beams in collider experiments. This dissertation is divided into two parts. The first part of this dissertation presents the optics design and beam dynamics studies in a dual energy storage ring. The second part of the dissertation presents the cooling performance to cool the 275 GeV EIC proton beam.

From scratch, the optics design of such a storage ring based cooler is carried out using the MAD-X software package. Particle tracking simulation is carried out using ELEGANT particle tracking simulation code. Numerical calculations were performed using PYTHON and MATHEMATICA software packages. After the optics design is completed, single and many particle tracking simulations were performed using ELEGANT particle tracking. Dynamic aperture and momentum aperture calculations were carried out using a numerically intensive procedure in ELEGANT. Based on the momentum aperture, the Touschek lifetime is calculated for each ring and the whole ring both analytically and in simulation using ELEGANT.

Furthermore, the damped equilibrium emittance and energy spread of an electron beam in a dual energy storage ring are estimated based on newly derived formulas. Equilibrium is achieved with a balance between radiation damping, quantum excitation, and intra-beam scattering (IBS). Since the radiation damping effect dominates the IBS effect, we calculate the damped equilibrium emittance and energy spread considering the radiation damping and quantum excitation only. We derived the new formulas for damped equilibrium emittance and energy spread for the first time. Damped equilibrium parameters are obtained from analytical calculations and compared to tracking simulations with low energy ring at 150 MeV and high energy ring at 500 MeV, respectively.

Electron beam temperatures were calculated based on the damped equilibrium parameters in a dual energy storage ring. Using these parameters, cooling simulations were performed using the JSPEC simulation codes. The RHIC lattice is being used, and 275 GeV proton beam parameters were taken from the EIC-CDR. Cooling simulations were performed considering different cases of dispersion and IBS effects in the cooler section for the proton

beam. Cooling performance shows that the dual energy storage ring cooler may provide a feasible path to cool the hadron beams at higher energy, eventually improving the collider performance with higher luminosity. The cooling performance of a two-energy ring has better damped parameters than for Brookhaven's single energy ring design. The JSPEC simulation shows that 275 GeV proton beam emittances are under better control than Brookhaven's single energy cooling simulation results.

6.1 FUTURE WORKS

In this thesis, we have not answered all questions concerning two-energy ring stability. In the future, we suggest working on the following topics. For example, the beam optics can perhaps be better optimized, HOM studies should be undertaken, and identifying the potential issues such as CSR and beam-break up should be studied and solved. We are also exploring the possible applications of dual energy storage ring design besides beam cooler design.

6.1.1 OPTICS OPTIMIZATION

It may be possible to change the beam optics in our dual energy storage ring to get better cooling performance. This dissertation summarizes the dual energy storage ring design for the specific case of a low energy ring at 150 MeV and the high energy ring at 500 MeV. The low energy ring at 150 MeV is chosen for the cooling requirement of hadron beam energy at 275 GeV. The high energy ring at 500 MeV is chosen to get the sufficient synchrotron radiation damping. Further optics study should be carried out to study whether this design can be used to cool the hadron beam at lower energies, say 100 GeV or 41 GeV.

In the future, optics optimization should be carried out including emittance coupling in the design directly. We calculated the damped equilibrium horizontal emittance and take 5% coupling to get the vertical emittance. ELEGANT particle tracking simulations to calculate equilibrium beam parameters do not introduce coupling.

6.1.2 HOM STUDIES

In a dual energy storage ring cooler, SRF cavities are used to accelerate or decelerate the high average current and high bunch charge beams. Different eigenmodes of frequencies are excited when the beam passes through these cavities. Higher order modes (HOM) are parasitic eigenmodes with frequencies higher than that of the fundamental operating mode.

HOMs are one of the dominating factors that need to be considered in designing high-current cavities. These modes can limit the performance and operation of SRF cavities. In general, multi-pass multi-bunch instabilities are driven by high impedance dipole modes, resulting in the beam breakup. Further power loss into the HOMs must be removed from these SRF cavities. The future work involves identifying and investigating possible trapped HOM modes that might result in multi bunch instabilities in a dual energy storage ring cooler.

6.1.3 IDENTIFY POTENTIAL ISSUES

Some possible potential issues such as coherent synchrotron radiation (CSR) and beam-break up studies should be carried out. CSR eventually leads towards the collective instabilities and may affects the operation of the electron storage ring. Future work involves studying such effects in a dual energy storage ring.

6.1.4 POSSIBLE APPLICATIONS OF A DUAL ENERGY STORAGE RING

A dual-energy electron storage ring configuration was initially proposed as an electron cooler to cool the ion beam in a collider. In this novel configuration of a dual energy storage ring, an energy recovery linac structure is a sandwich between two rings that continuously accelerates and decelerates the electron beam. Such a configuration may have various applications in the field of accelerator science. A dual energy storage ring design concept can be used for the following applications [55]:

- Electron cooler for hadron beam cooling at high energy.
- Ultra-short bunches for light source applications.
- Compton source of radiation
- Fundamental studies such as Electric Dipole Moment (EDM) search, dark matter search, low-energy electron physics, and figure-8 ring test.
- Test of beam-beam effects with both co- and counter-propagating beams with interesting beam-beam tune shifts.
- Tests of cryomodules, HOM couplers, and crab cavities at high currents.
- Isotope production test.
- Positron production tests and low – energy positron physics and applications.

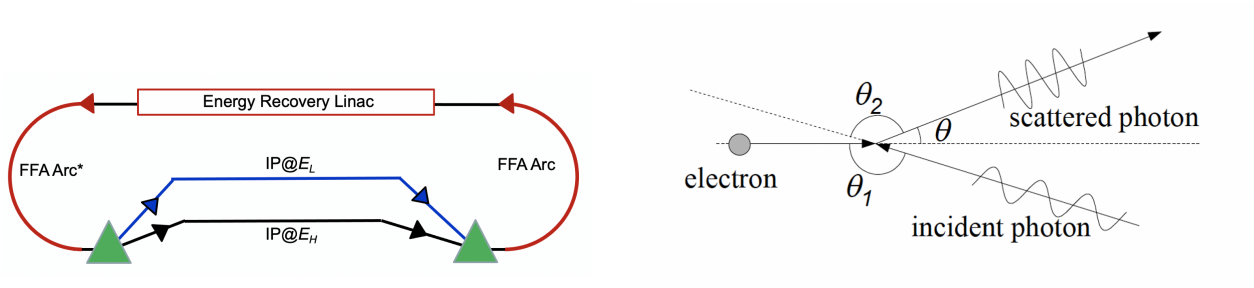

FIG. 16: Schematic Drawing of a Dual-Color Compton Light Source (Left) and Compton Scattering Process (Right).

- Serve as a driver beam for tests of a plasma afterburner.

Among the above-listed possible applications based on a dual energy storage ring configuration, we briefly discuss two possible applications: a dual-color Compton light source and electric dipole moment measurement.

When a relativistic electron beam interacts with a high-field laser beam, intense and highly collimated electromagnetic radiation will be generated through Compton scattering. This process generates highly energetic polarized photons along the electron beam motion [56]. Because the intense radiation is produced with desirable properties, many Compton light source facilities worldwide exist. We propose a new design concept for Compton light sources based on a dual energy storage ring. The schematic drawing of a dual-color Compton light source is shown in Fig. 16. In this design concept, an ERL is used to accelerate and decelerate the beam at two different energies: E_L for the low energy loop and E_H for the high energy loop respectively. Fixed Field Alternating Gradient (FFA) optics is used in the arc design since the FFA arcs are able to contain beams of significantly different energies [57]. Due to different beam rigidity, low energy electron beam bends more and moves along the path indicated by solid blue line whereas high energy electron beam bends less and moves along the solid black line. A high-power laser incident at Interaction Point (IP) interacts with an electron beam and undergoes Compton scattering. As a result, high-energy X-ray radiation is produced. The theory of Compton scattering of a laser photon by a relativistic

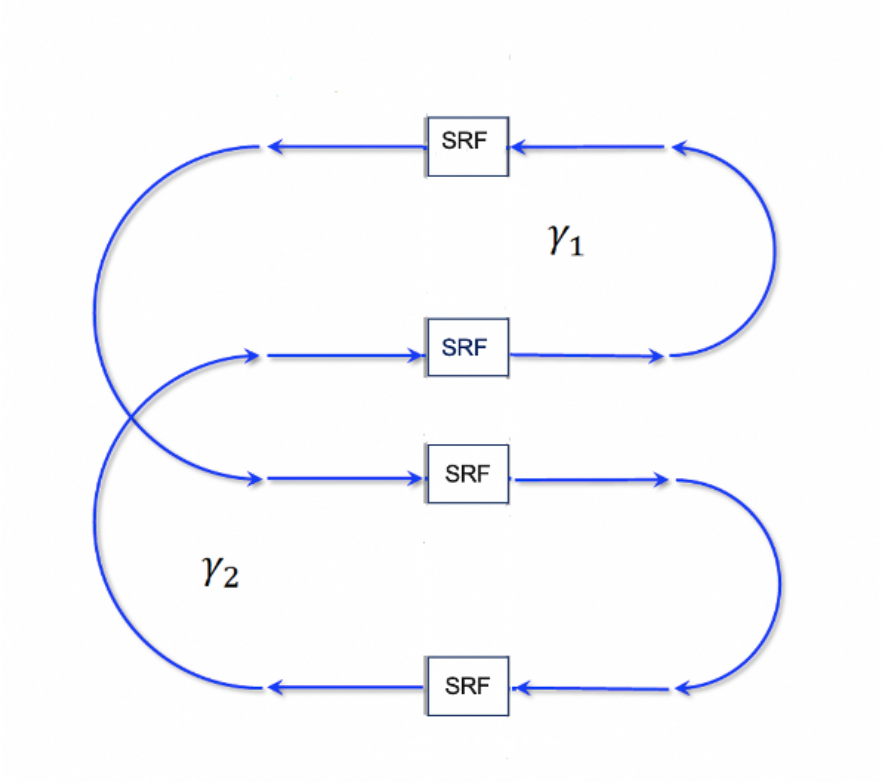

FIG. 17: Layout of a Dual Energy Storage Ring for Measuring the Electron Electric Dipole Moment.

electron is discussed in [58]. The great advantage of this dual-color Compton light source design is that it can provide two beams with different photon energies for one experiment.

A dual-energy storage ring design can be used to perform experiments to measure the permanent Electric Dipole Moment (EDM) of the electron relevant to CP violation and matter-antimatter asymmetry in the universe and to search for dark energy and ultra-light dark matter. The simplest layout design of a ring for measuring the electron EDM is presented in Fig. 17 [59]. A dual energy storage ring in Fig. 17 is configured in the figure-8 spin transparency mode so the net bend at each energy is zero. This eliminates the spin precession due to the Magnetic Dipole Moment (MDM). SRF cavities accelerate and decelerate the

electron beam going from the low energy ring to the high energy ring and vice-versa. The beam directions in the two arcs of each energy are opposite to one another, making the net bending angle zero. This principle is equally applicable to hadron beams. However, while electrostatic acceleration and deceleration may be sufficient for electrons, hadron beams require a more significant energy difference that an electrostatic field cannot provide. Such a significant energy difference may be achieved using Energy Recovering Linacs (ERLs).

The optics design of such a ring system to measure the EDM must provide a high efficiency in terms of the EDM spin rotation rate, a long spin coherence time, adequate momentum acceptance and dynamic aperture, low emittance growth rates due to Intra-Beam Scattering (IBS), and acceptable stored beam size. Since there is a change in the bending direction between the adjacent arcs, each arc must be achromatic.

The dispersion can be suppressed in each arc by varying the bending direction within the arc, keeping its net bend fixed at 180°. This allows for an achromatic weak-focusing arc design with constant horizontal and vertical focusing strengths [60]. A conventional Mott polarimeter can be used to measure the electron beam polarization in the energy range from a few keV to a few MeV. The principle of Mott polarimetry and the experimental procedure to measure the electron EDM are discussed in [61]. The SRF structure in this design has time-varying magnetic fields accompanying the oscillating electric fields. The effect of these magnetic fields on the spins requires further study.

6.1.5 EFFICIENCY IN A DUAL ENERGY STORAGE RING COOLER

Next consider a dual energy storage ring cooler as a heat pump. The electron beam temperature in such a cooler arises from the radiative equilibrium formed between quantized emission and radiation damping in the ring. The RF system provides the operating energy to the beam by acceleration. The work on each electron, per pass, exactly balances the amount of radiation it emits. The following thermodynamics argument is applicable in a dual energy storage ring cooler.

In the cooler, the electrons pick up heat ΔQ from the ion beam at temperature T_{cool}. The entropy change in the electron beam is $\Delta Q/T_{\text{cool}}$. This entropy change causes a slight temperature (emittance) increase in the electron beam. Suppose the average temperature the beam radiates the heat away is T_{rad}. For the same amount of entropy to leave the electron beam $\Delta Q_{\text{rad}} = (T_{\text{rad}}/T_{\text{cool}})\Delta Q$, and the difference $\Delta Q_{\text{rad}} - \Delta Q = W$ is the additional work needed to run the cooler [62]. The work done W_{cooler}, and efficiency $\varepsilon_{\text{cooler}}$ of such a cooler

is defined by

$$W_{\text{cooler}} = \left(\frac{T_{\text{rad}} - T_{\text{cool}}}{T_{\text{cool}}} \right) \Delta Q, \rightarrow \varepsilon_{\text{cooler}} = \frac{T_{\text{cool}}}{T_{\text{rad}} - T_{\text{cool}}}. \tag{185}$$

Based on the analysis of the Carnot cycle, the efficiency ε of a refrigerator or heat pump cannot exceed

$$\varepsilon = \frac{T_2}{T_1 - T_2}, \tag{186}$$

where T_2 is the (lower) temperature at which heat is put into the working fluid, and T_1 is the temperature at which heat leaves the working fluid and is rejected into the environment. A storage ring electron cooler operates with this maximum efficiency.

Consistent with this analysis, the following conclusion can be made: The storage ring must be designed be such that $T_{\text{rad}} > T_{\text{cool}}$. If it is not so designed, as in the reversible heat pump, the cycle actually runs in the opposite direction. Some heat that is not radiated is transferred and the "cooler" actually rejects heat into the higher temperature ion beam and a beam heater results. Also $T_{\text{rad}} \neq T_{\text{cool}}$. According to the second law of thermodynamics, no net heat flow can develop between two systems at the same temperature.

In a beam, no energy enters or leaves it except through the RF and the synchrotron radiation. Any beam compression or decompression is adiabatic to a good approximation. Hence a beam can be considered a very good physical model of a Carnot cycle, as long as the beam temperature at which the synchrotron radiation emits can be well quantified. Whether there exists any precision thermodynamics experiment that could be done with a dual energy storage ring cooler is an interesting question for future work.

BIBLIOGRAPHY

[1] F. Willeke, "Electron Ion Collider Conceptual Design Report 2021," 10.2172/1765663 (2021).

[2] D. Cline, A. Garren, H. Herr, F. E. Mills, C. Rubbia, A. Ruggiero, and D. Young, "High energy electron cooling to improve the luminosity and lifetime in colliding beam machines," IEEE Transactions on Nuclear Science **26**, 10.1109/TNS.1979.4330070 (1979).

[3] H. Zhao, J. Kewisch, M. Blaskiewicz, and A. Fedotov, "Ring-based electron cooler for high energy beam cooling," Phys. Rev. Accel. Beams **24**, 043501 (2021).

[4] H. Zhang, S. V. Benson, M. W. Bruker, and Y. Zhang, "Jspec: a program for ibs and electron cooling simulation," in *12th International Particle Accelerator Conference, Campinas, SP, Brazil* (2021).

[5] E. D. Courant, M. S. Livingston, and H. S. Snyder, "The Strong-Focusing Synchroton—A New High Energy Accelerator," Phys. Rev. **88**, 10.1103/PhysRev.88.1190 (1952).

[6] A. W. Chao, K. H. Mess, M. Tigner, and F. Zimmermann, *Handbook of Accelerator Physics and Engineering*, 2nd ed. (WORLD SCIENTIFIC, 2013).

[7] H. Wiedemann, *Particle Accelerator Physics*, 4th ed. (Springer, Switzerland, Jan. 2015).

[8] S. Y. Lee, *Accelerator Physics*, 3rd ed. (World Scientific Publishing Company, 2018).

[9] R. Wideröe, "Über ein neues prinzip zur herstellung hoher spannungen," Archiv für Elektrotechnik **21**, 387–406 (1928).

[10] K. W. Robinson, "Radiation effects in circular electron accelerators," Phys. Rev. **111**, edited by C. Pellegrini and A. M. Sessler, 373–380 (1958).

[11] B. Dhital, Y. Derbenev, D. Douglas, A. Hutton, G. Krafft, F. Lin, V. Morozov, and Y. Zhang, "Estimates of Damped Equilibrium Energy Spread and Emittance in a Dual Energy Storage Ring", in *12th International Particle Accelerator Conference, Campinas, SP, Brazil* (2021).

[12] B. Dhital, *Damping Times in a Dual Energy Storage Ring*, tech. rep. (Jefferson Lab, VA (US), 2021).

[13] W. Herr and B. Muratori, "Concept of luminosity," 10.5170/CERN-2006-002.361 (2006).

[14] S. van der Meer, *Stochastic damping of betatron oscillations in the ISR*, tech. rep. (CERN, Geneva, 1972).

[15] D. Mohl, "Stochastic cooling for beginners," Conf. Proc. C **831011**, 97–161 (1983).

[16] D. Möhl, G. Petrucci, L. Thorndahl, and S. van der Meer, "Physics and technique of stochastic cooling," Physics Reports **58**, 73–102 (1980).

[17] J. Marriner, "Stochastic cooling overview," Nuclear Instruments and Methods in Physics Research Section A: Accelerators, Spectrometers, Detectors and Associated Equipment **532**, International Workshop on Beam Cooling and Related Topics, 11–18 (2004).

[18] J. Wei, *Stochastic cooling and intra-beam scattering in RHIC,* tech. rep. (Brookhaven National Lab, Upton, NY (United States), 1993).

[19] G. I. Budker, "An effective method of damping particle oscillations in proton and anti-proton storage rings," Sov. Atom. Energ. **22**, 438–440 (1967).

[20] T. W. Hansch and A. L. Schawlow, "Cooling of gases by laser radiation," Optics Communications **13**, 68–69 (1975).

[21] S. Chu, L. Hollberg, J. E. Bjorkholm, A. Cable, and A. Ashkin, "Three-dimensional viscous confinement and cooling of atoms by resonance radiation pressure," Phys. Rev. Lett. **55**, 48–51 (1985).

[22] D. V. Neuffer, "Principles and applications of muon cooling," Part. Accel. **14**, 75 (1983).

[23] D. Prasuhn, J. Dietrich, R. Maier, R. Stassen, H. Stein, and H. Stockhorst, "Electron and stochastic cooling at COSY," Nuclear Instruments and Methods in Physics Research Section A: Accelerators, Spectrometers, Detectors and Associated Equipment **441**, 167–174 (2000).

[24] H. Poth, "Applications of electron cooling in atomic, nuclear and high-energy physics," Nature **345**, 399–405 (1990).

[25] P. Kienle, "The heavy ion cooler and synchrotron ring at GSI," Nucl. Phys. A **447**, edited by H. A. Gustafsson, B. Jakobsson, I. Otterlund, and K. Aleklett, 419C–434C (1986).

[26] M. Gentner, R. Brinkmann, Y. Derbenev, D. Husmann, and C. Steier, "On the possibilities of electron cooling for HERA," Nuclear Instruments and Methods in Physics Research Section A: Accelerators, Spectrometers, Detectors and Associated Equipment **424**, 277–295 (1999).

[27] S. Y. Lee, P. Colestock, and K. Y. Ng, "Electron cooling in high-energy colliders," (1997).

[28] L. Spitzer, *Physics of Fully Ionized Gases*, Provided by the SAO/NASA Astrophysics Data System (1956).

[29] G. Krafft and D. Douglas, "Energy Recovered Loop Accelerators," Jefferson Lab, 2015.

[30] G. Krafft, B. Dhital, F. Lin, and V. Morozov, "Multiple energy storage rings," `10.48550/ARXIV.1907.13461` (2019).

[31] B. Dhital, J. Delayen, Y. Derbenev, D. Douglas, G. Krafft, F. Lin, V. Morozov, and Y. Zhang, "Equilibria and synchrotron stability in two energy storage rings," in *10^{th} International Particle Accelerator Conference, Melbourne, Australia* (2019).

[32] F. Lin, Y. Derbenev, D. Douglas, J. Guo, R. Johnson, G. Krafft, V. Morozov, and Y. Zhang, "Storage-ring electron cooler for relativistic ion beams," in *7^{th} International Particle Accelerator Conference, Busan, Korea* (2016).

[33] M. Borland, "Elegant: a flexible sdds-compliant code for accelerator simulation," in *6^{th} International Computational Accelerator Physics Conference (ICAP)* (2000).

[34] M. Borland, "Private communications," Argonne National Lab, 2020.

[35] J. M. Byrd, S. De Santis, G. Stover, D. Teytelman, J. Fox, J. Jacob, V. Serriere, and M. Georggson, "Harmonic cavities and longitudinal beam stability in electron storage rings," Conf. Proc. C **0106181**, edited by P. W. Lucas and S. Webber, 380–384 (2001).

[36] K. Wille and J. McFall, *The Physics of Particle Accelerators: An Introduction,* (Oxford University Press, 2000).

[37] A. Piwinski, J. D. Bjorken, and S. K. Mtingwa, "Wilson Prize article: reflections on our experiences with developing the theory of intrabeam scattering," Phys. Rev. Accel. Beams **21**, 114801 (2018).

[38] A. Piwinski, "Intra-beam-scattering," in *9^{th} International Conference on High-Energy Accelerators* (1974), pp. 405–409.

[39] J. D. Bjorken and S. K. Mtingwa, "Intrabeam scattering," Part. Accel. **13**, 115–143 (1983).

[40] S. Nagaitsev, "Intrabeam scattering formulas for fast numerical evaluation," Phys. Rev. ST Accel. Beams **8**, 064403 (2005).

[41] M. P. Ehrlichman, W. Hartung, B. Heltsley, D. P. Peterson, N. Rider, D. Rubin, D. Sagan, J. Shanks, S. T. Wang, R. Campbell, and R. Holtzapple, "Intrabeam scattering studies at the Cornell Electron Storage Ring Test Accelerator," Phys. Rev. ST Accel. Beams **16**, 104401 (2013).

[42] B. Dhital, J. Delayen, Y. Derbenev, D. Douglas, G. Krafft, F. Lin, V. Morozov, and Y. Zhang, "Beam dynamics study in a dual energy storage ring for ion beam cooling," in *12th International Particle Accelerator Conference* (2021).

[43] Y. Li and L. Yang, "Multi-objective dynamic aperture optimization for storage rings," Int. J. Mod. Phys. A **31**, edited by L. R. Flores Castillo and K. Prokofiev, 1644019 (2016).

[44] C. Steier, D. Robin, L. Nadolski, W. Decking, Y. Wu, and J. Laskar, "Measuring and optimizing the momentum aperture in a particle accelerator," Phys. Rev. E **65**, 056506 (2002).

[45] A. Xiao and M. Borland, "Touschek effect calculation and its application to a transport line," in 2007 IEEE Particle Accelerator Conference (PAC) (2007), pp. 3453–3455.

[46] A. Piwinski, "The Touschek Effect in Strong Focusing Storage Rings," `10.48550/ARXIV.PHYSICS/9903034` (1999).

[47] V. Parkhomchuk and I. Ben-Zvi, *Electron cooling for RHIC*, tech. rep. (Brookhaven National Lab (BNL), Upton, NY (United States), 2001).

[48] H. Poth, "Electron cooling: Theory, experiment, application," Physics Reports **196**, 135–297 (1990).

[49] Y. S. Derbenev, "Theory of electron cooling," `10.48550/ARXIV.1703.09735` (2017).

[50] Y. S. Derbenev and A. N. Skrinsky, "The kinetics of electron cooling of beams on heavy particle storage rings," Part. Accel. **8**, 1–20 (1977).

[51] Y. S. Derbenev and A. N. Skrinsky, "The effect of an accompanying magnetic field on electron cooling," Part. Accel. **8**, 235–243 (1978).

[52] M. Martini, *Intrabeam scattering in the ACOL-AA machines*, tech. rep. (CERN, Geneva, 1984).

[53] I. N. Meshkov, "Electron cooling: Status and perspectives," Phys. Part. Nucl. **25**, 631–661 (1994).

[54] H. Zhao and M. Blaskiewicz, "Rate redistribution in dispersive electron cooling," Phys. Rev. Accel. Beams **24**, 083502 (2021).

[55] V. Morozov, "Private communications," Jefferson Lab, 2021.

[56] G. A. Krafft and G. Priebe, "Compton Sources of Electromagnetic Radiation," Reviews of Accelerator Science and Technology **03**, 147–163 (2010).

[57] W. Lou et al., "The Beam Optics of the FFAG Cell of the CBETA ERL Accelerator," in *9th International Particle Accelerator Conference, Vancouver, BC, Canada* (June 2018).

[58] R. Hajima, "Status and Perspectives of Compton Sources," Physics Procedia **84**, 35–39 (2016).

[59] R. Suleiman, V. S. Morozov, and Y. S. Derbenev, "On Possibilities of High Precision Experiments in Fundamental Physics in Storage Rings of Low Energy Polarized Electron Beams," `10.48550/ARXIV.2105.11575` (2021).

[60] J. Flanz and C. Sargent, "Operation of an isochronous beam recirculation system," Nuclear Instruments and Methods in Physics Research Section A: Accelerators, Spectrometers, Detectors and Associated Equipment **241**, 325–333 (1985).

[61] J. M. Grames, C. K. Sinclair, M. Poelker, X. Roca-Maza, M. L. Stutzman, R. Suleiman, M. A. Mamun, M. McHugh, D. Moser, J. Hansknecht, B. Moffit, and T. J. Gay, "High precision 5 MeV Mott polarimeter," Phys. Rev. C **102**, 015501 (2020).

[62] G. Krafft, "Private communications," Jefferson Lab, 2021.

APPENDIX A

FUNDAMENTALS OF RF CAVITY

An ideal cavity is a vacuum volume enclosed by perfectly conducting surfaces. The electromagnetic fields in a cavity are solutions of Maxwell equations in a vacuum defined as

$$\begin{aligned} \vec{\nabla} \cdot \vec{E} &= 0, \\ \vec{\nabla} \cdot \vec{B} &= 0, \\ \vec{\nabla} \times \vec{E} &= -\frac{\partial \vec{B}}{\partial t}, \\ \vec{\nabla} \times \vec{B} &= \frac{1}{c^2} \frac{\partial \vec{E}}{\partial t}. \end{aligned} \tag{187}$$

The boundary condition near a perfect conductor is that, outside the conductor the electric field is perpendicular to the surface whereas the magnetic field must be parallel to the surface, i.e. $\hat{n} \times \vec{E} = 0, \hat{n} \cdot \vec{H} = 0$ and $\vec{B} = \mu_0 \vec{H}$, μ_0 is the permeability of free-space. We assume that the spatial and temporal variation of the fields in a cavity with a cylindrical geometry can be represented as

$$\begin{aligned} \vec{E}(x,t) &= \vec{E}(\rho,\phi) e^{ikz - i\omega t} \\ \vec{H}(x,t) &= \vec{H}(\rho,\phi) e^{ikz - i\omega t}, \end{aligned} \tag{188}$$

where k is the wave number, ω is the angular frequency of the cavity, . Maxwell's equations defined in Eq. 187 combine to yield the wave equations

$$\left(\nabla^2 - \frac{1}{c^2} \frac{\partial^2}{\partial t^2}\right) \begin{Bmatrix} \vec{E} \\ \vec{H} \end{Bmatrix}. \tag{189}$$

Now, substituting the values of fields in Eq. 188 into the Eq. 189, we get the following two sets of solutions

$$\begin{aligned} \nabla_\perp^2 \vec{E} + \left(\frac{\omega^2}{c^2} - k^2\right) \vec{E} = 0, \\ \nabla_\perp^2 \vec{B} + \left(\frac{\omega^2}{c^2} - k^2\right) \vec{B} = 0. \end{aligned} \tag{190}$$

The term $\nabla_\perp^2$ refers to the transverse components of the Laplace differential operator. Under the boundary conditions in cylindrical symmetric geometry, the solutions given by Eq. 190 are

known as the eigenmodes of the cavity, each with a characteristic frequency. This transverse solution can be divided into two types as a transverse electric (TE) and the transverse magnetic (TM) modes.

Consider a cylindrical cavity which has radius R and height L, the solutions for transverse magnetic modes TM_{mnp} are given by

$$\begin{aligned}
E_z &= E_0 \cos\Big(\frac{p\pi z}{L}\Big) J_m\Big(\frac{x_{mn}\rho}{R}\Big)\cos(m\phi),\\
E_\rho &= -E_0\Big(\frac{p\pi R}{L x_{mn}}\Big)\sin\Big(\frac{p\pi z}{L}\Big) J'_m\Big(\frac{x_{mn}\rho}{R}\Big)\cos(m\phi),\\
E_\phi &= E_0\frac{mp\pi R^2}{\rho L x_{mn}^2}\sin\Big(\frac{p\pi z}{L}\Big) J_m\Big(\frac{x_{mn}\rho}{R}\Big)\sin(m\phi),\\
H_z &= 0,\\
H_\rho &= iE_0\frac{m\omega_{mnp}R^2}{\eta c\rho x_{mn}^2}\cos\Big(\frac{p\pi z}{L}\Big) J_m\Big(\frac{x_{mn}\rho}{R}\Big)\sin(m\phi),\\
H_\phi &= iE_0\frac{\omega_{mnp}R}{\eta c x_{mn}}\cos\Big(\frac{p\pi z}{L}\Big) J'_m\Big(\frac{x_{mn}\rho}{R}\Big)\cos(m\phi).
\end{aligned} \tag{191}$$

Similarly, the solutions for the transverse electric modes TE_{mnp} are

$$\begin{aligned}
H_z &= H_0 \sin\Big(\frac{p\pi z}{L}\Big) J_m\Big(\frac{x'_{mn}\rho}{R}\Big)\cos(m\phi),\\
H_\rho &= H_0\Big(\frac{p\pi R}{L x_{mn}}\Big)\cos\Big(\frac{p\pi z}{L}\Big) J'_m\Big(\frac{x'_{mn}\rho}{R}\Big)\cos(m\phi),\\
H_\phi &= -H_0\frac{mp\pi R^2}{\rho L x_{mn}'^2}\cos\Big(\frac{p\pi z}{L}\Big) J_m\Big(\frac{x'_{mn}\rho}{R}\Big)\sin(m\phi),\\
E_z &= 0,\\
E_\rho &= iH_0\frac{m\eta\omega_{mnp}R^2}{c\rho x_{mn}'^2}\sin\Big(\frac{p\pi z}{L}\Big) J_m\Big(\frac{x'_{mn}\rho}{R}\Big)\sin(m\phi),\\
E_\phi &= iH_0\frac{\eta\omega_{mnp}R}{\eta c x'_{mn}}\sin\Big(\frac{p\pi z}{L}\Big) J'_m\Big(\frac{x'_{mn}\rho}{R}\Big)\cos(m\phi)
\end{aligned} \tag{192}$$

where c is the speed of the light, η is the free space impedance, ω is the frequency of each mode, J_m is the m^{th} order Bessel function of first kind and J'_m is its derivative. The x_{mn} and x'_{mn} are the n^{th} zero of the Bessel functions J_m and J'_m of order m respectively. m, n, and p in TM_{mnp} and TE_{mnp} are integers that corresponds to the number of sign changes of E_z or H_z in ϕ, ρ, and z directions considering a cylindrical coordinates system. The frequency of TM and TE modes are given by

$$\begin{aligned}
\omega_{mnp}(TM) &= c\sqrt{\Big(\frac{x_{mn}c}{R}\Big)^2 + \Big(\frac{p\pi}{L}\Big)^2},\\
\omega_{mnp}(TE) &= c\sqrt{\Big(\frac{x'_{mn}c}{R}\Big)^2 + \Big(\frac{p\pi}{L}\Big)^2}.
\end{aligned} \tag{193}$$

APPENDIX B

ELECTRON BEAM TEMPERATURE CALCULATION

We get the damped equilibrium emittance and energy spread of electron beam by considering the combined effect of synchrotron radiation, and quantum excitation. With damped equilibrium beam parameters, Electron beam temperature are calculated in the cooler section to be used to run in JSPEC simulation.

- Matched beta function for a solenoid: $\beta_s = \frac{2p}{eB_s} = \frac{2\times 3.3357(\mathrm{Tm/(GeV/c)}\times p(\mathrm{GeV/c})}{B_s}$, where B_s is the longitudinal magnetic field applied in the cooling solenoid.
- Normalized drift emittance (in the lab frame) $\varepsilon_d^N = \frac{\beta\gamma\langle r^2\rangle}{\beta_s}$.
- Un-normalized drift emittance : $\varepsilon_d = \frac{\langle r^2\rangle}{\beta_s} = \frac{2\langle x^2\rangle}{\beta_s}$ for around beam.
- Un-normalized drift emittance : $\varepsilon_d = \frac{\langle r^2\rangle}{\beta_s} = \frac{\langle x^2\rangle+\langle y^2\rangle}{\beta_s}$, for a flat beam.
- Normalized Larmor emittance (in the lab frame) : $\varepsilon_L^N = \frac{\beta\gamma V_\perp^2}{c^2}\beta_s$.
- Un-normalized Larmor emittance : $\varepsilon_L = \frac{V_\perp^2}{c^2}\beta_s$.
- Transverse temperature (defined in the beam frame) : $T_\perp = m_e V_\perp^2[eV]\gamma^2 = m_e c^2 \frac{\varepsilon_L}{\beta_s}\gamma^2, V_\perp^2 = V_x^2 + V_y^2$.
- Longitudinal temperature : $T_\parallel = m_e c^2(\frac{\Delta p}{p})^2$.
- Traditional temperature $\varepsilon = \sqrt{\varepsilon_d \varepsilon_L}$.
- In our calculation of cooling rates, $\varepsilon_d = \frac{\varepsilon_x}{2}$, ($\varepsilon_x$ is the damped emittance), $\varepsilon_L = \frac{\varepsilon_y}{2}$. Then $\varepsilon_L \to T_\perp, \frac{\Delta p}{p} \to T_\parallel$

APPENDIX C

ELEGANT TRACKING FILE

```
&change_particle
name = electron
&end

&run_setup
lattice       = SR_500MeV.lte,
use_beamline  = SR_cooler,
p_central     = 293.541002921706, !LER 150 MeV
!    p_central     = 978.4751765220160,!HER 500 MeV
parameters = "%s.param",
!    default_order = 2,
!    concat_order  = 3,
centroid      = "%s.cen",
always_change_p0 = 0,
!    random_number_seed = 0,
&end

&alter_elements name=*, type=CSBEND, item=N_KICKS, value=150,
allow_missing_elements=1 &end
&alter_elements name=*, type=KSEXT, item=N_KICKS, value=200,
allow_missing_elements=1 &end
&alter_elements name=*, type=KQUAD, item=N_KICKS, value=150,
allow_missing_elements=1 &end

!&alter_elements name=B*, type=CSBEND, item=SYNCH_RAD, value=1 &end
!&alter_elements name=B*, type=CSBEND, item=ISR, value=1 &end

!&alter_elements name=Q*, type=KQUAD, item=SYNCH_RAD, value=1 &end
```

```
!&alter_elements name=Q*, type=KQUAD, item=ISR, value=1 &end

!&alter_elements name=S*, type=*SEXT*, item=SYNCH_RAD, value=1 &end
!&alter_elements name=S*, type=*SEXT*, item=ISR, value=1 &end

&run_control
!    n_indices = 1
!    n_steps = 1
n_passes = 1000
&end

&bunched_beam n_particles_per_bunch = 1,
centroid[0] = 0.0,0.0,0.0,0.0,0.0,0.0 &end

&track &end
&stop &end
!Bunched beam case
&bunched_beam
bunch = "%s.bun"
n_particles_per_bunch = 5,
sigma_dp = 1e-03
sigma_s = 14e-02
!  emit_z = 1e-06,
!  beta_z = 99.0668359, alpha_z = -0.071976102,
distribution_type[0] = 3*"uniform-ellipse",
distribution_cutoff[0] = 1,1,1,
&end

&track &end
&stop &end
```

APPENDIX D

ELEGANT TWISS SET-UP FILE

```
&change_particle
name = electron
&end

! comment the below : divide_elements when matching elements
 in momentum aperture run

&divide_elements name=*, type=CSBEND, divisions=5 &end

!&divide_elements name=*, type=KQUAD, divisions=5 &end
!&divide_elements name=*, type=KSEXT, divisions=5 &end

&run_setup
lattice       = SR_500MeV.lte,
use_beamline  = SR_cooler,
!    p_central     = 293.541002921706, !LER 150 MeV
p_central     = 978.4751765220160, !HER 500 MeV
default_order = 2,
concat_order  = 2,
!    centroid     = %s.cen,
!    acceptance   = %s.acc,
!    final        = %s.fin,
output = %s.out ,
!    always_change_p0 = 1
parameters    = %s.param,
magnets       = "%s.mag",
!   rootname=<rootname>
&end
```

```
!there is no need to set synch_rad=1 for twiss parameter output

&run_control
!        n_steps  = 1,
n_passes = 1
&end

&twiss_output
filename             = "%s.twi",
!   concat_order         = 2,
matched              = 1,
!   output_at_each_step  = 1,
radiation_integrals  = 1,
higher_order_chromaticity = 1,
higher_order_chromaticity_range  = 3e-6,
higher_order_chromaticity_points = 7,
compute_driving_terms     = 1,
&end

&bunched_beam n_particles_per_bunch = 1 &end

&matrix_output
printout = "%s.mpr"
printout_order = 1
&end

&track &end
&stop &end
```

APPENDIX E

ELEGANT LATTICE FILE

```
DLMT12:DRIFT,L=1.4
QLMT12:KQUAD,L=0.25,K1=-1.1373174212,TILT=0,N_KICKS=10
DLMT11:DRIFT,L=2.9
QLMT11:KQUAD,L=0.25,K1=1.2148799268,TILT=0,N_KICKS=10
QLMT10:KQUAD,L=0.25,K1=-1.207033748,TILT=0,N_KICKS=10
DLMT10:DRIFT,L=2.9
QLMT09:KQUAD,L=0.25,K1=1.052500738,TILT=0,N_KICKS=10
DLMT09:DRIFT,L=2.9
QLMT08:KQUAD,L=0.25,K1=-0.7339796576,TILT=0,N_KICKS=10
DLMT08:DRIFT,L=2.9
QLMT07:KQUAD,L=0.25,K1=0.40639472,TILT=0,N_KICKS=10
DLMT07:DRIFT,L=2.9
QLMT06:KQUAD,L=0.25,K1=-0.519852988,TILT=0,N_KICKS=10
DLDS01:DRIFT,L=1.25
BXLDS:CSBEND,L=1, ANGLE=0.1963495408,TILT=0,&
E1=0.0,E2=0.0,K1=0.0,N_KICKS=10
QLDS04:KQUAD,L=0.25,K1=1.044472586,TILT=0,N_KICKS=10
QLDS03:KQUAD,L=0.25,K1=-1.165652134,TILT=0,N_KICKS=10
QLDS02:KQUAD,L=0.25,K1=1.3305682628,TILT=0,N_KICKS=10
QLARC01:KQUAD,L=0.25,K1=-1.3842288308,TILT=0,N_KICKS=10
DLARC01:DRIFT,L=0.25
SXLARC01:KSEXT,L=0.25,k2=-12.60302638,TILT=0,N_KICKS=10
!SXLARC01:KSEXT,L=0.25,k2=0.0,TILT=0,N_KICKS=10
DLARC02:DRIFT,L=0.75
BXLARC:CSBEND,L=1, ANGLE=0.3926990817,TILT=0,&
E1=0.0,E2=0.0,K1=0.0,N_KICKS=10
DLARC03:DRIFT,L=1.25
QLARC02:KQUAD,L=0.25,K1=0.8192991508,TILT=0,N_KICKS=10
```

```
! yeslai uncomment garne ho hai zero test paxi
SXLARC02:KSEXT,L=0.25,k2=8.216007204,TILT=0,N_KICKS=10

!SXLARC02:KSEXT,L=0.25,k2=0.0,TILT=0,N_KICKS=10

DLMT06:DRIFT,L=0.5
QLMT05:KQUAD,L=0.25,K1=-2.4865962008,TILT=0,N_KICKS=10
DLMT05:DRIFT,L=1.8
QLMT04:KQUAD,L=0.25,K1=3.1614112472,TILT=0,N_KICKS=10
DLMT04:DRIFT,L=1.8
QLMT03:KQUAD,L=0.25,K1=2.57976146,TILT=0,N_KICKS=10
DLMT03:DRIFT,L=1.8
QLMT02:KQUAD,L=0.25,K1=-3.1431037448,TILT=0,N_KICKS=10
DLMT02:DRIFT,L=0.6
QLMT01:KQUAD,L=0.25,K1=2.5366239528,TILT=0,N_KICKS=10
DLMT01:DRIFT,L=0.3
SOL_H:DRIFT,L=12.5
MXBTAC1:EMATRIX,L=0,ORDER=1,&
R11=1.82574185791,R12=-6.00987037913e-10,R13=0.0,R14=0.0,R15=0.0,
R16=-1.59614632155e-19,&
R21=1.11846643058e-11,R22=0.547722557581,R23=0.0,R24=0.0,R25=0.0,
R26=-2.38332706462e-21,&
R31=0.0,R32=0.0,R33=1.82574185883,R34=1.61828328515e-10,
R35=0.0,R36=0.0,&
R41=0.0,R42=0.0,R43=1.64295105298e-11,R44=0.54772255743,
R45=0.0,R46=0.0,&
R51=0.0,R52=5.16987882846e-26,R53=0.0,R54=0.0,
R55=1.0,R56=0.0,&
R61=0.0,R62=0.0,R63=0.0,R64=0.0,R65=0.0,R66=1.0
DHMT12:DRIFT,L=1.4
QHMT12:KQUAD,L=0.25,K1=0.4263975716,TILT=0,N_KICKS=10
DHMT11:DRIFT,L=2.9
QHMT11:KQUAD,L=0.25,K1=-0.16420329672,TILT=0,N_KICKS=10
QHMT10:KQUAD,L=0.25,K1=-0.8568511784,TILT=0,N_KICKS=10
```

```
DHMT10:DRIFT,L=2.9
QHMT09:KQUAD,L=0.25,K1=1.010767854,TILT=0,N_KICKS=10
DHMT09:DRIFT,L=2.9
QHMT08:KQUAD,L=0.25,K1=-0.305278963,TILT=0,N_KICKS=10
DHMT08:DRIFT,L=2.9
QHMT07:KQUAD,L=0.25,K1=0.4287427224,TILT=0,N_KICKS=10
DHMT07:DRIFT,L=2.9
QHMT06:KQUAD,L=0.25,K1=-0.909010916,TILT=0,N_KICKS=10
DHDS01:DRIFT,L=1.25
BXHDS:CSBEND,L=1, ANGLE=-0.1963495408,TILT=0,&
E1=0.0,E2=0.0,K1=0.0,N_KICKS=10
QHDS04:KQUAD,L=0.25,K1=1.044472586,TILT=0,N_KICKS=10
QHDS03:KQUAD,L=0.25,K1=-1.165652134,TILT=0,N_KICKS=10
QHDS02:KQUAD,L=0.25,K1=1.3305682628,TILT=0,N_KICKS=10
QHARC01:KQUAD,L=0.25,K1=-1.3842288308,TILT=0,N_KICKS=10
DHARC01:DRIFT,L=0.25
! yslai uncomment garne ho hai zero test paxi
SXHARC01:KSEXT,L=0.25,k2=12.60302638,TILT=0,N_KICKS=10

!SXHARC01:KSEXT,L=0.25,k2=0.0,TILT=0,N_KICKS=10

!SXHARC01:KSEXT,L=0.25,k2=25.255828880,TILT=0,N_KICKS=10
DHARC02:DRIFT,L=0.75
BXHARC:CSBEND,L=1, ANGLE=-0.3926990817,TILT=0,&
E1=0.0,E2=0.0,K1=0.0,N_KICKS=10
DHARC03:DRIFT,L=1.25
QHARC02:KQUAD,L=0.25,K1=0.8192991508,TILT=0,N_KICKS=10
! yeslai uncomment garne la zero test paxi
SXHARC02:KSEXT,L=0.25,k2=-8.216007189,TILT=0,N_KICKS=10

!SXHARC02:KSEXT,L=0.25,k2=0.0,TILT=0,N_KICKS=10

!SXHARC02:KSEXT,L=0.25,k2=-16.420585953,TILT=0,N_KICKS=10
QHMT31:KQUAD,L=0.25,K1=-1.3229761492,TILT=0,N_KICKS=10
```

```
DHMT31:DRIFT,L=1.585
QHMT32:KQUAD,L=0.25,K1=1.134552496,TILT=0,N_KICKS=10
DHMT32:DRIFT,L=1.585
QHMT33:KQUAD,L=0.25,K1=-0.756561852,TILT=0,N_KICKS=10
DHMT33:DRIFT,L=1.585
QHMT34:KQUAD,L=0.25,K1=1.0511401528,TILT=0,N_KICKS=10
DHMT34:DRIFT,L=1.585
QHMT35:KQUAD,L=0.25,K1=-1.41462735,TILT=0,N_KICKS=10
DHMT35:DRIFT,L=1.585
QHTT02:KQUAD,L=0.25,K1=1.220298132,TILT=0,N_KICKS=10
DHTT01:DRIFT,L=3.5
QHTT01:KQUAD,L=0.25,K1=-1.209560824,TILT=0,N_KICKS=10
MXBTDC1:EMATRIX,L=0,ORDER=1,&
R11=0.547722557568,R12=-1.32296174016e-09,R13=0.0,R14=0.0,R15=0.0,
R16=5.86642694277e-19,&
R21=4.1597489342e-11,R22=1.82574185808,R23=0.0,R24=0.0,R25=0.0,
R26=-4.61126049634e-20,&
R31=0.0,R32=0.0,R33=0.547722557527,R34=-5.5315418912e-11,
R35=0.0,R36=0.0,&
R41=0.0,R42=0.0,R43=1.62173503793e-11,R44=1.82574185806,
R45=0.0,R46=0.0,&
R51=1.29246970711e-26,R52=0.0,R53=0.0,R54=0.0,R55=1.0,
R56=0.0,&
R61=0.0,R62=0.0,R63=0.0,R64=0.0,R65=0.0,R66=1.0

! Making very small M56
MSLIP: EMATRIX, L=0, ORDER=1, &
R11=1.0, R12=0.0, R13=0.0, R14=0.0, R15=0.0, R16=0.0, &
R21=0.0, R22=1.0, R23=0.0, R24=0.0, R25=0.0, R26=0.0, &
R31=0.0, R32=0.0, R33=1.0, R34=0.0, R35=0.0, R36=0.0, &
R41=0.0, R42=0.0, R43=0.0, R44=1.0, R45=0.0, R46=0.0, &
R51=0.0, R52=0.0, R53=0.0, R54=0.0, R55=1.0, R56=-12.30, &
R61=0.0, R62=0.0, R63=0.0, R64=0.0, R65=0.0, R66=1.0
```

```
!original, with radiation on
!97.7 MHz, CSBEND+QUAD+SEXT (Syn_rad+ISR)
!ACRF:RFCA,L=0,VOLT=393750000.0,PHASE=90.0,FREQ=97777085.5029211000,
CHANGE_T=1,CHANGE_P0=0
!HMRF1:RFCA,L=0,VOLT=-43750000.0,PHASE=90.0,FREQ=293331256.508763000,
CHANGE_T=1,CHANGE_P0=0
!DCRF:RFCA,L=0,VOLT=393750000.0,PHASE=270.0,FREQ=97777085.5029211000,
CHANGE_T=1,CHANGE_P0=0
!HMRF2:RFCA,L=0,VOLT=-43750000.0,PHASE=270.0,FREQ=293331256.508763000,
CHANGE_T=1,CHANGE_P0=0
!BUCRF:RFCA,L=0,VOLT=80.0,PHASE=180.0,FREQ=97777085.5029211000,
CHANGE_T=1,CHANGE_P0=0
!COM_RF:RFCA,l=0.0,VOLT=1643.6751269522,FREQ=97777085.5029211000,
PHASE=90, CHANGE_T=1,CHANGE_P0=0



en1: energy, central_momentum=293.541002921706,     ! 150 MeV
en2: energy, central_momentum=978.4751765220160,    ! 500 MeV


!MA: malign,dp=3.0E-03,on_pass=1   ! put MA after en1
!MA: malign,on_pass=1

!w1: watch,filename="%s.w1",mode="centroid"
w1: watch,filename="%s.w1",mode="coordinates"
w2: watch,filename="%s.w2",mode="coordinates"
w3: watch,filename="%s.w3",mode="coordinates"
w4: watch,filename="%s.w4",mode="coordinates"
w5: watch,filename="%s.w5",mode="coordinates"
w6: watch,filename="%s.w6",mode="coordinates"
w7: watch,filename="%s.w7",mode="coordinates"
```

```
w8: watch,filename="%s.w8",mode="coordinates"
w9: watch,filename="%s.w9",mode="coordinates"
wemit1:watch,filename="%s.wemit1",mode="parameter"
wemit2:watch,filename="%s.wemit2",mode="parameter"

LER: LINE=(&
DLMT12,QLMT12,DLMT11,QLMT11,DLMT11,QLMT10,DLMT10,
QLMT09,DLMT09,QLMT08,&
DLMT08,QLMT07,DLMT07,QLMT06,DLDS01,
BXLDS,DLDS01,QLDS04,DLDS01,BXLDS,&
DLDS01,QLDS03,DLDS01,BXLDS,DLDS01,
QLDS02,DLDS01,BXLDS,DLDS01,QLARC01,&
DLARC01,SXLARC01,DLARC02,BXLARC,
DLARC03,QLARC02,DLARC01,SXLARC02,DLARC02,BXLARC,&
DLARC03,QLARC01,DLARC01,SXLARC01,
DLARC02,BXLARC,DLARC03,QLARC02,DLARC01,SXLARC02,&
DLARC02,BXLARC,DLARC03,QLARC01,DLDS01,BXLDS,
DLDS01,QLDS02,DLDS01,BXLDS,&
DLDS01,QLDS03,DLDS01,BXLDS,DLDS01,
QLDS04,DLDS01,BXLDS,DLDS01,DLMT06,&
QLMT05,DLMT05,QLMT04,DLMT04,QLMT03,
DLMT03,QLMT02,DLMT02,QLMT01,DLMT01,&
SOL_H,w2,SOL_H,DLMT01,QLMT01,DLMT02,
QLMT02,DLMT03,QLMT03,DLMT04,QLMT04,&
DLMT05,QLMT05,DLMT06,DLDS01,BXLDS,DLDS01,
QLDS04,DLDS01,BXLDS,DLDS01,&
QLDS03,DLDS01,BXLDS,DLDS01,QLDS02,DLDS01,
BXLDS,DLDS01,QLARC01,DLARC01,&
SXLARC01,DLARC02,BXLARC,DLARC03,QLARC02,
DLARC01,SXLARC02,DLARC02,BXLARC,DLARC03,&
QLARC01,DLARC01,SXLARC01,DLARC02,BXLARC,
DLARC03,QLARC02,DLARC01,SXLARC02,DLARC02,&
BXLARC,DLARC03,QLARC01,DLDS01,BXLDS,DLDS01,
QLDS02,DLDS01,BXLDS,DLDS01,&
```

```
QLDS03,DLDS01,BXLDS,DLDS01,QLDS04,DLDS01,
BXLDS,DLDS01,QLMT06,DLMT07,&
QLMT07,DLMT08,QLMT08,DLMT09,QLMT09,
DLMT10,QLMT10,DLMT11,QLMT11,DLMT11,&
QLMT12,DLMT12)


HER: LINE=(&
DHMT12,QHMT12,DHMT11,QHMT11,DHMT11,QHMT10,DHMT10,&
QHMT09,DHMT09,QHMT08,DHMT08,QHMT07,DHMT07,
QHMT06,DHDS01,BXHDS,DHDS01,&
QHDS04,DHDS01,BXHDS,DHDS01,QHDS03,DHDS01,
BXHDS,DHDS01,QHDS02,DHDS01,&
BXHDS,DHDS01,QHARC01,DHARC01,SXHARC01,
DHARC02,BXHARC,DHARC03,QHARC02,DHARC01,&
SXHARC02,DHARC02,BXHARC,DHARC03,QHARC01,
DHARC01,SXHARC01,DHARC02,BXHARC,DHARC03,&
QHARC02,DHARC01,SXHARC02,DHARC02,BXHARC,
DHARC03,QHARC01,DHDS01,BXHDS,DHDS01,&
QHDS02,DHDS01,BXHDS,DHDS01,QHDS03,DHDS01,
BXHDS,DHDS01,QHDS04,DHDS01,&
BXHDS,DHDS01,QHMT31,DHMT31,QHMT32,DHMT32,
QHMT33,DHMT33,QHMT34,DHMT34,&
QHMT35,DHMT35,QHTT02,DHTT01,QHTT01,DHTT01,
QHTT02,DHTT01,QHTT01,DHTT01,&
QHTT02,DHTT01,QHTT01,DHTT01,QHTT02,DHMT35,
QHMT35,DHMT34,QHMT34,DHMT33,&
QHMT33,DHMT32,QHMT32,DHMT31,QHMT31,
DHDS01,BXHDS,DHDS01,QHDS04,DHDS01,&
BXHDS,DHDS01,QHDS03,DHDS01,BXHDS,DHDS01,
QHDS02,DHDS01,BXHDS,DHDS01,&
QHARC01,DHARC01,SXHARC01,DHARC02,BXHARC,
DHARC03,QHARC02,DHARC01,SXHARC02,DHARC02,&
BXHARC,DHARC03,QHARC01,DHARC01,SXHARC01,DHARC02,
```

```
BXHARC,DHARC03,QHARC02,DHARC01,&
SXHARC02,DHARC02,BXHARC,DHARC03,QHARC01,
DHDS01,BXHDS,DHDS01,QHDS02,DHDS01,&
BXHDS,DHDS01,QHDS03,DHDS01,BXHDS,DHDS01,
QHDS04,DHDS01,BXHDS,DHDS01,&
QHMT06,DHMT07,QHMT07,DHMT08,QHMT08,DHMT09,
QHMT09,DHMT10,QHMT10,DHMT11,&
QHMT11,DHMT11,QHMT12,DHMT12)

!Twiss
SR_cooler: LINE=(HER)
!SR_cooler: LINE=(LER,MXBTAC1,HER,MXBTDC1)
RETURN
```

APPENDIX F

DAMPING AND IBS TIME CALCULATIONS

Damping times in a dual energy storage ring design are calculated using ELEGANT. This method uses the individual ring optics. Damped equilibrium energy spread and emittance values are taken for each rings. The following syntax in ELEGANT is used:

```
ibsEmittance twissFile resultFile -particles=6.9E10 -coupling=0.05
-isRing=1 -emitInput=damped emittance
-deltaInput=damped energy spread
-length=bunch length (mm)
```

To get the damping times values, use the following command

```
sddsprintout resultFile -par=taux -par=tauy -par=taudelta
```

taux, tauy, and taudelta printout the horizontal, vertical and longitudinal damping times. To get the IBS rates, use the following command

```
sddsprintout resultFile -par=xGrowthRateInitial
-par=yGrowthRateInitial -par=zGrowthRateInitial
```

xGrowthRateInitial, yGrowthRateInitial, and zGrowthRateInitial printout the horizontal, vertical and longitudinal IBS rates respectively. The total damping and IBS times calculation after this follows the methods explained in Chapter 4.

Reference:

```
https://ops.aps.anl.gov/manuals/elegant_latest
/elegantsu94.html#x103-1020008.9
```

In a storage ring, damping times can be calculated theoretically using the following formulas

$$\tau_x = \frac{2E_0T_0}{J_xU_0}, \quad \tau_y = \frac{2E_0T_0}{J_yU_0}, \tau_z = \frac{2E_0T_0}{J_zU_0}, \tag{194}$$

where τ_x, τ_y, and τ_z are the horizontal, vertical, and longitudinal damping times, respectively. E_0, T_0, U_0 are the beam energy, revolution time, and the energy loss per turn due to synchrotron radiation. J_x, J_y, and J_z are the damping partition numbers such that $J_x + J_y + J_z = 4$.

APPENDIX G

ELEGANT FILE TO CALCULATE DYNAMIC APERTURE

```
!DA calculation
!Tracking  ==========================================================================
&run_setup
lattice       = SR_500MeV.lte,
use_beamline  = SR_cooler,
p_central     = 293.541002921706, !LER 150 MeV
!    p_central     = 978.4751765220160,! HER 1000 MeV
parameters = "%s.param",
acceptance = %s.acc
!    default_order = 2,
!    concat_order  = 3,
centroid      = "%s.cen",
!    always_change_p0 = 0,
!    random_number_seed = 0
&end

!&twiss_output
!      filename = "%s.twi",
!      concat_order = 1,
!      matched = 1,
!      radiation_integrals = 1
!     beta_x = 100
!     beta_y = 100
!      output_at_each_step = 0
!&end

&alter_elements name=*, type=CSBEND, item=N_KICKS, value=150,
allow_missing_elements=1 &end
```

```
&alter_elements name=*, type=KSEXT, item=N_KICKS, value=200,
allow_missing_elements=1 &end
&alter_elements name=*, type=KQUAD, item=N_KICKS, value=150,
allow_missing_elements=1 &end



&run_control
!    n_indices = 1
!    n_steps = 1
n_passes=500
&end

!&vary_element
!   index_number = 0,
!   index_limit = 11,
!   name = mal,
!   item = dp,
!   initial = -5,
!   final = 5,
!   multiplicative = 1
!&end

&find_aperture
output = "%s.aper",
mode = "n-line",
n_lines = 5,
xmin = -0.001,
xmax = 0.01,
ymin=0,
ymax = 0.01,
nx = 5,
ny = 9,
n_splits = 8,
```

```
split_fraction = 0.1,
verbosity = 1,
desired_resolution = 0.00001,
offset_by_orbit = 1
&end

&bunched_beam n_particles_per_bunch = 1 &end

&track &end
&stop &end
```

APPENDIX H

ELEGANT FILE TO CALCULATE MOMENTUM APERTURE

```
!Momentum Aperture Run

&run_setup
lattice = SR_500MeV.lte,
magnets = %s.mag
p_central = 293.54100292171,
!    p_central = 978.4751765220,
use_beamline= SR_cooler,
default_order = 3,
concat_order = 0,
centroid="%s.cen"
parameters = %s.paramOpt,
magnets = %s.mag,
losses = %s.lost
&end

!&insert_elements
!   name = *,
!   type = *[QLMT]*,
!   skip = 1,
!   element_def = "TEST: TSCATTER",
!&end

&twiss_output
filename = "%s.twi",
statistics=1,
radiation_integrals=1,
&end
```

```
!&alter_elements name=Q*, type=KQUAD, item=SYNCH_RAD, value=1 &end
!&alter_elements name=B*, type=CSBEN*, item=SYNCH_RAD, value=1 &end
!&alter_elements name=S*, type=*SEXT*, item=SYNCH_RAD, value=1 &end


&run_control
n_passes = 1000
&end

&momentum_aperture
output = %s.mmap,
x_initial = 1e-5,
y_initial = 1e-5,
delta_negative_start = 0.0
delta_negative_limit = -0.01
delta_positive_start = 0.0,
delta_positive_limit = 0.01
delta_step_size = 0.001,
!        oversteps = 1,
steps_back = 1,
split_step_divisor = 10,
splits = 10,
s_start = 0.0,
s_end = 343.4,
skip_elements = 0,
!        include_name_pattern = TEST,
verbosity = 4
soft_failure = 1
&end
&track &end
&stop &end
```

APPENDIX I

PYTHON SCRIPTS TO CALCULATE DAMPED PARAMETERS

```
! The following python codes calculate the damped emittances
import pandas as pd
import numpy as np
from math import sqrt

E_L = 150 !(Low energy ring energy in MeV)
E_H = 500 !(High energy ring enerhy in MeV)
mc2 = 0.510999 !(Rest mass of an electron in MeV)
g_L = E_L/mc2 !(relativisitic gamma for LER)
g_H = E_H/mc2
bg_L = sqrt((g_L*g_L)-1) !(Relativisitc beta for LER)
bg_H = sqrt((g_H*g_H)-1)
h_bar = 1.05457e-34
m = 9.10938356e-31
c = 299792458
a = 55*sqrt(3)/(24*4)
A = a*h_bar/(m*c)
! damping partition numbers in x, y, and s
Jx = 0.2144927 #(1 -xi) in the formula
Jy = 1
Js = 2.785507
!bending radius in meter
rho_L = 2.55 # bend radius for LER
rho_H = 2.55 # bend radius for HER
! radiation integrals
I5 = 0.74106
I2 = 1.85055
```

```
Ex_nu = A*(pow(g_H,6)*I5 + (pow(g_L,6)*I5))
Ex_den = Jx*(pow(g_H,3)*I2 + (pow(g_L,3)*I2))
! LER and HER emittances
Ex_L = Ex_nu/(g_L*Ex_den)
Ex_H = Ex_nu/(g_H*Ex_den)

!Normalized LER and HER emittances
noremitt_L = Ex_L*bg_L
noremitt_H = Ex_H*bg_H

k = 0.05 !coupling factor
!Vertical emittances for LER and HER
veremitt_L = Ex_L*k/(1+k)
veremitt_H = Ex_H*k/(1+k)

!! The following codes calculate the energy spread
es_square_nu = A*(pow(g_L,7)+ pow(g_H,7))*(1/pow(rho_L,3))
 !numerator term
es_square_den = Js*(pow(g_L,3)+pow(g_H,3))*(1/pow(rho_L,2))
!denominator term
es_squ_Low = es_square_nu/((pow(g_L,2)*es_square_den))
es_Low = sqrt(es_squ_Low) ! energy spread for LER
es_squ_High = es_square_nu/(pow(g_H,2)*es_square_den)
es_High = sqrt(es_squ_High) ! energy spread for HER
```

APPENDIX J

PYTHON SCRIPTS TO CALCULATE TOUSCHEK LIFETIME

```
import pandas as pd
import numpy as np

r_e = 2.817e-15
c = 3e8
n = 6.9e10
e = 1.6e-19
q=n*e
E_e = 150
mc2 = 0.511
gamma = E_e/mc2
pi = 3.1416
C = 171.7
sigma_s = 0.025
A = r_e*r_e*c*q/(8*pi*e*gamma*gamma*gamma*sigma_s*C)

df1=pd.read_csv("twiss_param_1.txt",sep="\s+")
df2=pd.read_csv("twiss_param_2.txt",sep="\s+")
df3=pd.read_csv("mom_aper.txt",sep="\s+")
#Merging two sets of dataframe
df4 = df1.reset_index().merge(df2.reset_index(), left_index=True,
right_index=True, how='left')
df = df3.reset_index().merge(df4.reset_index(), left_index=True,
right_index=True, how='left')
for ind, row in df.iterrows():
df.loc[ind,"eta*delta_pos"] = row["deltaPositive"] * row["etax"]
for ind, row in df.iterrows():
df.loc[ind,"eta*delta_pos_square"] = row["eta*delta_pos"] *
```

```
 row["eta*delta_pos"]
for ind, row in df.iterrows():
df.loc[ind,"sigma_x^2"] = row["sigma_x1"] +
row["eta*delta_pos_square"]
for ind, row in df.iterrows():
df.loc[ind,"sigma_x"] = np.sqrt(row["sigma_x1"] +
 row["eta*delta_pos_square"])
for ind, row in df.iterrows():
df.loc[ind,"H(s)"] = (row["gamma_x"]*row["etax"]*row["etax"])
 + (2* row["alphax"]*row["etax"]*row["etaxp"]) +
(row["betax"]*row["etaxp"]*row["etaxp"])

df[['H(s)']].mean()

ex = 2.287e-06
sigma_delta = 6.9E-04
sigma_delta_sqr = sigma_delta*sigma_delta
ratio = sigma_delta_sqr / ex
for ind, row in df.iterrows():
df.loc[ind,"sigma_div"] = (ex /row["sigma_x"])*
np.sqrt(1 + row["H(s)"]*ratio)

gamma_L = 293.54
for ind, row in df.iterrows():
df.loc[ind,"denominator"] = row["sigma_div"]*gamma_L

for ind, row in df.iterrows():
df.loc[ind,"x"] = row["deltaPositive"]/row["denominator"]

for ind, row in df.iterrows():
df.loc[ind,"x^2"] = row["x"]*row["x"]

# Integrating F(x) and getting array values of integration
 for all values of x
```

```
from scipy.integrate import quad
import math
from math import log
x_values = df["x^2"].to_numpy()
I1 = np.empty(len(x_values))
def f(u,x):
return (1/u - 0.5*np.log(1/u) - 1)*np.exp(-x/u)
for i, x in enumerate(x_values):
I1[i] = quad(f, 0, 1, args=(x))[0]

for ind, row in df.iterrows():
df.loc[ind,"Pdel_square"] = row["deltaPositive"]*
row["deltaPositive"]
for ind, row in df.iterrows():
df.loc[ind,"I2"] = row["sigma_x"]*row["sigmay"]*
row["sigma_div"]*row["Pdel_square"]
df["I1"] = pd.Series(I1) # Convert numpy array into
 dataframe column
for ind, row in df.iterrows():
df.loc[ind,"I"] = row["I1"] / row["I2"]
I_sum = df["I"].sum()
pos_trate = A*I_sum
pos_tlifetime = 1/pos_trate/3600 ! lifetime in hour
```

VITA

Bhawin Dhital
Department of Physics
Old Dominion University
Norfolk, VA 23529

Bhawin Dhital enrolled in the physics graduate program at Old Dominion University in the 2016 Fall semester. Mr. Dhital joined the beam dynamics group of the Center for Advanced Studies of Accelerators (CASA) at Jefferson Lab in 2018. After joining CASA, he continued his research on the possibility of a novel accelerator design to cool hadron beams. He received an EIC Center Fellowship at Jefferson Lab to carry out his research work. He defended his doctoral thesis on September 07 2022. Bhawin Dhital is a member of the American Physical Society.

Typeset using LaTeX.